

1 ~~Exploring the sensitivity of the Northern Hemisphere~~ The Eurasian and North American ice  
2 ~~sheets at the last two~~ Last and Penultimate glacial maxima ~~to~~ : coupled  
3 ~~climate~~ atmosphere-ice sheet model ~~parameters~~ sensitivity and calibration

4 Violet L. Patterson<sup>1</sup>, Lauren J. Gregoire<sup>1</sup>, Ruza F. Ivanovic<sup>1</sup>, Niall Gandy<sup>2</sup>, Stephen Cornford<sup>3</sup>, Jonathan  
5 Owen<sup>4</sup>, Sam Sherriff-Tadano<sup>5</sup>, Robin S. Smith<sup>6</sup>

6 <sup>1</sup>School of Earth and Environment, University of Leeds, Leeds, UK

7 ~~<sup>2</sup>Department~~<sup>2</sup>Institute of the Natural and Built Environment Social Science, Sheffield Hallam University, Sheffield, UK

8 ~~<sup>3</sup>School~~<sup>3</sup>School of Geographical Sciences, University of Bristol, Bristol, UK

9 ~~<sup>4</sup>School~~<sup>4</sup>School of Mathematical and Physical Sciences, University of Sheffield, Sheffield, UK

10 <sup>5</sup>Faculty of Science, University of the Ryukyus, Okinawa, Japan

11 <sup>6</sup>NCAS, Department of Meteorology, University of Reading, Reading, UK

12 *Correspondence to:* Violet L. Patterson (ee17vp@leeds.ac.uk)

13 **Abstract.** ~~Simulations of past periods are useful for testing the ability of numerical models to simulate ice sheet changes under~~  
14 ~~significantly different climate conditions to present day. This can help improve projections of future sea level rise made by~~  
15 ~~these same models and avoid over tuning to particular (e.g. modern) stationary climate conditions. The Last Glacial Maximum~~  
16 ~~(LGM; ~21 thousand years ago (ka)) has been extensively used for this purpose since it is relatively well constrained by~~  
17 ~~empirical evidence. However, less is known about the Penultimate Glacial Maximum (PGM; ~140 ka) and why the vast ice~~  
18 ~~sheets covering much of the Northern Hemisphere (NH), differed to the LGM. The answer likely lies, at least in part, in the~~  
19 ~~different orbital configurations between the two periods, and the resulting impact on climate-ice sheet interactions.~~

20 The configuration of the Northern Hemisphere ice sheets during the Last and Penultimate Glacial Maxima (LGM; PGM)  
21 influenced millennial-scale climate changes, as well as solid Earth and sea level changes that occurred during the subsequent  
22 deglaciations, due to their effects on the atmosphere, ocean circulation, and the solid Earth. Thus, realistic simulations of these  
23 ice sheets are crucial for the initialisation of deglaciation experiments that can help improve our understanding of interactions  
24 between the climate, ice sheets and sea levels. Here, we ~~perform and compare~~produce the first large ensembles of complex  
25 coupled ~~climate~~atmosphere-ice sheet model (FAMOUS-BISICLES) simulations of the ~~LGM and PGM to better understand~~  
26 ~~how NH ice sheets interact with the climate and quantify how sensitive the simulations are to the choice of uncertain model~~  
27 ~~inputs, including physical parameter values. Specifically, we vary~~PGM and LGM, varying 12 uncertain parameters that control  
28 the ~~model representations of~~ ice sheet albedo, ice dynamics and climate. ~~The ensembles are evaluated against palaeo-evidence~~  
29 ~~of global mean temperature, ice volume and extent to calibrate the model and find combinations of~~We quantify the sensitivity  
30 to input parameters ~~that simultaneously yield plausible ice sheets and climates for both periods. The sensitivity of the North~~  
31 ~~American ice sheet and the Eurasian ice sheet during the LGM and PGM, to each of the 12 parameter values, is explored using~~  
32 Gaussian Process emulators to perform a Sobol sensitivity analysis. ~~From the whole ensemble, we find two simulations that~~  
33 ~~meet our evaluation constraints for the LGM ice sheets. The parameter values that influence the albedo of the ice sheet~~ Albedo

34 parameters have the largest influence on the ice volumes for both ice sheets and time periods. Parameters controlling  
35 precipitation and sliding have a larger effect on Eurasian than North American ice sheet size due to the differences in  
36 geographical and climatic settings. Out of 120 parameter combinations, we find four that produce LGM and PGM ice volumes  
37 and extents compatible with palaeo-evidence. The resulting ice sheet volumes, but several other parameters display different  
38 sensitivity indices depending on the ice sheet (North American versus Eurasian) and time period (PGM versus LGM). This  
39 includes parameters that affect the cloud liquid water, lapse rate, basal sliding and downscaling elevation  
40 heights. configurations provide new and improved reconstructions of PGM Northern Hemisphere ice sheets for use as inputs  
41 in climate, ice sheet and sea level models.

## 42 **1 Introduction**

43 During ~~glacial periods of~~ the last 800,000 years, glacial periods saw the accumulation of large ice sheets ~~built up over the~~  
44 Northern Hemisphere (NH) continents (Ehlers et al., 2018) ~~impacting the climate through their interactions with atmospheric~~  
45 ~~circulation, oceanic circulation and the energy budget (Lambeck et al., 2014; Scherrenberg et al., 2023b). However, the~~  
46 ~~evolution of the NH ice sheets differed between each glacial period leading to different geometries at the glacial maxima, the~~  
47 ~~periods during the glacials in which global ice volume is at its largest and global mean sea level is at its lowest (Ehlers et al.,~~  
48 ~~2018).~~

49 Geological evidence and numerical simulations of the last two glacial maxima, the Penultimate Glacial Maximum (PGM; ~140  
50 ka) and the Last Glacial Maximum (LGM; ~21 ka), for example, suggest very different configurations of the North American  
51 ice sheet (NAIS) and the Eurasian ice sheet (EIS) (Svendsen et al., 2004; Colleoni et al., 2016; Batchelor et al., 2019) despite  
52 similarities in Greenhouse Gas (GHG) concentrations (CO<sub>2</sub> ~190 ppm), global average insolation and global ice volume (~  
53 130 meters sea level equivalent (m s.l.e.)) (Berger and Loutre, 1991; Loulergue et al., 2008; Rabineau et al., 2006; Masson-  
54 Delmotte et al., 2010; Bereiter et al., 2015; Rohling et al., 2017). Geomorphological evidence suggests that the extent of the  
55 Penultimate EIS could have been ~50% larger than during the Last Glacial Cycle and expanded 200 km further south and 1000  
56 km further east in Siberia (Batchelor et al., 2019; Knies et al., 2001; Svendsen et al., 2004). However, there are large  
57 uncertainties in its maximum extent at the PGM since there is evidence of two major ice advances in Europe, the more extensive  
58 Drenthe (~160 ka), which was followed by partial melting and sea level rise ~157-154 ka under increasing summer insolation,  
59 and then a readvance after 150 ka during the less extensive Warthe (Hughes and Gibbard, 2018). Thus, current reconstructions  
60 of the maximum may incorrectly incorporate previous advances during MIS 6 (195-123 ka) (Ehlers et al., 2018; Margari et al.,  
61 2014; Svendsen et al., 2004).

62 Since the volume of ice sheets cannot be directly inferred from empirical evidence, it must be indirectly estimated from datasets  
63 such as relative sea level proxies through glacial isostatic adjustment (GIA) inversion modelling and numerical ice sheet  
64 modelling (e.g. Lambeck et al., 2006; Tarasov et al., 2012; Rohling et al., 2017). Consequently, there is even larger uncertainty  
65 in volume estimates than there are in extent estimates. Nonetheless, ice volume estimates support the ice extent derived

66 ~~evidence that EIS volume was indeed larger at the PGM, with most estimates ranging from ~40–70 m s.l.e. compared to ~13–~~  
67 ~~24 m s.l.e. at the LGM (Lambeck et al., 2006; Peyaud, 2006; Pollard et al., 2023; Rohling et al., 2017; Simms et al., 2019;~~  
68 ~~Tarasov et al., 2012).~~  
69 In contrast, whilst there is some evidence that, during the PGM, the NAIS. Their size, shape, and evolution exerted a strong  
70 influence on the climate through their interactions with atmospheric and oceanic circulation, as well as the energy budget  
71 (Beghin et al., 2015; Fyke et al., 2018; Izumi et al., 2023; Roberts et al., 2019). Thus, reconstructing their extent and thickness  
72 is key to deciphering the causes of past climatic and environmental changes.  
73 Beyond impacting the energy balance through their high albedo, ice sheets have direct effects on ocean circulation, atmospheric  
74 circulation, and precipitation patterns. They affect deep water formation and circulation in the North Atlantic, either through  
75 their freshwater release near sites of deep water formation, their impact on energy balance, or their effect on wind patterns  
76 (Gregoire et al., 2018; Sherriff-Tadano et al., 2018, 2021; Smith and Gregory, 2012; Ullman et al., 2014). Not only can they  
77 be responsible for hemispheric-scale, century-scale cooling events, such as the 8.2 kyr event (Matero et al., 2017), but their  
78 size has also been shown to affect the stability of the Atlantic Meridional Overturning Circulation (Sherriff-Tadano et al.,  
79 2021; Zhang et al., 2014). Even subtle differences in the topographical profile of the Eurasian ice sheet can control whether  
80 the ocean responds to meltwater fluxes linearly or non-linearly (Romé, 2024). The geometry of an ice sheet also influences its  
81 stability. An ice sheet made of multiple domes can produce large sea level rises due to the Saddle Collapse instability (Gregoire  
82 et al., 2012), while marine ice sheets can be susceptible to marine ice sheet instability (MISI; Reed et al., 2024). Thus, knowing  
83 the shape and size of past ice sheets is key to understanding past abrupt climate and sea level changes in the Quaternary, as  
84 well as climate-ice sheet mechanisms relevant for the future. One period that has recently gained a lot of interest is the  
85 penultimate deglaciation (~140–128 ka). This period was the precursor to the last interglacial period (~129–116 ka) when sea  
86 level was last higher than today (by up to 9 m; Dutton et al., 2015; Dutton and Lambeck, 2012). Knowledge of the Penultimate  
87 Glacial Maximum (PGM; ~140 ka) ice sheets and their influence on the atmosphere and ocean during the subsequent  
88 deglaciation is key for interpreting climate and sea level records of the last interglacial period, which hold information on the  
89 sensitivity of Greenland and Antarctica ice sheets to climate warmer than today (Barnett et al., 2023; Capron et al., 2017;  
90 Pollard et al., 2024). Despite this interest, there are very few reconstructions or simulations of the PGM and the subsequent  
91 deglaciation. Climate simulations of the period thus either use ice sheet configurations from the LGM (e.g. Clark et al., 2020;  
92 Quiquet and Roche, 2024) or ice sheet reconstructions that have large disagreements with reconstructions of ice extent (e.g.  
93 Menviel et al., 2019). Indeed, reconstructing the geometry, size, and volume of ice sheets prior to the Last Glacial Maximum  
94 (LGM; ~21 ka) is extremely challenging as the last deglaciation has erased traces left of the previous glaciations and  
95 deglaciations, and dating glacial features is challenging and uncertain (Capron et al., 2017; Govin et al., 2015; Parker et al.,  
96 2022). Coupled climate-ice sheet modelling thus offers the best tool to produce ice sheet reconstructions informed by our  
97 knowledge of climate and ice sheet physics as well as the available geological evidence.  
98

99 [The extent of the Eurasian ice sheet \(EIS\) could have been ~50% larger during the penultimate glacial cycle than during the](#)  
100 [last glacial cycle, expanding 200 km further south and 1000 km further east in Siberia according to geomorphological evidence](#)  
101 [\(Batchelor et al., 2019; Knies et al., 2001; Svendsen et al., 2004\). However, the exact extent at the PGM is more uncertain](#)  
102 [because there were two major ice advances in Europe: the more extensive Drenthe \(~160 ka\), followed by partial melting and](#)  
103 [sea level rise ~157-154 ka, and then the less extensive Warthe readvance after 150 ka \(Hughes and Gibbard, 2018\). Current](#)  
104 [reconstructions \(e.g. Batchelor et al., 2019\) of the PGM may incorrectly incorporate previous MIS 6 \(195-123 ka\) advances](#)  
105 [\(Ehlers et al., 2018; Margari et al., 2014; Svendsen et al., 2004\). The volume of PGM ice sheets is even more uncertain than](#)  
106 [their extent since it is indirectly estimated from sea level datasets through glacial isostatic adjustment \(GIA\) and ice sheet](#)  
107 [modelling \(e.g. Lambeck et al., 2006; Tarasov et al., 2012; Rohling et al., 2017\). Estimates of EIS volume range from ~40-70](#)  
108 [m s.l.e. compared to ~13-24 m s.l.e. at the LGM \(Lambeck et al., 2006; Peyaud, 2006; Pollard et al., 2023; Rohling et al.,](#)  
109 [2017; Simms et al., 2019; Tarasov et al., 2012\) reflecting the huge uncertainties in PGM ice sheet size compared to the better](#)  
110 [known LGM.](#)

111 [In contrast, the North American ice sheet \(NAIS\) was smaller at the PGM than at the LGM, though some evidence suggests it](#)  
112 [extended slightly further south in the regions known today as Illinois and Wisconsin \(Batchelor et al., 2019; Hughes and](#)  
113 [Gibbard, 2018\).](#) ~~most available evidence suggests that the NAIS was smaller in extent and volume compared to the LGM.~~  
114 [This. Evidence for smaller PGM NAIS volume](#) includes relative sea level assessment studies (e.g. Rohling et al., 2017),  
115 reduced ice-rafted debris layers in the North Atlantic (pointing to reduced iceberg discharge from the Hudson Bay region;  
116 Hemming, 2004; Naafs et al., 2013; Obrochta et al., 2014), climate and ice sheet modelling studies (Abe-Ouchi et al., 2013;  
117 Colleoni et al., 2016; Wekerle et al., 2016) and GIA modelling studies (Dyer et al., 2021; Wainer et al., 2017). The relative  
118 lack of geomorphological evidence of the PGM NAIS further supports the hypothesis that PGM NAIS was smaller than LGM  
119 NAIS because it implies a larger ice advance at the LGM destroyed most traces of the previous glacial maximum (Dalton et  
120 al., 2022; Dyke et al., 2002; Rohling et al., 2017). Therefore, the footprint of the PGM NAIS remains very uncertain, while  
121 LGM NAIS ice extent is ~~relatively~~ well constrained from a range of glacial geological evidence, ~~which has been updated in~~  
122 ~~recent years (e.g. Dalton et al., 2020). As with the EIS, the~~ [The](#) volume of the NAIS is ~~more difficult to assess from empirical~~  
123 ~~evidence and mostly relies on modelling, which estimates it~~ [estimated](#) at ~~being between~~ ~39-59 m s.l.e. at the PGM compared  
124 to ~68-88 m s.l.e. at the LGM (Rohling et al., 2017; Simms et al., 2019).

125 [Recently, Pollard et al. \(2023\) used simple ice sheet modelling and sea level modelling to reconstruct a range of plausible](#)  
126 [Eurasian ice sheet shapes at the PGM, providing vital new information for climate and sea level models. However, such](#)  
127 [methodology neglects the influence of ice sheet dynamics and climate. Another possible way of reconstructing Quaternary ice](#)  
128 [sheets is to use dynamical ice sheet models \(Abe-Ouchi et al., 2013; Alder and Hostetler, 2019; Charbit et al., 2007; Gregoire](#)  
129 [et al., 2016; Niu et al., 2019; Scherrenberg et al., 2023b; Wekerle et al., 2016; Zweck and Huybrechts, 2005\). Their results](#)  
130 [highly depend on how the surface mass balance \(SMB\) is prescribed and this is the largest source of uncertainty. PGM](#)  
131 [modelling has so far relied on simple positive degree day SMB schemes, where the SMB is prescribed as a function of](#)

132 [temperature, and SMB evolution is derived from faraway climate proxy records producing unrealistic ice sheets \(e.g. Abe-](#)  
133 [Ouchi et al., 2013; Clark et al., 2020; Wekerle et al., 2016\).](#)

134 [Progress in ice sheet and climate modelling now allow us to use coupled climate-ice sheet models to simulate the co-evolution](#)  
135 [of climate and ice sheets. In such models, the SMB can be simulated as a function of the surface energy budget and moisture](#)  
136 [fluxes, and techniques exist to downscale low resolution climate onto the higher resolution surface of the ice sheet \(Smith et](#)  
137 [al., 2021; Ziemen et al., 2014\). Such methods not only allow us to investigate the interactions between the climate and the ice](#)  
138 [sheets, but are also a powerful way to simulate ice sheet evolution accounting for the feedbacks between ice sheet geometry](#)  
139 [and surface mass balance.](#)

140 [Only a handful of coupled climate-ice sheet models have been used to simulate the evolution of past ice sheets during the](#)  
141 [Quaternary. Some climate models, such as CESM, have high complexity and climate resolution limiting the duration of the](#)  
142 [simulations to century time scales \(Bradley et al., 2024; Sommers et al., 2021\). Other models like CLIMBER-2 and](#)  
143 [LOVECLIM have lower complexity and resolution enabling simulations over glacial-interglacial timescales \(e.g. Ganopolski](#)  
144 [et al., 2010; Quiquet et al., 2021; Quiquet and Roche, 2024\). The model we use in our study, FAMOUS-ice, has the complexity](#)  
145 [of a full GCM but a sufficiently low atmospheric resolution to enable us to run 10,000 year long simulations and large](#)  
146 [ensembles to investigate uncertainty \(Gandy et al., 2023; Patterson et al., 2024; Sherriff-Tadano et al., 2024\). This is an ideal](#)  
147 [model to produce physically consistent reconstructions of Quaternary ice sheets.](#)

148 [In a previous study, Patterson et al., \(2024\) used FAMOUS coupled to the Glimmer ice sheet model to simulate the North](#)  
149 [American ice sheet](#)~~The differences in the shape and size of the ice sheets between the LGM and PGM are not well understood.~~  
150 ~~They result from complex interactions occurring between different components of the earth system (e.g. atmosphere, ocean,~~  
151 ~~ice sheets, and solid earth) leading up to and at the glacial maximum. Despite similar levels of average global incoming solar~~  
152 ~~radiation between the LGM and PGM, the seasonal and latitudinal patterns differed between the two periods, as did its~~  
153 ~~evolution prior to the maxima, as a result of different orbital situations (Berger, 1978; Berger and Loutre, 1991). The orbital~~  
154 ~~forcing, along with concentrations of GHGs, would have altered the radiative balance between the periods. As well as affecting~~  
155 ~~the ice sheet evolutions directly, this also would have influenced the sources and pathways of moisture advection (Hughes and~~  
156 ~~Gibbard, 2018; Krinner et al., 2011; Rohling et al., 2017), sea surface temperatures (SSTs) and sea ice concentration (Clark et~~  
157 ~~al., 2009; Colleoni et al., 2011; Kageyama et al., 1999; Kageyama and Valdes, 2000), vegetation distribution (Colleoni et al.,~~  
158 ~~2009b; Kageyama et al., 2004; Stone and Lunt, 2013), dust deposition (Colleoni et al., 2009a; Krinner et al., 2006; Naafs et~~  
159 ~~al., 2012) and pro-glacial lake coverage (Colleoni et al., 2009a; Krinner et al., 2004), which all have important feedbacks onto~~  
160 ~~the climate. Additionally, feedbacks on the climate from the ice sheets themselves are very important in regulating ice sheet~~  
161 ~~surface mass balance (SMB), for example through the influence of the ice albedo and temperature elevation feedbacks on~~  
162 ~~surface temperature and energy balance (Abe-Ouchi et al., 2007; Patterson et al., 2024), and interactions between atmospheric~~  
163 ~~and oceanic circulation, surface temperature and precipitation patterns (Beghin et al., 2014, 2015; Liakka et al., 2012). Some~~  
164 ~~studies have also concluded that the topography of the NAIS had a large influence in the size and configuration of the EIS~~  
165 ~~through its effect on the jet stream and stationary waves (Beghin et al., 2015; Liakka et al., 2016).~~

166 Direct observations of processes occurring during glacial cycles are not available and while proxy evidence can provide  
167 important constraints on how the ice sheets changed, it cannot reveal the mechanisms behind these changes. Numerical  
168 modelling is therefore required to understand the response of the NH ice sheets to external and internal forcings and unpack  
169 why they differed between glacial periods. This is an important source of information in the context of understanding how ice  
170 sheets may respond to future climate change (Gregory et al., 2012). Currently there are large uncertainties in projections of  
171 future sea level rise (Edwards et al., 2021; Intergovernmental Panel On Climate Change, 2021) mainly as a result of limited  
172 knowledge of several important ice sheet processes, such as non-linear behaviours of the ice sheet system, and climate and ice  
173 sheet interactions (Golledge et al., 2019; Gregoire et al., 2012; Kopp et al., 2017). Simulations of past periods can help improve  
174 our understanding of these processes as well as help evaluate and refine the numerical models used for these projections  
175 (Braconnot et al., 2012; Gandy et al., 2018; Harrison et al., 2016; Masson-Delmotte et al., 2013; Schmidt et al., 2014). The  
176 LGM has been extensively used for this purpose because the climate and ice sheet states are relatively well constrained by  
177 empirical evidence and thus allow evaluation of model performance, helping constrain climate and ice sheet models and future  
178 sea level projections (Gandy et al., 2023; Ziemen et al., 2014). Furthermore, the EIS has large marine-based sectors in the  
179 Barents Kara and North Sea regions and thus it is often considered an analogue of the current West Antarctic Ice Sheet.  
180 Modelling and identifying the mechanisms responsible for the different EIS evolutions might help with understanding the  
181 processes in effect in West Antarctica and its vulnerabilities to climate change (van Aalderen et al., 2023; Gandy et al., 2018).  
182 Many previous studies simulating the NH LGM and PGM climate and ice sheets have treated the components independently.  
183 Either prescribing the ice sheets as a boundary condition in a climate model, which neglects any affects the climate has on the  
184 ice sheets (Beghin et al., 2015; Colleoni et al., 2016; Hofer et al., 2012; Merz et al., 2015; Ullman et al., 2014), or forcing ice  
185 sheet models with climate output from GCMs, which introduces large uncertainties depending on the model used and can  
186 produce unrealistic ice sheets (Abe-Ouchi et al., 2013; Alder and Hostetler, 2019; Charbit et al., 2007; Gregoire et al., 2016;  
187 Niu et al., 2019; Scherrenberg et al., 2023b; Wekerle et al., 2016; Zweck and Huybrechts, 2005). Thus, the use of directly  
188 coupled climate-ice sheet models to perform these simulations will explicitly resolve some of these important feedbacks and  
189 interactions between the climate and the ice sheets, reducing some of the uncertainties and inconsistencies caused by  
190 prescribing one of the components, and provide a better understanding of these processes (Abe-Ouchi et al., 2013; Niu et al.,  
191 2019; Quiquet et al., 2021; Ziemen et al., 2014).

192 Recent developments have allowed the two-way coupling between GCMs and ice sheet models, but previous studies using  
193 this method have focused on just one time period and/or one ice sheet and there have so far been no coupled GCM-ISM  
194 simulations of the NH ice sheets at the PGM (Gandy et al., 2023; Gregory et al., 2012; Patterson et al., 2024; Quiquet et al.,  
195 2021; Sherriff-Tadano et al., 2024; Ziemen et al., 2014). Additionally, it has been shown that uncertainties in certain model  
196 parameters can have a large influence on the resulting ice volumes simulated by the coupled model through altering the strength  
197 of important climate-ice sheet feedbacks (Gandy et al., 2023; Patterson et al., 2024; Sherriff-Tadano et al., 2024). Patterson et  
198 al., (2024) evaluated a range of model parameter values based on whether they produced plausible NAIS configurations for  
199 both the LGM and PGM. However, the different processes operating on the Eurasian ice sheet (see Sect. 2.1), the interactions

200 that may occur between both ice sheets and the use of a different ice sheet model with more advanced physics and an updated  
201 experimental design, require additional uncertainty quantification to be carried out through a large ensemble analysis, to re-  
202 evaluate the collection of parameter combinations that yield model output consistent with observation data (up to the assessed  
203 uncertainties), referred to as the ‘Not Ruled Out Yet’ (NROY) parameter space (Williamson et al., 2013).

204 The aim of this work is therefore to perform and compare ensemble simulations of the NH ice sheets at the LGM and PGM  
205 using a coupled climate-ice sheet model (FAMOUS-BISICLES). After performing some sensitivity tests to optimise the model  
206 for ice streaming in the NH ice sheets, we assess the ability of the model to produce reasonable simulations of both the NAIS  
207 and EIS for both periods. We evaluate the impact of uncertainty in model parameters on the resulting ice sheets and whether  
208 both ice sheets show similar sensitivities to the parameters. The model is evaluated against an implausibility metric based on  
209 ice sheet volume and extent data, and the representation of ice streams is assessed.

## 210 and the Last and Penultimate Glacial Maximum. **2 Methods**

### 211 **2.1 Models**

212 The climate model used in this study, FAMOUS, is sufficiently efficient that it is suitable for running long (multi-millennial)  
213 ~~palaeo simulations (e.g. Gregory et al., 2012; Gregoire et al., 2012; Roberts et al., 2014; Dentith et al., 2020) and large~~  
214 ~~ensembles for uncertainty quantification (Gandy et al., 2023; Gregoire et al., 2011; Sherriff-Tadano et al., 2024), whilst still~~  
215 ~~resolving the same complex processes as represented in an Atmosphere-Ocean General Circulation Model (AOGCM). It is~~  
216 ~~based on HadCM3 AOGCM (Gordon et al., 2000; Pope et al., 2000) but has half the spatial resolution and a longer time-step,~~  
217 ~~thus requiring only 10 % of the computational costs of the parent GCM.~~

218 ~~We use the atmospheric component of FAMOUS, which is a hydrostatic, primitive equation grid point model with a horizontal~~  
219 ~~resolution of 7.5° longitude by 5° latitude with 11 vertical levels and a 1-hour time step (Williams et al., 2013). FAMOUS can~~  
220 ~~also be run coupled with a dynamical ocean (e.g. Dentith et al., 2020), however, in this study, we prescribe sea surface~~  
221 ~~temperatures and sea ice (see Sect. 2.3.1). The land surface scheme MOSES2.2 (Essery et al., 2003) is used to represent land~~  
222 ~~processes on a set of sub-grid scale tiles in each grid-box representing fractions of nine different surface types, including land~~  
223 ~~ice (Smith et al., 2021).~~

224 This study uses a version of FAMOUS developed to have bi-directional coupling to an ice sheet model (FAMOUS-ice; Smith  
225 et al., 2021) accounting for the mismatch between the atmosphere and ice sheet grid sizes by using sub-grid scale elevation  
226 tiles. The atmospheric surface air temperature and long-wave radiation is calculated in FAMOUS at the mean elevation within  
227 each grid-cell and for ice sheet grid-cells, these quantities are downscaled onto 10 vertical “ice tiles” with different elevations;  
228 100 m, 300 m, 550 m, 850 m, 1150 m, 1450 m, 1800 m, 2250 m, 2750 m, 3600 m. The air temperature downscaling is done  
229 by using a constant lapse rate (*tgrad*) to adjust for the differences in the elevation between each tile and the mean elevation,  
230 and humidity and downwelling longwave are adjusted to be consistent with the temperature adjustment. No downscaling is  
231 applied to precipitation and shortwave radiation in this version of the model. The surface energy fluxes and SMB are calculated

232 on the 10 ice tiles based on the energy budget equation and a multi-layer deep snowpack model. Then the SMB is passed onto  
233 the ice sheet model, which projects and linearly interpolates this coarse 3D lat lon SMB field onto the higher resolution ice  
234 sheet surface. The resulting changes in ice extent and surface elevation simulated by the ice sheet model are passed back to  
235 FAMOUS to update the fraction of ice present within each ice tile and the orography fields. Within FAMOUS, the mean of  
236 the surface fluxes weighted by ice fraction within the ice tiles sets the land atmosphere exchanges within FAMOUS. In this  
237 study, this process is run at 10 times ice sheet model acceleration meaning one year of climate integrated in FAMOUS is used  
238 to force 10 years of ice sheet integration in the dynamical ice sheet model before the ice cover and orography fields are passed  
239 back (Gregory et al., 2020).

240 ~~In a previous study, Patterson et al., (2024) used FAMOUS coupled to the Glimmer ice sheet model to simulate the North~~  
241 ~~American ice sheet.~~ However, the coarse resolution and the use of Shallow Ice Approximation (SIA) in the Glimmer ice sheet  
242 model used in that study does not resolve the small-scale processes or longitudinal stresses required to accurately simulate ice  
243 stream evolution or grounding line migration. Whilst these processes are not as important to capture in an equilibrium spin up  
244 of a continental size terrestrial ice sheet, such as NAIS, they have a large influence on the behaviour, configuration and stability  
245 of a marine ice sheet (Hubbard et al., 2009; Pattyn et al., 2012; Stokes and Clark, 2001). In particular, the Eurasian ice sheet  
246 has many ice streams within marine sectors (e.g. North Sea and Barents Sea) that are vulnerable to processes that may cause  
247 instabilities of retreat, for example ~~Marine Ice Sheet Instability (MISI)~~, and are likely to have been important in its evolution  
248 and deglaciation (Kopp et al., 2017). These processes are similar to those in operation today in West Antarctica, currently  
249 forming a large source of uncertainty in future sea level projections (~~van Aalderen et al., 2023; Alvarez-Solas et al., 2019;~~  
250 ~~Edwards et al., 2019; Gandy et al., 2019, 2021; Petrini et al., 2020)~~([van Aalderen et al., 2023](#); [Alvarez-Solas et al., 2019](#);  
251 [Edwards et al., 2019](#); [Gandy et al., 2019, 2021](#); [Petrini et al., 2020](#)).

252 [FAMOUS-ice has also been used to simulate the LGM North American and Greenland ice sheet with a more complex ice](#)  
253 [sheet model, BISICLES \(Sherriff-Tadano et al., 2024\). BISICLES is a model well suited to simulate the past evolution of](#)  
254 [marine ice sheets, such as the Eurasian ice sheet, due to its use of L1L2 physics which includes longitudinal stresses that enable](#)  
255 [the representation of ice-shelves and fast-flowing ice streams \(Cornford et al., 2013; Hindmarsh, 2009\). It also uses Adaptive](#)  
256 [Mesh Refinement \(AMR\) which allows smaller scale processes, such as grounding line migration, to be simulated at higher](#)  
257 [resolutions whilst the rest of the domain \(i.e. the slower moving interior of the ice sheet\) remains at a lower resolution for](#)  
258 [efficiency \(Cornford et al., 2013\). This also allows for better physical accuracy in representing ice streams within the North](#)  
259 [American ice sheet compared to SIA models. BISICLES has previously been used to simulate the ice streams and retreat of](#)  
260 [the marine-based British-Irish Ice Sheet at the Last Deglaciation \(Gandy et al., 2018, 2019, 2021\), the final retreat of the NAIS](#)  
261 [during the early Holocene \(Matero et al., 2020\), present-day Greenland \(Lee et al., 2015\) and the future evolution of the](#)  
262 [Antarctic Ice Sheet \(Cornford et al., 2015; Siahaan et al., 2022\).](#)

263  
264 [Here, we use the FAMOUS-ice coupled climate ice sheet model with the complex BISICLES ice sheet model to simulate the](#)

265 [North American, Eurasian and Grenland ice sheets at the Last and Penultimate Glacial Maxima. We build on the work of](#)  
266 [Sherriff-Tadano et al. \(2024\) and Patterson et al., \(2024\) by including the first interactive simulation of the Eurasian ice sheet](#)  
267 [with FAMOUS and BISICLES and by improving the spin-up procedure and downscaling parameterisation. Furthermore, we](#)  
268 [deploy sophisticated statistical tools to assess the sensitivity of the ice sheets to uncertain model inputs, evaluate the](#)  
269 [performance of the model and produce realistic ice sheet simulations for use as initial conditions for subsequent work on](#)  
270 [deglaciations or inputs to climate and sea level models.](#)

## 271 2 Methods

### 272 2.1 Climate model and coupling

273 [We use a coupled atmosphere-ice sheet model called FAMOUS-ice. FAMOUS is an Atmosphere-Ocean General Circulation](#)  
274 [Model \(AOGCM\) sufficiently efficient for running multi-millennial palaeo simulations \(e.g. Gregory et al., 2012; Gregoire et](#)  
275 [al., 2012; Roberts et al., 2014; Dentith et al., 2020\) and large ensembles for uncertainty quantification \(Gandy et al., 2023;](#)  
276 [Gregoire et al., 2011; Sherriff-Tadano et al., 2024\).](#)

277 [We use the atmospheric component of FAMOUS, a hydrostatic, primitive equation grid point model with a horizontal](#)  
278 [resolution of 7.5° longitude by 5° latitude with 11 vertical levels and a 1-hour time step \(Williams et al., 2013\). The land](#)  
279 [processes are simulated using the MOSES2.2 scheme \(Essery et al., 2003\) with vegetation prescribed to present-day](#)  
280 [distributions as in Patterson et al. \(2024\). A high-latitude cold bias in FAMOUS, also seen in other GCMs, can produce overly](#)  
281 [large ice sheets \(Gregoire et al., 2016\). Thus, we chose to prescribe sea surface temperatures and sea ice \(see Sect. 2.3.1\),](#)  
282 [rather than using FAMOUS' dynamical ocean component \(e.g. Dentith et al., 2020\), to correct for model biases.](#)

283 [FAMOUS-ice has bi-directional coupling between the atmosphere and the Glimmer or BISICLES ice sheet model \(FAMOUS-](#)  
284 [ice; Smith et al., 2021\), accounting for the mismatch between the atmosphere and ice sheet grid sizes using sub-grid scale](#)  
285 [downscaling. The atmospheric surface air temperature and longwave radiation is calculated in FAMOUS at the mean](#)  
286 [orography and downscaled onto 10 vertical "ice tiles" distributed vertically \(at 100, 300, 550, 850, 1150, 1450, 1800, 2250,](#)  
287 [2750, 3600 m elevation\) using a constant lapse rate, \*tgrad\*. No downscaling is applied to precipitation and downwelling](#)  
288 [shortwave radiation. SMB is calculated on the 10 ice tiles based on the energy budget equation and a multi-layer deep snowpack](#)  
289 [model. Then the SMB is passed onto the ice sheet model, which projects and linearly interpolates the coarse 3D lat-long-](#)  
290 [elevation SMB field onto the higher resolution ice sheet surface on its Cartesian grid. The resulting changes in ice extent and](#)  
291 [surface elevation simulated by the ice sheet model are passed back to FAMOUS to update the fraction of ice present within](#)  
292 [each ice tile and the orography fields. ~~BISICLES is well suited to simulating marine ice sheet dynamics due to its use of the~~](#)  
293 [~~L1L2 physics for approximating the sliding and flow of the ice sheet, instead of SIA \(Cornford et al., 2013\). The L1L2~~](#)  
294 [~~approximation is a variant of Glen's flow law that includes longitudinal and lateral stresses and approximates vertical shear~~](#)  
295 [~~strains in vertically integrated models \(Schoof and Hindmarsh, 2010\). This makes it able to represent ice shelves and fast-~~](#)  
296 [~~flowing ice streams \(Hindmarsh, 2009\). Additionally, some ice sheet processes, such as ice streaming and grounding line~~](#)

297 migration, require high resolution to simulate accurately. BISICLES enables this to be feasible in millennial scale and large  
298 ensemble simulations through its adaptive mesh refinement (AMR). Where required, the model can simulate at high resolution,  
299 whilst the rest of the domain (i.e. the slower moving interior of ice sheets) remains at a lower resolution, thus increasing the  
300 efficiency of the model (Cornford et al., 2013). With these features, BISICLES is a model well suited to simulate the past  
301 evolution of marine ice sheets such as the Eurasian ice sheet. It also allows for better physical accuracy in the representation  
302 of ice streams within the North American ice sheet. BISICLES has previously been used to successfully simulate the ice  
303 streams and retreat of the marine based British Irish Ice Sheet at the Last Deglaciation (Gandy et al., 2018, 2019, 2021), the  
304 final retreat of the NAIS during the early Holocene (Matero et al., 2020), produce an initial condition of the present day  
305 Greenland Ice Sheet (Lee et al., 2015) and model the future evolution of the Antarctic Ice Sheet (Cornford et al., 2015; Siahaan  
306 et al., 2022). Additionally, FAMOUS-BISICLES has been used to explore the sensitivity of the NAIS and Greenland Ice Sheet  
307 at the LGM to model parameter values through large ensemble analysis (Sherriff-Tadano et al., 2024).

308 We use the updated version of BISICLES developed by Gandy et al., (2019), which implements a pressure limited basal sliding  
309 law that is sensitive to the presence of till water. This is mostly found to be applicable near the grounding line and the inclusion  
310 of the Coulomb sliding law has been shown to have an effect on ice sheet stability in models, with greater grounding line  
311 retreat occurring in simulations that include this law than those without (Nias et al., 2018; Schoof, 2006; Tsai et al., 2015).  
312 [The mean of the surface fluxes weighted by ice fraction within the ice tiles sets the land-atmosphere exchanges within FAMOUS.](#)  
313 [The full details of the climate-ice sheet coupling within FAMOUS-ice are described in Smith et al., \(2021\), including a](#)  
314 [description of how the snowpack model deals with the meltwater percolation and runoff. Since our simulations do not include](#)  
315 [an interactive ocean, there is no need to close the climate system hydrological cycle, and so routing of surface and basal](#)  
316 [meltwater that have the potential to modify ocean circulation are not involved in the coupling. In this study, we use a 10 times](#)  
317 [acceleration meaning one year of climate integrated in FAMOUS is used to force 10 years of ice sheet integration \(Gregory et](#)  
318 [al., 2020\).](#)

319 [Sherriff-Tadano et al. \(2024\) found that some of the FAMOUS-BISICLES simulations of the NAIS at the LGM exhibit a](#)  
320 [strong local melting of the ice sheet from parts of the interior. This phenomenon is caused by warm temperature biases over](#)  
321 [the ice sheet interior in the atmospheric model, which are amplified by the downscaling method and a positive height-mass](#)  
322 [balance feedback. A similar temperature bias was pointed out by Smith et al., \(2021\) using the same model under the modern](#)  
323 [Greenland ice sheet, which produced a higher Equilibrium Line Altitude \(ELA\) \(around 2 km high in places\) compared to a](#)  
324 [high-resolution regional atmospheric model \(at about 1 km high\). The warm temperature bias comes from the low resolution](#)  
325 [of the atmospheric model. In reality, a very cold atmospheric layer often forms at the surface of the ice sheet, especially in the](#)  
326 [interior, which induces a stable boundary layer and isolates the cold surface from the ambient warm air. However, a global](#)  
327 [climate model cannot resolve the effect of the stable boundary layer and overestimates the exchange of heat between the](#)  
328 [surrounding atmosphere and the ice sheet surface. As a result, FAMOUS overestimates the temperature in the ice sheet interior](#)  
329 [and causes a high ELA bias, which results in surface melt.](#)

330 Here, we take a practical approach to mitigate the effect of the warm temperature bias in FAMOUS. This is done by modifying  
331 the height adjustment of atmospheric surface temperature to the ice tiles through the introduction of a new parameter in the  
332 model, *elevcon*, which is intended to make the parts of the ice sheet surface well inside the margins colder. Appendix A  
333 includes a description of how the *elevcon* parameter is implemented and works to affect the surface temperature and SMB  
334 during height correction, and of sensitivity experiments performed to validate the effect of different values of *elevcon* on the  
335 modern and LGM ice sheets and climates. Since the optimal value of this adjustment is uncertain, we include *elevcon* in the  
336 ensemble as a varied parameter value, between the range of 1 and 1.5 (0-50 %). These values were chosen based on testing  
337 that showed that a value of 1.5 produced an equilibrium line altitude height that represents an upper limit determined by  
338 empirical data (Fig. A1).

## 339 **2.2 Ice sheet model**

340 The BISICLES marine ice sheet model uses the L1L2 approximation which is a variant of Glen’s flow law that includes  
341 longitudinal and lateral stresses and approximates vertical shear strains in vertically integrated models (Schoof and Hindmarsh,  
342 2010). In this set-up, we also use a pressure-limited Coulomb basal sliding law that is sensitive to the presence of till water  
343 (Gandy et al., 2019; Tsai et al., 2015). This is mostly found to be applicable near the grounding line and the inclusion of the  
344 Coulomb sliding law has been shown to have an effect on ice sheet stability in models, with greater grounding line retreat  
345 occurring in simulations that include this law than those without (Nias et al., 2018; Schoof, 2006; Tsai et al., 2015). The upper  
346 surface temperature boundary condition in the ice sheet model (surface heat flux) is determined by the climate model and the  
347 basal boundary condition (basal heat flux) is set as a constant flux ( $3 \times 10^6 \text{ J a}^{-1} \text{ m}^{-2}$ ). The effective pressure, and therefore the  
348 basal sliding, depends on the basal water pressure and thus the depth of the till water layer. Once the englacial drainage water  
349 fraction ( $w$ ) grows beyond a certain value (0.01) it is drained to a till layer at a rate proportional to the water fraction, up until  
350 a maximum water fraction (0.05). The till water is then transported elsewhere by the basal hydrology model (Van Pelt and  
351 Oerlemans, 2012). It is lost vertically at a rate proportional to the till water depth which is determined by the specified till  
352 water drain factor ( $drain$ ). A maximum till water thickness of 2 m is set following previous studies (Bueler and van Pelt, 2015;  
353 Gandy et al., 2019; Moreno-Parada et al., 2023). A recent comparison study by Drew and Tarasov (2023) shows that this  
354 simplified ‘leaky bucket’ hydrology scheme produces similar results to more complete models over centennial or longer  
355 timescales and continental scale ice sheets. Additionally, the implementation of this basal sliding scheme coupled with this  
356 hydrology parameterisation allows the simulation of spontaneous ice stream generation and evolution (Gandy et al., 2019,  
357 2021).

358 The upper surface thickness flux (i.e. accumulation/melt) is calculated by the climate model and the lower surface (basal)  
359 thickness flux (i.e. oceanic melt) is set to zero for grounded ice and is proportional to the SSTs for floating ice, according to  
360 the linear relationship;

$$361 \textit{Subshelf melt rate} (\text{myr}^{-1}) = c(T_{ocn} - T_f) \quad (1)$$

362 Where  $c$  is a constant,  $T_{ocn}$  is the prescribed sea surface temperature and  $T_f$  is the freezing point of seawater, assumed to be -  
363 1.8 °C at the surface (Alvarez-Solas et al., 2019; Beckmann and Goosse, 2003; Gandy et al., 2018; Martin et al., 2011; Rignot  
364 and Jacobs, 2002). Since the freezing point of sea water varies with depth of the ice shelf base and with salinity, and the surface  
365 temperatures are used rather than subsurface, this is a highly idealised parameterisation. In addition, many studies have found  
366 a quadratic relationship to be a better fit to present-day observations (e.g. DeConto and Pollard, 2016; Favier et al., 2019;  
367 Holland et al., 2008). However, the lack of constraints on ice shelves, ocean temperatures, and sub-shelf melt rates for the  
368 periods covered in this study makes this a large source of uncertainty in our modelling. In this context, it is preferable to choose  
369 a simple linear representation of sub-shelf melt over a more complex quadratic relationship. We account for this uncertainty  
370 in the wide range of sub-shelf melt constant ( $c$ ) values used (1 – 50 m yr<sup>-1</sup> °C<sup>-1</sup>). This relationship produces an average sub-  
371 shelf melt rate across the ice shelves of between around 1.6 – 28 m yr<sup>-1</sup>, which are not unrealistic when compared to the  
372 estimates from present-day Antarctica of 0 – 43 m yr<sup>-1</sup> (Depoorter et al., 2013; Jourdain et al., 2022; Rignot et al., 2013).  
373 However, some regions in some simulations display very large rates of 100s of metres per year.

374 Glacial isostatic adjustment (GIA) of bedrock topography due to changes in the ice sheet load is included through coupling  
375 BISICLES to a simple Elastic Lithosphere Relaxing Asthenosphere (ELRA) model, which approximates this response by  
376 assuming a fully elastic lithosphere above a uniformly viscous asthenosphere (Kachuck et al., 2020). A relaxation time of 3000  
377 years is applied in this model based on previous studies (Pollard and DeConto, 2012). This method does not account for  
378 changes in the gravitational pull that ice sheets exert on sea level or adjustments in Eustatic sea level caused by changing  
379 global ice sheet volume (e.g. Gomez et al., 2010).

380 ~~IceSherriff-Tadano et al. (2024) found that some of the FAMOUS-BISICLES simulations of the NAIS at the LGM exhibit a~~  
381 ~~strong local melting of the ice sheet from parts of the interior. This phenomenon is caused by warm temperature biases over~~  
382 ~~the ice sheet interior in the atmospheric model, which are amplified by the downscaling method and a positive height-mass~~  
383 ~~balance feedback. A similar temperature bias was pointed out by Smith et al., (2021) using the same model under the modern~~  
384 ~~Greenland ice sheet, which produced a higher Equilibrium Line Altitude (ELA) (around 2 km high in places) compared to a~~  
385 ~~high-resolution regional atmospheric model (at about 1 km high). The warm temperature bias comes from the low-resolution~~  
386 ~~of the atmospheric model. In reality, a very cold atmospheric layer often forms at the surface of the ice sheet, especially in the~~  
387 ~~interior, which induces a stable boundary layer and isolates the cold surface from the ambient warm air. However, a global~~  
388 ~~climate model cannot resolve the effect of the stable boundary layer and overestimates the exchange of heat between the~~  
389 ~~surrounding atmosphere and the ice sheet surface. As a result, FAMOUS overestimates the temperature in the ice sheet interior~~  
390 ~~and causes a high ELA bias, which results in surface melt.~~

391 ~~Here, we take a practical approach to mitigate the effect of the warm temperature bias in FAMOUS. This is done by modifying~~  
392 ~~the height adjustment of atmospheric surface temperature to the ice tiles through the introduction of a new parameter in the~~  
393 ~~model, *elcreon*, which is intended to make the parts of the ice sheet surface well inside the margins colder. Appendix A~~  
394 ~~includes a description of how the *elcreon* parameter is implemented and works to affect the surface temperature and SMB~~  
395 ~~during height correction, and of sensitivity experiments performed to validate the effect of different values of *elcreon* on the~~

396 ~~modern and LGM ice sheets and climates. Since the optimal value of this adjustment is uncertain, we include *cleveon* in the~~  
397 ~~ensemble as a varied parameter value, between the range of 1 and 1.5 (0-50 %). These values were chosen based on testing~~  
398 ~~that showed that a value of 1.5 produced an equilibrium line altitude height that represents an upper limit determined by~~  
399 ~~empirical data (Fig. A1).~~

## 400 **2.2 Ice dynamics in BISICLES**

401 ~~It has been established that ice~~ streams exert an important control on the behaviour and geometry of an ice sheet and therefore  
402 it is crucial that in our study, the simulated location and dynamics of at least the major ice stream features, are consistent with  
403 reconstructions. Gandy et al. (2019) highlighted that the most important model ingredient necessary to successfully model ice  
404 streams is the representation of idealised subglacial hydrology. The till water layer coupled with the Coulomb sliding law  
405 described ~~in Sect. 2.1~~ [above](#) is crucial for the spontaneous generation of ice streams. However, this scheme is highly sensitive  
406 to the drainage and temperature structure of the ice sheets. Inadequate consideration of these factors can lead to a poor  
407 representation of ice streams (e.g. Sherriff-Tadano et al., 2024). Therefore, we perform a spin up of BISICLES that results in  
408 the internal temperatures of the ice sheet being more conducive for ice stream generation over shorter integration times. We  
409 also perform sensitivity tests varying the level of refinement of the ice streams and the rate of till water drainage to find an  
410 optimum set-up that balances computational cost with the representation of ice dynamics. These methods are described in ~~the~~  
411 ~~following sections~~ [appendices B and C](#).

### 412 **2.2.1 Temperature spin-up**

413 ~~The internal temperature of ice sheets is an important factor in controlling the deformation, rheology and velocity of the ice~~  
414 ~~due to the temperature dependence of the sliding law and enthalpy scheme (Blatter et al., 2010). The ice sheets start with a~~  
415 ~~uniform internal temperature of 268 K and it can take tens of thousands of years for the process of cold ice advection from the~~  
416 ~~interior and heat conduction from the bed to occur and reach an equilibrium, which is important for the formation of ice streams~~  
417 ~~(Fyke et al., 2014; Heine and Metigue, 1996). Thus, we perform ice sheet model only spin-ups for the LGM and the PGM to~~  
418 ~~allow the ice sheet internal temperatures to reach close to equilibrium. This temperature profile is then used as the internal ice~~  
419 ~~sheet temperature in the initial condition for the sensitivity tests (Sect. 2.2.2 and 2.2.3) and coupled simulations.~~

420 ~~The spin-ups were run at 32 km resolution for 20,000 years using single surface mass balance and surface temperature fields~~  
421 ~~taken from a FAMOUS BISICLES equilibrium simulation that used climate model parameters identified to be NROY in~~  
422 ~~simulations of the NAIS by Patterson et al., (2024), default ice sheet model parameters and an *cleveon* value of 1.2 (Fig. B1).~~  
423 ~~The initial ice sheet configurations were the same as used in the coupled simulations (described in Sect. 2.3.1; Fig. 1). The~~  
424 ~~sliding law was set to a temperature dependent Weertman sliding without till water dependent Coulomb sliding enabled since~~  
425 ~~the bulk of the temperature field is not affected much by Coulomb sliding near the coast. The resulting temperature profiles~~  
426 ~~are shown in Appendix B (Figs. B2 and B3).~~

### 2.2.2 Drain factor sensitivity tests

In their study, Sherriff-Tadano et al., (2024) used much higher values of *drain* ( $0.2\text{--}0.6\text{ m yr}^{-1}$ ) than has typically been used in previous studies ( $0.001\text{--}0.005\text{ m yr}^{-1}$ ; Gandy et al., 2019; Kazmierczak et al., 2022; Moreno-Parada et al., 2023). This was to prevent large till water depths leading to too large velocities across the entire ice sheet and long simulation times, as high velocities require more iterations and smaller timesteps to solve. This resulted in the till water drainage outpacing the supply and thus very small till water depths, leading to mostly Weertman sliding across the whole ice sheet. Slow till drainage (low values of *drain*) can lead to isolated regions of fast flow,  $> 50\text{ km yr}^{-1}$ , which have a disproportionate effect on simulation time. To prevent this we introduce an artificial drag term rising with the fourth power of ice speed and calibrated to be negligible for ice speeds below  $1\text{ km yr}^{-1}$ . This drag factor is also used in the coupled simulations throughout the rest of this study. We then perform sensitivity tests with different values of *drain* spanning the range  $0.001\text{--}0.06\text{ m yr}^{-1}$  but all other factors kept constant. The results of some of these tests are shown in Fig. C1. Values of *drain* above 0.05 prevent much of the coulomb sliding at the coasts and the representation of some of the major ice streams, particularly the Hudson Strait Ice Stream, is poor. Low values usually used in ice sheet models ( $0.001\text{--}0.005$ ) cause too large velocities and ice streams that remove much of the ice sheet, especially in Eurasia. Therefore, in this study, we implement a range of  $0.01\text{--}0.05$  to cover values just below the default till water supply rate of 0.02, to where no coulomb sliding occurs. For studies that seek to examine ice streaming of the glacial maximum ice sheets, we would recommend performing additional sensitivity tests that vary ice shelf basal melt parameterisation and geothermal heat flux, but this is beyond the scope of the present study.

### 2.2.3 Spatial resolution sensitivity tests

The base resolution of the ice sheet model is 32 km. The AMR allows the areas covered by ice to be refined once to 16 km, which shows some improvement to the simulated ice streams, although the difference is only about  $1.2\text{ m yr}^{-1}$  on average over the whole ice sheet (Figs. C2a and C2b). Additional sensitivity simulations were performed refining only the areas of ice streaming up to 8 km and up to 4 km (Figs. C2c and C2d). These tests showed that after refining the entire ice sheet to 16 km, the difference in average ice velocity for any further refinement of the ice streams converges to zero (Fig. C3) and the pattern of major ice stream features (Fig. C2), the position of the marine margins and the ice volume across the NH ice sheets is not significantly changed, except across the southern area of the Eurasian ice sheet (Fig. C4). However, computational costs are quadrupled with each level of refinement. Thus, we determine one level of refinement (16 km) to be sufficient for this study in which we are focussing more on the large scale geometry of the ice sheet rather than the finer details of the ice streams. This is a similar conclusion to that drawn from the simulations presented by Albrecht et al., (2020) and Gandy et al., (2019), the latter further showing anything finer than 4 km does not improve the match of simulated ice streams to empirical data. There is an increase in the velocity of up to around  $3000\text{ m yr}^{-1}$  at the centre of some of the ice streams at the higher resolutions, which could be important during simulations of the deglaciation (Robel and Tziperman, 2016). We performed an additional simulation refining the ice streams across the marine section of the Eurasian ice sheet to 2 km to see if any marine processes

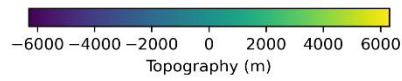
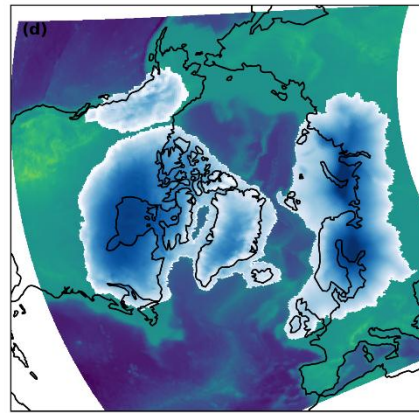
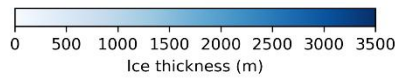
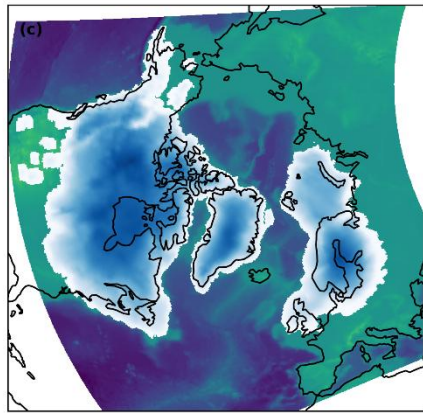
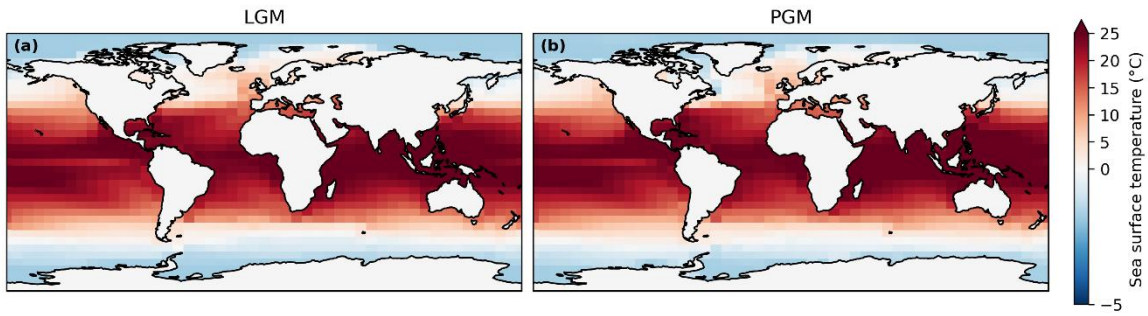
459 ~~would be captured that could not have been resolved at lower resolutions. This did not lead to any significant difference in the~~  
460 ~~ice velocity in this region compared to the 4 km simulation (Fig. C2e), but again could be important in deglaciation simulations~~  
461 ~~when MISI could be triggered (Gandy et al., 2020; Patton et al., 2015; Petriai et al., 2020; van Aalderen et al., 2024).~~

## 462 2.3 Experiment design

### 463 2.3.1 Boundary and initial conditions

464 The coupled simulations broadly follow the PMIP4 protocols for the LGM (Kageyama et al., 2017) and the PGM (Menviel et  
465 al., 2019), which prescribe greenhouse gases, orbital parameters and the Antarctic Ice Sheet configuration. Following the  
466 method of Patterson et al., (2024), we also prescribe SSTs and Sea ice from HadCM3 simulations of 21 ka and 140 ka (Figs.  
467 1a ~~and 1b-c~~). A description of the HadCM3 simulations, the justification for this choice of approach, and a discussion on how  
468 these SSTs may affect the result is also presented by Patterson et al., (2024). Vegetation is kept at pre-industrial distribution,  
469 which could have an effect on the results since studies have shown the importance of the albedo-vegetation feedback during  
470 glacials, particularly for the PGM (~~Colleoni et al., 2009b; Crucifix and Hewitt, 2005; Stone and Lunt, 2013; Willeit et al.,~~  
471 ~~2024~~)([Colleoni et al., 2009](#); [Crucifix and Hewitt, 2005](#); [Stone and Lunt, 2013](#); [Willeit et al., 2024](#)).

472 The interactive ice sheet model domain covers the whole NH, including the North American, Greenland and Eurasian ice  
473 sheets. Patterson et al., (2024) showed that the initial ice sheet model conditions used in the glacial maxima simulations  
474 overwhelmingly determined the configurations of the final ice sheets due to the ice-albedo feedback, and that the climate at  
475 the glacial maxima had an opposite impact on the difference in NAIS ice volume between the LGM and PGM to what was  
476 expected. This suggests that the evolution of the climate and the ice sheets leading up to the glacial maximum are important  
477 in determining the configurations of the ice sheets at the glacial maximum. We, therefore, chose to initialise the LGM and  
478 PGM simulations from the respective ice sheet reconstructions available to ensure realistic ice sheet geometry for each period,  
479 accounting for the evolution of the climate and ice sheets prior to the glacial maxima. With this approach, we can examine  
480 how the differences in ice geometry and background climate between the two time periods affect the sensitivity to the model  
481 parameters that control key earth system feedbacks (e.g. ice-albedo feedback, ice-elevation feedback and climate-ice sheet  
482 interactions). The LGM orography was initiated from the GLAC-1D reconstruction (Briggs et al., 2014; Ivanovic et al., 2016;  
483 Tarasov et al., 2012; Fig. [1e1d](#)) and the PGM was initiated from a combination of a simulated PGM NAIS by Patterson et al.,  
484 (2024) and simulated PGM EIS by Pollard et al., (2023) (Fig. [1e1e](#)) and their corresponding topographies.



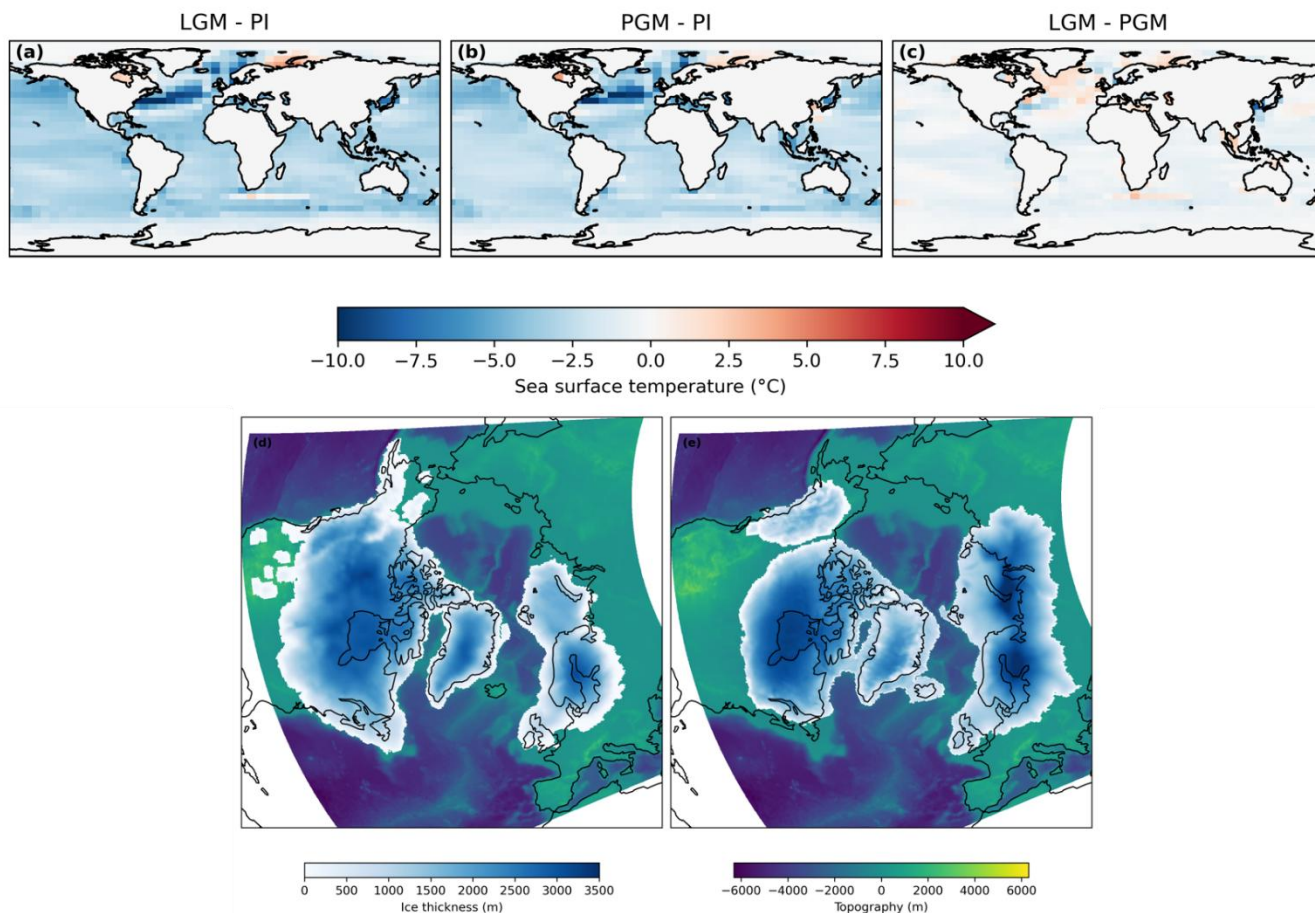


Figure 1: Boundary and initial conditions for the LGM and PGM simulations. Sea surface **temperatures prescribed in the FAMOUS atmosphere model** **temperature anomaly from a HadCM3 pre-industrial control run** for (a) LGM and (b) PGM; (c) **the difference between the prescribed LGM and PGM sea surface temperatures**; and initial topography (meters above sea level) and ice thickness in the BISICLES ice sheet model interactive domain for (c) LGM and (d) PGM.

### 2.3.2 Ensemble design

As well as the initial ice sheet conditions, modelled ice sheet volumes and areas are also sensitive to a number of **parameterisations** **uncertain parameters** related to climate processes, surface mass balance and ice sheet dynamics. To assess this sensitivity, we design an ensemble using maximin Latin Hypercube Sampling (Williamson, 2015; Santner et al., 2003), that consists of 120 combinations of 12 uncertain climate and ice sheet model parameters, varied over a specified range (Table 1). These 120 simulations are each run with the LGM and PGM initial conditions described in Sect. 2.3.1, resulting in 240 total simulations. Each was integrated for 500 climate years (5000 ice sheet years). Since we start from a glacial maximum configuration and spun-up internal temperatures, this is enough time for the ice sheets to (i) reach equilibrium (or close to it), and (ii) give an indication of whether the parameters are producing reasonable ice sheets and form ice streams. Each simulation took around 35 hours **running** on 8 cores to complete (~280 core hours).

502 The choice and range of parameters is adapted from several previous ensemble studies (Gandy et al., 2023; Gregoire et al.,  
503 2011; Patterson et al., 2024; Sherriff-Tadano et al., 2024). We vary three uncertain parameters related to ice sheet dynamics  
504 in BISICLES; the basal friction coefficient in the power law relation (*beta*), the till water drain factor (*drain*), and the sub-  
505 shelf melt constant (*c*). The *elevcon* parameter controls the magnitude of the height adjustment applied and the remaining  
506 parameters control the climatic conditions and ice albedo in the simulations.

507  
508 **Table 1: Parameters varied in the ensemble and the ranges sampled.**

Parameter	Unit	Ensemble range	Notes
<b>Weertman friction coefficient, <i>beta</i></b>	Pa m <sup>-1/3</sup> a <sup>1/3</sup>	20,000 to 60,000	Represents the resistance of ice at the base to motion. The higher the value, the stronger the friction between the ice and the bedrock over which it is flowing.
<b>Till water drain factor, <i>drain</i></b>	yr <sup>-1</sup>	0.01 to 0.05	Controls the rate of vertical till-stored drainage and therefore water pressure in the till layer. The higher the value, the more rapidly till water is removed.
<b>Sub-shelf melt constant, <i>c</i></b>	m yr <sup>-1</sup> °C <sup>-1</sup>	1 to 50	Characterises the relationship between ocean thermal forcing and sub-shelf melt rate.
<b>Lapse rate, <i>tgrad</i></b>	K m <sup>-1</sup>	-0.01 to -0.002	Air temperature lapse rate used <del>during downscaling to the ice sheet</del> calculate surface temperature at each ice elevation tile in FAMOUS. The more negative the number, the stronger the lapse rate effects (Smith et al., 2021).
<b>Sensitivity of bare ice albedo, <i>daice</i></b>	K <sup>-1</sup>	-0.4 to 0	The sensitivity of bare ice albedo to surface air temperatures above the melt threshold (mimics darkening of the surface due to melt ponds forming in summer). The minimum value reduces the bare ice albedo to as low as 0.15 (Smith et al., 2021).
<b>Surface snow density threshold, <i>fsnow</i></b>	kg m <sup>-3</sup>	350 to 800	The density threshold for snow beyond which the surface is regarded as bare ice. The higher the value, the higher the albedo for denser snow, tending to increase ice sheet albedo overall (Smith et al., 2021).
<b>Sensitivity to surface grain size, <i>av_gr</i></b>	µm <sup>-1</sup>	0 to 0.01	The sensitivity of the surface snow albedo to increasing grain size. The higher the value, the more the albedo decreases over time, reducing snow albedo overall (Smith et al., 2021).

<b>Relative humidity threshold, <math>rh_{crit}</math></b>	Pa <sup>-1</sup>	0.6 to 0.9	The threshold of relative humidity above which large-scale clouds form (Smith, 1990).
<b>Precipitating ice fall out speed, <math>v_{fI}</math></b>	m s <sup>-1</sup>	1 to 2	<del>The precipitating ice fall out speed (Heymsfield, 1977)</del> <a href="#">The precipitating ice fall out speed (Heymsfield, 1977)</a> .
<b>Cloud liquid water conversion rate, <math>ct</math></b>	s <sup>-1</sup>	5x10 <sup>-5</sup> to 4x10 <sup>-4</sup>	Rate of conversion of cloud liquid water droplets to precipitation (Smith, 1990).
<b>Cloud liquid water threshold, <math>cw</math></b>	kg m <sup>-3</sup>	1x10 <sup>-4</sup> to 2x10 <sup>-3</sup>	The threshold of cloud liquid water (over land) above which precipitation forms (Smith, 1990).
<b>Height correction, <math>elev_{con}</math></b>		1 to 1.5	Scaling factor for the height of the vertical levels read by the ice sheet model (this study).

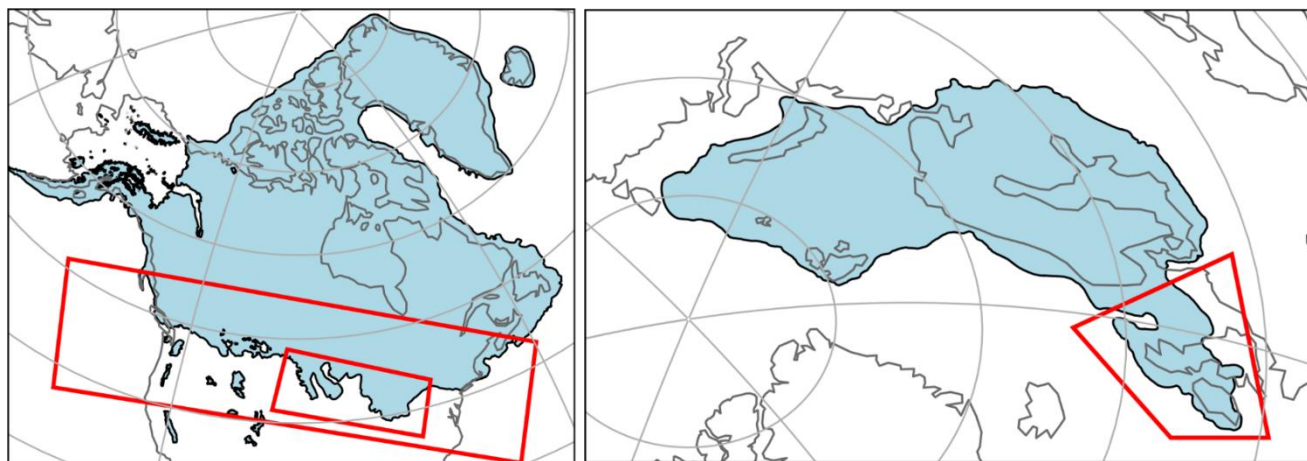
509

## 510 2.4 Evaluating the ensemble

511 To evaluate the performance of the LGM ensemble members and find sets of model parameters that produce [Not Ruled Out](#)  
512 [Yet \(NROY\)](#) ice sheet configurations, we employ an implausibility metric. This allows a robust comparison of model output  
513 to empirical evidence and previous modelling studies, taking into account their uncertainties. The implausibility metric  
514 considers constraints on LGM ice volume, ice extent and Global Mean Air Temperature (GMT) derived from studies using  
515 palaeo-records of past climate and ice sheets and numerical modelling (Table 2). Since the PGM is poorly constrained in these  
516 areas, we are unable to evaluate the performance of the PGM ensemble in the same way. Instead, we opt to select the PGM  
517 ensemble members that correspond to the selected LGM members to enable comparison, see whether the same parameter  
518 values produce plausible PGM ice sheets based on known configuration differences and allow us to learn more about the PGM  
519 without the restriction of uncertain constraints.

520 The NAIS area is evaluated based on the southern extent of the ice sheet reconstructed by Dalton et al., (2020), within  $\pm 3$   
521 times the area of the ice lobes (Fig 2a). We set this envelope of uncertainty (based on ice-lobe area) to account for known  
522 common model biases, such as over-estimated Alaskan ice, and limitations such as the inability to simulate the dynamic ice  
523 lobes (Patterson et al., 2024). Similarly, the plausible range of the EIS is considered to be within  $\pm 3$  times the area of the BIIS  
524 (Fig. 2b) based on the reconstruction from Hughes et al., (2016), since none of our simulations maintain ice over this area (see  
525 Sect. 3.1) and we do not want to compensate for/hide this limitation by over-estimating ice elsewhere. The GMT range is

526 determined from different estimated levels of LGM cooling, and their uncertainties, relative to a pre-industrial GMT of  $13.7 \pm$   
 527  $0.1 \text{ }^\circ\text{C}$  (1880-1900; NOAA National Centers for Environmental Information, 2023; Sherriff-Tadano et al., 2024).



528  
 529 **Figure 2: Reconstructions used in the implausibility metric. (a) North American Ice sheet extent from Dalton et al., (2020); the large**  
 530 **red box delimits the southern extent footprint used in the implausibility metric; the smaller red box indicates the area of the lobes**  
 531 **used to calculate the range of plausible values. (b) Eurasian ice sheet extent from Hughes et al., (2016); the red box indicates the area**  
 532 **of the BIIS used to calculate the range of plausible ice areas.**

533  
 534 **Table 2: The ranges of plausible values for ice sheet volume and extent (expressed in metres global mean sea level equivalent; m sle),**  
 535 **and global mean surface air temperature (GMT; given in  $^\circ\text{C}$ ) used in our implausibility metric, and references to the published**  
 536 **work used to derive these ranges.**

Metric		Plausible range	References
North American Ice Sheet (NAIS)	Volume (m s.l.e.)	68 – 88	Abe-Ouchi et al., 2015; Gregoire et al., 2012; Lambeck et al., 2017; Moreno-Parada et al., 2023; Peltier et al., 2015; Simms et al., 2019; Tarasov et al., 2012
	Area (km <sup>2</sup> )	$2.0 \times 10^6 - 7.16 \times 10^6$	Dalton et al., 2020
Eurasian Ice Sheet (EIS)	Volume (m s.l.e.)	13 – 23.5	Abe-Ouchi et al., 2015; Hughes et al., 2016; Lambeck et al., 2006; Patton et al., 2016; Peltier et al., 2015; Tarasov et al., 2012
	Area (km <sup>2</sup> )	$3.83 \times 10^6 - 8.02 \times 10^6$	Hughes et al., 2016
Global Mean surface air Temperature (GMT; $^\circ\text{C}$ )		5.6 - 12.1	Annan et al., 2022; Annan and Hargreaves, 2013; Holden et al., 2010; Liu et al., 2023; Osman et al., 2021; Schmittner et al., 2011; Schneider von Deimling et al., 2006; Zhu et al., 2022

## 537 2.5 Gaussian process emulation and Sobol sensitivity analysis

538 To determine which of the model parameters had the most influence on the uncertainty in modelled ice sheet configurations,  
539 and whether this differed for each of the NH ice sheets and each glacial maxima, we perform a Sobol Sensitivity Analysis  
540 (Saltelli, 2002; Sobol', 2001) on four diagnostics for each ensemble; NAIS ice volume, NAIS southern area, EIS ice volume  
541 and EIS area. This produces a first order sensitivity index which measures the contribution to the output variance by each  
542 model parameter alone; a second order index which measures the contribution from interactions between two parameters and;  
543 a total order index which is the contribution by a model parameter as a result of its first order sensitivity and all higher order  
544 interactions. An index value of 0.05 is often used as the threshold above which a parameter is considered to have an important  
545 influence on the output variance (Zhang et al., 2015).

546 The Sobol analysis requires a uniform sample of thousands of model inputs, for example, generated following Saltelli's  
547 extension of the Sobol sequence, which are outside of our initial parameter sample. This would therefore require additional  
548 evaluations of the model, which would require significant additional computational resources. To this end, we train  
549 [independent](#) Gaussian Process (GP) emulators (Kennedy and O'Hagan, 2001; Oakley and O'Hagan, 2004) on each of the four  
550 diagnostics from the two 120 member ensembles. These emulators are then employed to evaluate the additional parameter sets  
551 generated by the Sobol sequence. Using this sequence and the emulators, we are able to generate and evaluate more than  
552 200,000 samples in only a few minutes, a number which would have been computationally intractable using FAMOUS-  
553 BISICLES directly. Since we use a complex model with a large number of uncertain parameters, a sample of this size is  
554 necessary in order to increase the reliability of the Sobol analysis.

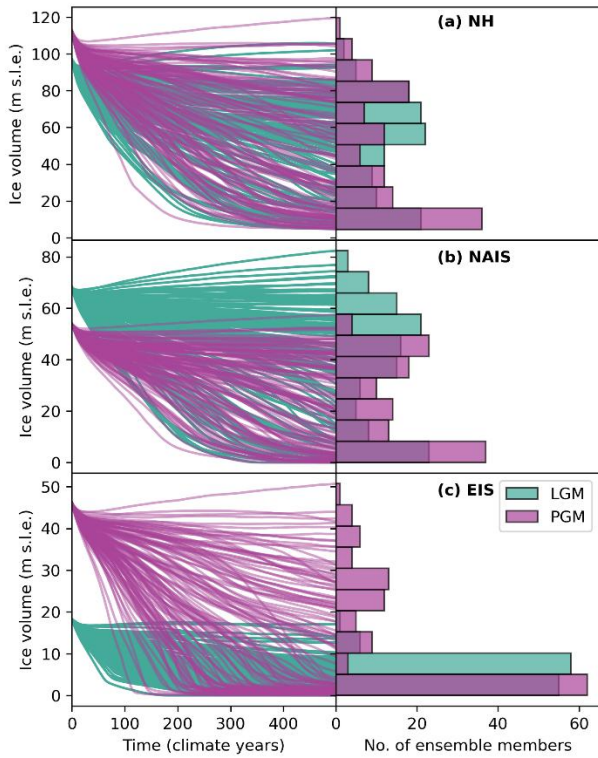
555 To evaluate the performance of our emulators and ensure their predicted output is sensible compared to the modelled output,  
556 we perform a Leave-One-Out Cross-Validation (LOOCV) on each emulator (Bastos and O'Hagan, 2009; Rougier et al., 2009).  
557 In general, leave-k-out cross-validation involves splitting the dataset of input parameters and output diagnostics into separate  
558 training sets and testing sets. ~~The~~ [An](#) emulator is ~~trained using~~ [fitted to](#) the training set and then fed the input parameters ~~off~~ [from](#)  
559 ~~the~~ [testing](#) set to evaluate. ~~The~~ values it then predicts ~~can be~~ [is then](#) compared to the actual modelled values. In the case of  
560 the LOOCV, all but one set of inputs and outputs are used as the training set and the emulator is used to predict the output left  
561 out. This process is then repeated for each of the 120 model outputs. We found that, compared to the modelled outputs, seven  
562 of the ensemble input parameter sets consistently produced poor predictions for four or more of the eight diagnostics.  
563 Therefore, to improve the quality of the emulator fit, we removed these seven inputs, re-trained the emulators, and once again  
564 performed the LOOCV. The predicted values (and their 95% credible intervals) compared to the modelled values for each  
565 emulator are shown in Appendix D (Fig D1). Overall, between 84-93% of the predicted intervals contain the true model output,  
566 which we determine is enough for the purposes of the Sobol analysis.

567 **3 Results and discussion**

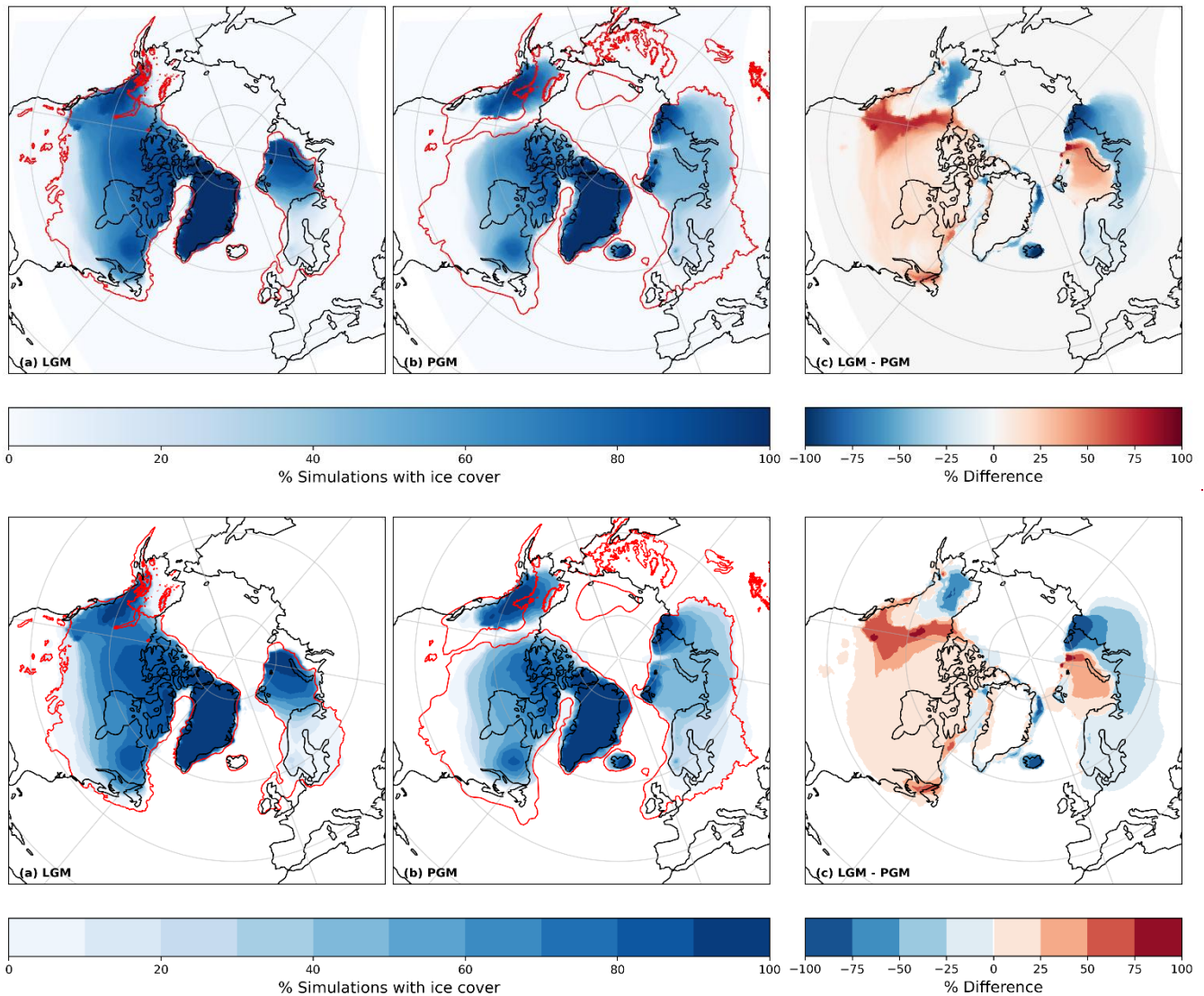
568 **3.1 Initial ensemble**

569 After running the ensembles of simulations for the LGM and PGM, we obtain two sets of 120 simulations with a wide spread  
570 of NH ice sheet configurations (Fig. 3). The ensemble mean volume of the NAIS at the LGM is 37.6 m s.l.e., with a smaller  
571 mean at the PGM of 22.8 m s.l.e.. In contrast, the LGM has a smaller mean EIS volume of 5.39 m s.l.e. compared to 12.6 m  
572 s.l.e. at the PGM. Both ensembles have a similar mean Greenland ice sheet volume of ~ 7 m s.l.e.. ~~The range in ice volume  
573 and extent across the ensembles are shown in Figs. 3 and 4 which reveal a larger spread in NAIS volume at the LGM but a  
574 larger EIS spread at the PGM. Figure 4a shows that the LGM simulations tended to have more extensive ice across the  
575 Laurentide ice sheet and in the area joining the Laurentide to the Cordilleran ice sheet, but that the PGM had more extensive  
576 ice to the south and east of the EIS and over Alaska while maintaining an ice free corridor between the Laurentide and  
577 Cordilleran. Whilst these relative volumes and extents between the LGM and PGM are consistent with knowledge of the  
578 different NH ice sheet configurations at each glacial maxima, the average values are much lower than current estimates suggest.  
579 This is due to a large proportion of the ensemble members deglaciating to very low or zero ice extent (Fig. 3). The differences  
580 in volume and extent between the LGM and PGM are primarily caused by the differences in initial conditions as demonstrated  
581 by Patterson et al., (2024). The evolution and distributions of ice volume across the ensembles shown in Fig. 3 reveals that ice  
582 sheets collapse in a significant proportion of simulations due to an unsuitable combination of parameter values, but that many  
583 simulations sustain the initial ice volume, and a few grow.~~

584 [At the LGM, the North American ice sheet maintains the connection between the Cordilleran and Laurentide ice sheets in a](#)  
 585 [significant proportion \(70-80 %\) of the ensemble \(Fig. 4a\), while the corridor between the two ice sheets remains free in all](#)  
 586 [the PGM simulations consistent with ice sheet reconstructions \(Dalton et al., 2020; Batchelor et al., 2019\).](#)



587 -  
 588 **Figure 3: Time series of ice volume over the 500 climate years (5000 ice sheet years) of simulation for each ensemble member (left**  
 589 **hand panels) and histograms of the distribution of final ice volumes across the ensembles (right hand panels) for the LGM and PGM**  
 590 **(a) Northern Hemisphere; (b) North American ice sheet and (c) Eurasian ice sheet.**



591

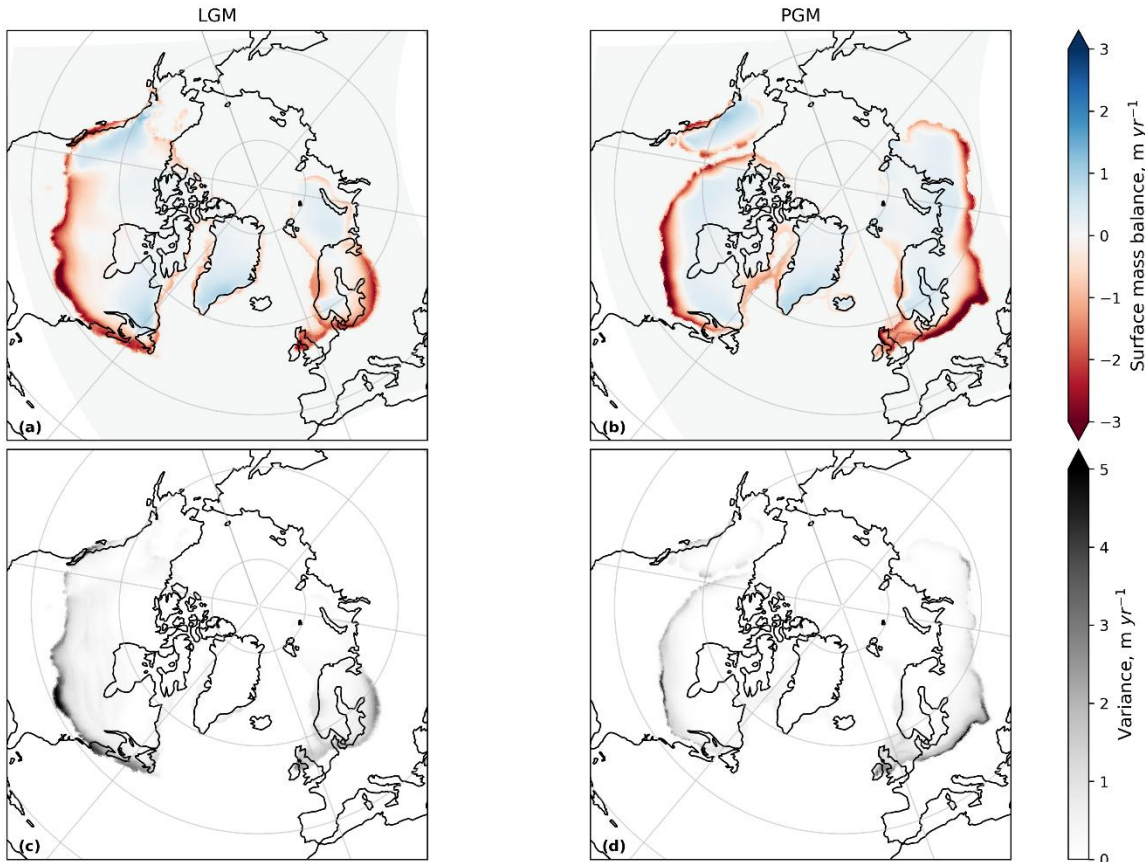
592

593 **Figure 4: Percentage of ensemble members that had ice over areas of the domain for (a) the LGM (with the extents of Dalton et al.,**  
 594 **(2020) and Hughes et al., (2016) in red); (b) the PGM (with Batchelor et al., (2019) extent in red); and (c) the difference between the**  
 595 **LGM and PGM ensembles.**

596

597 Some areas are systematically deglaciated in the ensembles of simulations. In particular, all simulations lack a British-Irish Ice  
 598 Sheet (BIIS), and most display a poor match to reconstructions over Scandinavia and ~~in the southern~~ the South-Eastern  
 599 Laurentide (North American) ice margin ~~and eastern marine extent of North America.~~ This is due to large negative SMB  
 600 values over these regions (Fig. 5) causing rapid deglaciation, with the BIIS disappearing in 600 ice sheet years or less. This is  
 601 a similar result to Bradley et al., (2024) who used ~~a GCM~~ the CESM2.1 model to simulate the SMB across the LGM ice sheets.  
 602 Their simulations showed large ablation areas across the BIIS, the southern margin of Scandinavia and the southern, Pacific

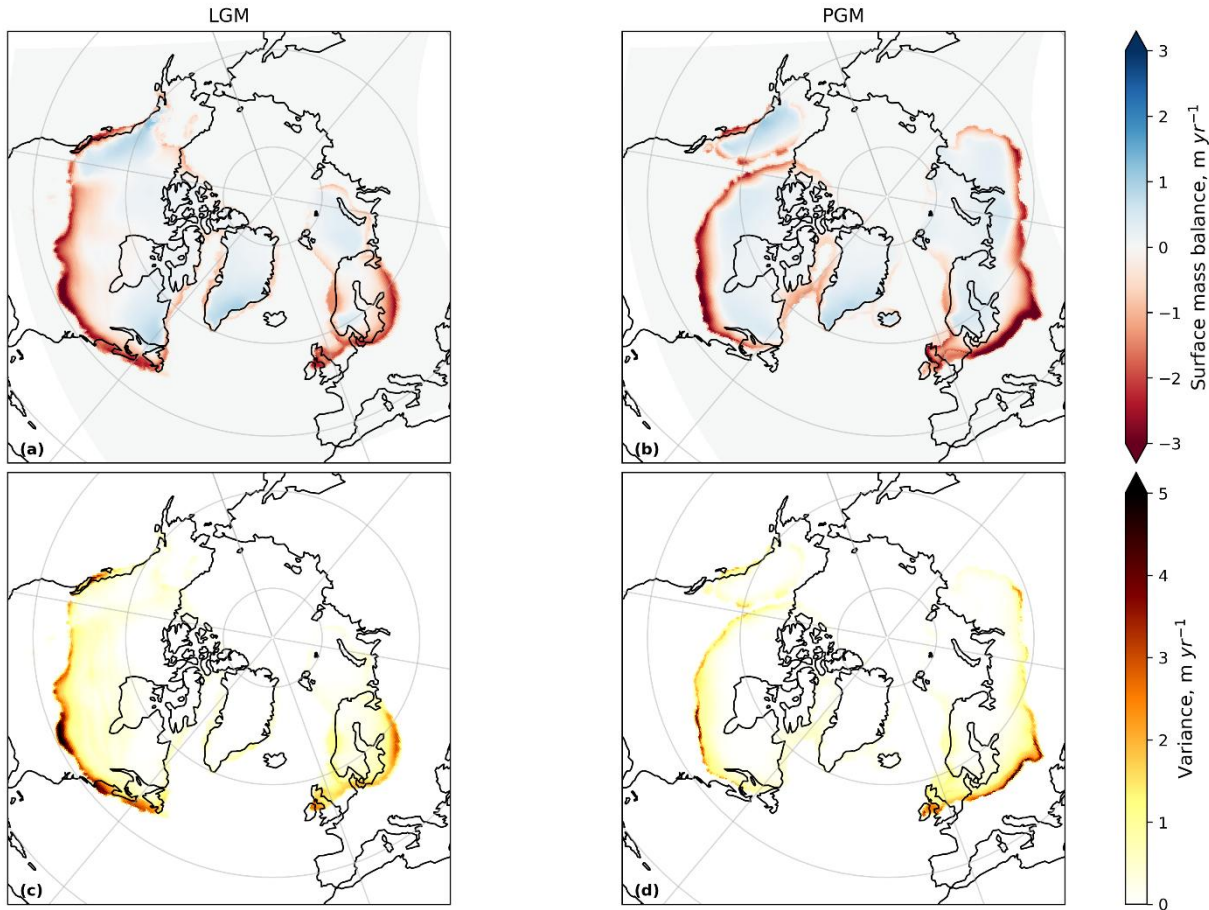
603 and Atlantic margins of the NAIS, but low melt rates across the Barents-Kara Ice Sheet and Greenland. Whilst they did not  
604 use a dynamical ice sheet model, they concluded that if this SMB pattern was applied to one, it would very likely drive rapid  
605 retreat of the southern margins of both ice sheets. [By testing 120 combinations of parameter values, our study is able to find](#)  
606 [model configurations with weaker ablation across some of these regions, reducing some of the SMB biases of Bradley et al.](#)  
607 [\(2024\).](#)



608 **Figure 5: Ensemble mean surface mass balance and variance at ice sheet year 200 for (a) and (c) the LGM and (b) and (d) the PGM.**  
609 ~~This result~~ [The underestimation of ice extent in particular regions, compared to reconstructions,](#) could reflect the asynchronous  
610 timing of the local maxima of the NH ice sheets since, for example, there is evidence that much of the NAIS reached its  
611 maximum extent at  $\sim 25$  ka (Dalton et al., 2022, 2023) and the BIIS reached its maximum at  $\sim 25$ -23 ka before starting its retreat  
612 at  $\sim 22$  ka due to a warming trend caused by a change in orbital parameters between 26–21 ka (Clark et al., 2022; Hughes et  
613 al., 2016). However, these reconstructions of the NAIS and BIIS still suggest there was extensive ice over these regions at 21  
614 ka even if not at their maxima. In addition, Bradley et al., (2024) also performed a simulation using boundary conditions for  
615 26 ka and obtained a similar result to 21 ka. They therefore concluded that the too negative SMBs are likely a result of biases  
616 in the simulated climate or ice sheet reconstruction, a highly non-equilibrated climate and ice sheet at the LGM, and/or the  
617

618 need to retune the model for LGM climate conditions (as also shown to be necessary by Gandy et al., 2023). Indeed, many  
619 other numerical modelling studies have also found it difficult to maintain extensive ice in these regions using a range of  
620 different models, boundary conditions and model parameters (van Aalderen et al., 2023; Quiquet et al., 2021; Scherrenberg et  
621 al., 2023b; Sherriff-Tadano et al., 2024; Ziemen et al., 2014; Zweck and Huybrechts, 2005)(van Aalderen et al., 2023; Quiquet  
622 et al., 2021; Scherrenberg et al., 2023b; Sherriff-Tadano et al., 2024; Ziemen et al., 2014; Zweck and Huybrechts, 2005).

623



624

625 **Figure 5: Ensemble mean surface mass balance and variance at ice sheet year 200 for (a) and (c) the LGM and (b) and (d) the PGM.**

626 In this present study, the compromise with using a coarse resolution [atmospheric](#) model is that it is not able to accurately  
627 capture some of the smaller scale atmospheric circulation effects that influence precipitation and temperature patterns. This  
628 leads to biases in the modelled climate that result in some areas of the ice sheets not matching reconstructions. For example,  
629 simulations of the NAIS have grown too much ice over Alaska and the southern extents are not extensive enough (Patterson  
630 et al., 2024; Sherriff-Tadano et al., 2024; Ziemen et al., 2014). This is likely a result of an underestimation of the stationary  
631 wave effect on temperature patterns; a common feature when using low resolution atmospheric models (Abe-Ouchi et al.,

2007; Ganopolski et al., 2010; Liakka et al., 2012; Roe and Lindzen, 2001). [Ziemen et al. \(2014\)](#) note that increasing the resolution of their AGCM from 3.75° to 1.9° reduces the cold bias over Alaska, and [van Kampenhout et al. \(2019\)](#) show that refining the grid over the Greenland ice sheet results in improvements to precipitation patterns and the distribution of accumulation. Thus, the use of a higher resolution model may result in a closer match to reconstructions in general across the ensemble members.

### 3.2 Non-implausible parameter sets

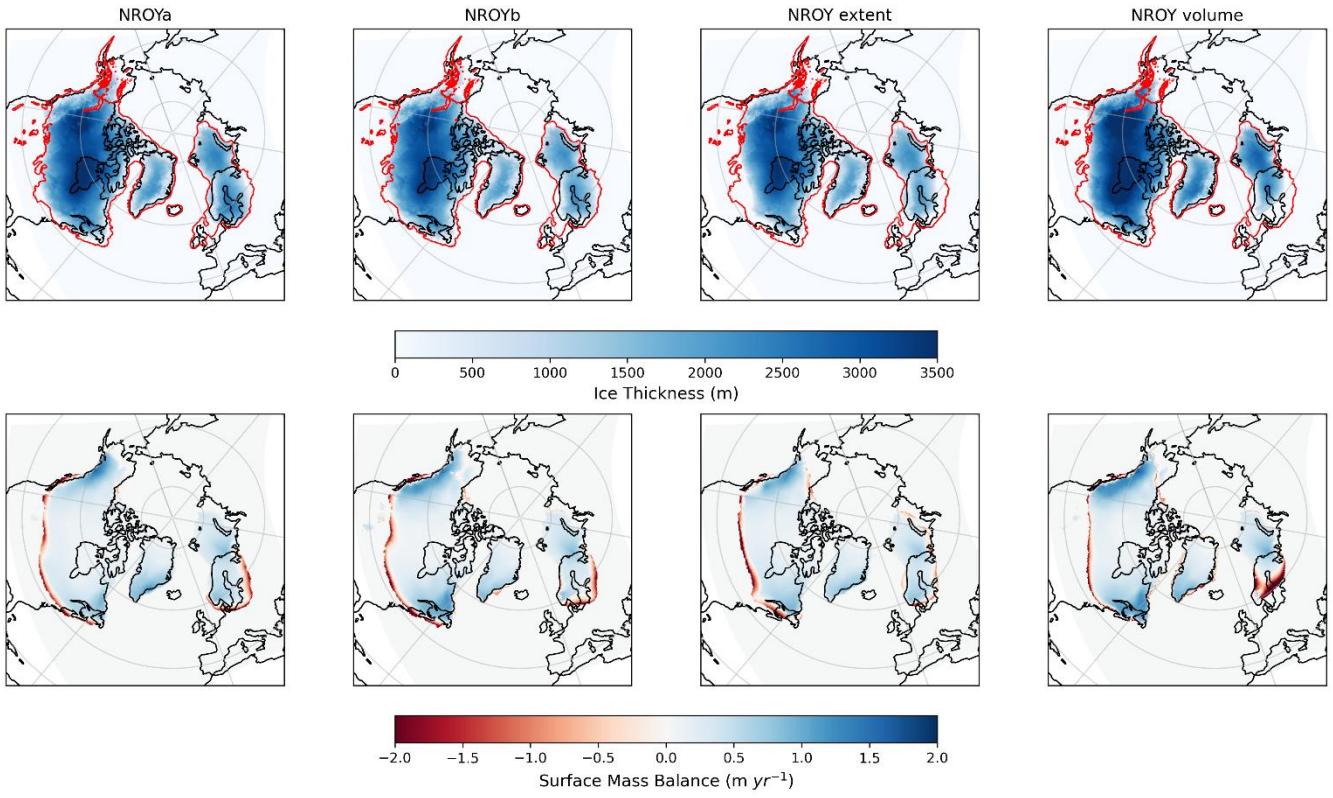
~~We apply the implausibility metric described in Sect. 2.4 to the ensemble of LGM simulations to see if there are any sets of model parameters that produce plausible ice sheets. All ensemble members have a GMT that falls within the range included in the implausibility metric due to the control in surface conditions imposed by the prescribed SSTs. The LGM simulations range from 6.34–9.20 °C and the PGM from 7.12–10.12 °C. This suggests that the SSTs used produce plausible LGM and PGM climates, causing a warmer PGM compared to the LGM, which is also in agreement with palaeo reconstructions and other dynamical models (Bintanja et al., 2005; Colleoni et al., 2016). However, due to ice extent and volume, only two LGM simulations are NROY (labelled as NROYa and NROYb). Furthermore, we acknowledge the risk that our evaluation metric may be too tightly constrained by uncertain palaeo reconstructions; ice sheet volume, in particular, is not well known. We therefore also~~  
We apply the implausibility metric described in Sect. 2.4 to the ensemble of LGM simulations to identify sets of model parameters that produce plausible ice sheets. All ensemble members have a global mean surface air temperature within the plausible range (6.3–9.2 °C at the LGM and 7.1–10.1 °C at the PGM) due to the prescribed SSTs. Two LGM simulations fit all four of our implausibility criteria for the volume and extent of both the NAIS and EIS, we label these NROYa and NROYb. The proportion of NROYs in an ensemble is highly dependent on the subjective choice of number and ranges of parameter values sampled. Previous work with FAMOUS-ice (Gandy et al., 2023; Patterson et al., 2024; Sherriff-Tadano et al., 2024) has shown that finding combinations of parameter values that produce realistic ice extent during glacial times is challenging, due to strong albedo-surface mass balance feedbacks. Thus, finding two parameter combinations that produce plausible results for both time periods and both ice sheets is a good outcome. Additional simulations from the NROY parameter space could be found by iterating this process and using emulators within the implausibility measures to efficiently identify such parameter combinations given the first ensemble, as was done in Patterson et al. (2024). This is computationally expensive and was not required for our purposes. Nevertheless, we apply the extent and volume constraints separately to explore additional plausible ice sheet configurations, especially since the volume constraint is still very uncertain and our minimum volume for the NAIS is less lenient than limits that have been used previously (e.g. Gandy et al., 2023; Sherriff-Tadano et al., 2024). This results in the selection of two more ensemble members; one that meets only the ice extent criteria (labelled as NROY extent) and one that meets only the ice volume criteria (labelled as NROY volume). All four ~~of these~~ NROY simulations are shown in Fig. 6, with the corresponding four PGM simulations ~~shown~~ presented in Fig. 7. ~~Time~~ The time series of ice volume, surface mass balance, sub-shelf melt plus calving rate, and surface air temperature for these simulations ~~can be found~~ are provided in Appendix E.

665 The final volumes and extents of the NROY simulations are outlined in Table 3. Overall, the LGM NROY simulations show  
666 a good match to the reconstructed extents of the LGM ice sheets and the equivalent PGM simulations display a smaller NAIS  
667 and larger EIS in line with empirical evidence and previous studies. Whilst the equivalent PGM simulations show a smaller  
668 NAIS than the extent of Batchelor et al., (2019), this [latter](#) reconstruction represents the maximum MIS 6 extent (190-132 ka)  
669 and therefore is likely larger than the 140 ka ice sheet would have been, particularly for the NAIS. These four NROY model  
670 simulations suggest the NAIS was ~25 m s.l.e. smaller at the PGM compared to the LGM, and the EIS ~24-27 m s.l.e. larger.  
671 There are very few existing reconstructions of the PGM ice sheets and none produced using a coupled climate-ice sheet model.  
672 Our simulations perform well in comparison to these reconstructions (Fig. 8) ~~and thus provide a great alternative for use as~~  
673 ~~boundary conditions in future climate and sea level modelling studies~~8) . For example, compared to the reconstruction of  
674 [Pollard et al., \(2023\)](#), our Eurasian ice sheet is more physically consistent with climate and ice sheet dynamics but is also more  
675 in line with empirical reconstruction of ice extent (e.g. [Batchelor et al., 2019](#)) compared to the dynamic ice sheet model  
676 reconstruction used in the PMIP4 protocol ([Abe-Ouchi et al., 2013](#); [Menviel et al., 2019](#)), which is missing most of the  
677 [Fennoscandian ice sheet \(Fig. 8\)](#). Thus, our NROY simulations provide new improved reconstructions of the PGM Northern  
678 [Hemisphere ice sheets for use as inputs for climate, ice sheets and sea level models](#).

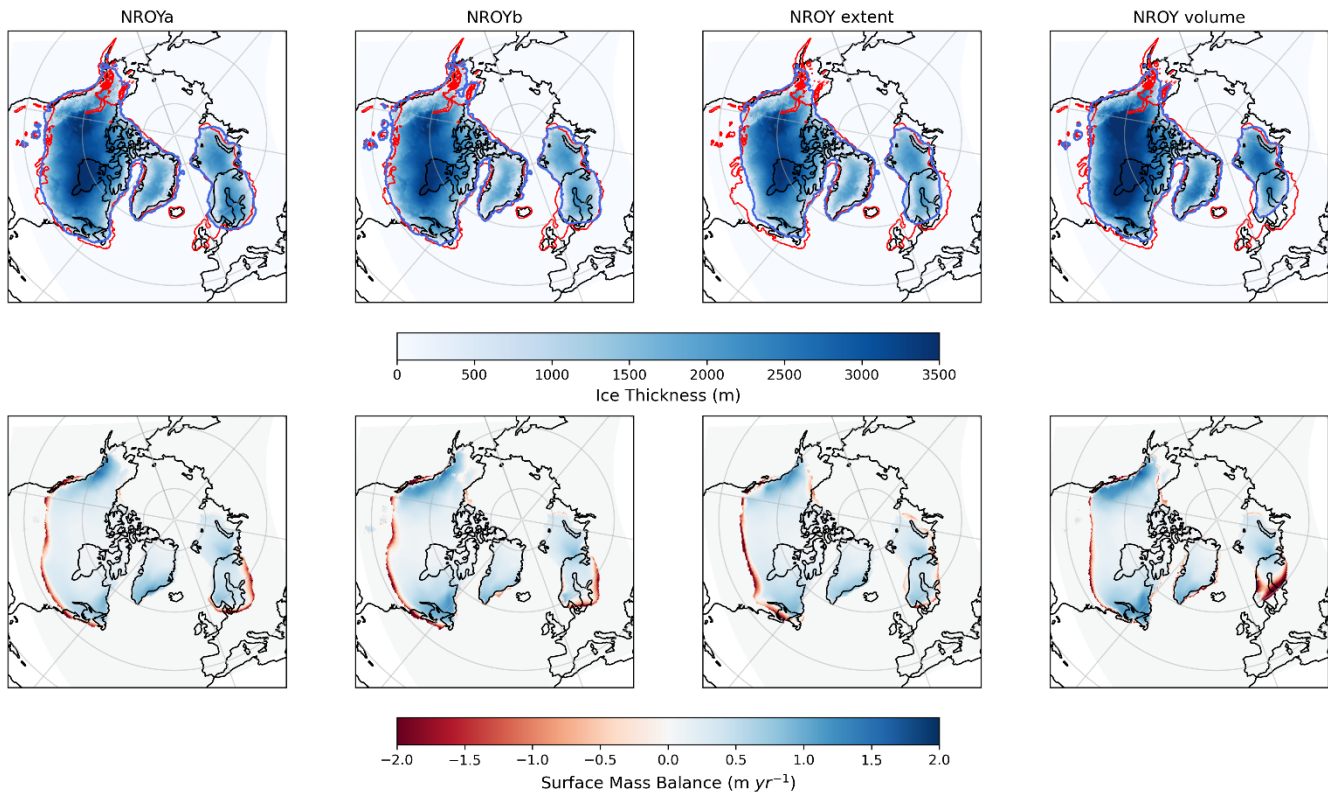
679  
680 **Table 3: Ice sheet volumes and extents at the end of the 5000 ice sheet years for the two NROY LGM simulations and the**  
681 **corresponding PGM simulations**

	LGM				PGM			
	NROYa	NROYb	NROY extent	NROY volume	NROYa	NROYb	NROY extent	NROY volume
<b>NAIS Volume (m s.l.e.)</b>	72.6	76.9	64.7	82.4	48.1	52.2	41.5	57.5
<b>EIS Volume (m s.l.e.)</b>	14.2	17.0	12.7	13.7	38.7	44.0	35.6	50.7
<b>NAIS area (southern area) (x10<sup>6</sup> km<sup>2</sup>)</b>	14.2 (4.44)	13.9 (4.17)	12.4 (2.91)	13.1 (3.51)	10.9 (1.87)	10.8 (1.66)	9.31 (0.75)	10.1 (1.32)
<b>EIS area (x10<sup>6</sup> km<sup>2</sup>)</b>	4.53	5.0	4.08	3.56	9.86	10.1	9.04	9.61

682



683



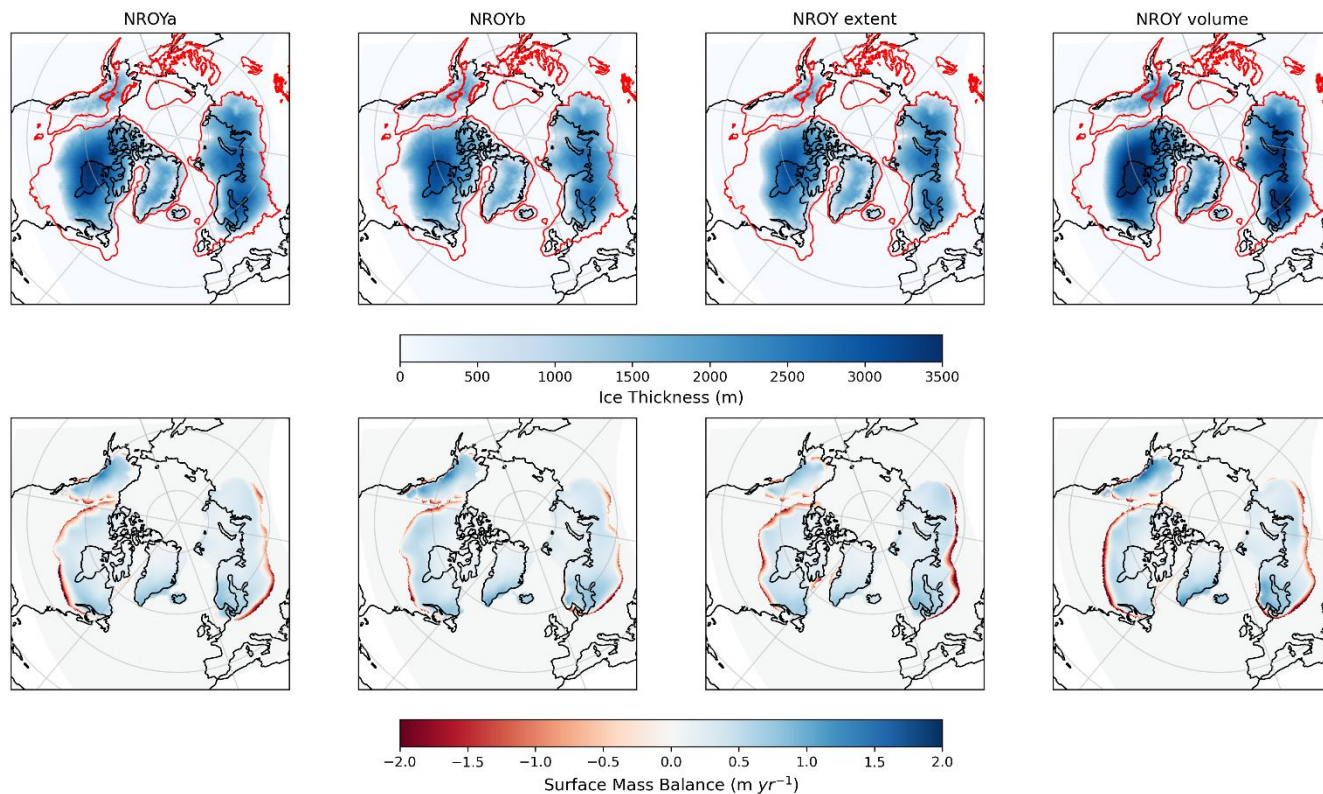
684

685 **Figure 6: Final ice thickness and surface mass balance for the four NROY LGM simulations. The red contours indicate the**  
 686 **reconstructed LGM ice sheet extents of Dalton et al., (2020) and Hughes et al., (2016) and the blue contours indicate the**  
 687 **modelled ice sheets displayed in the figure.**

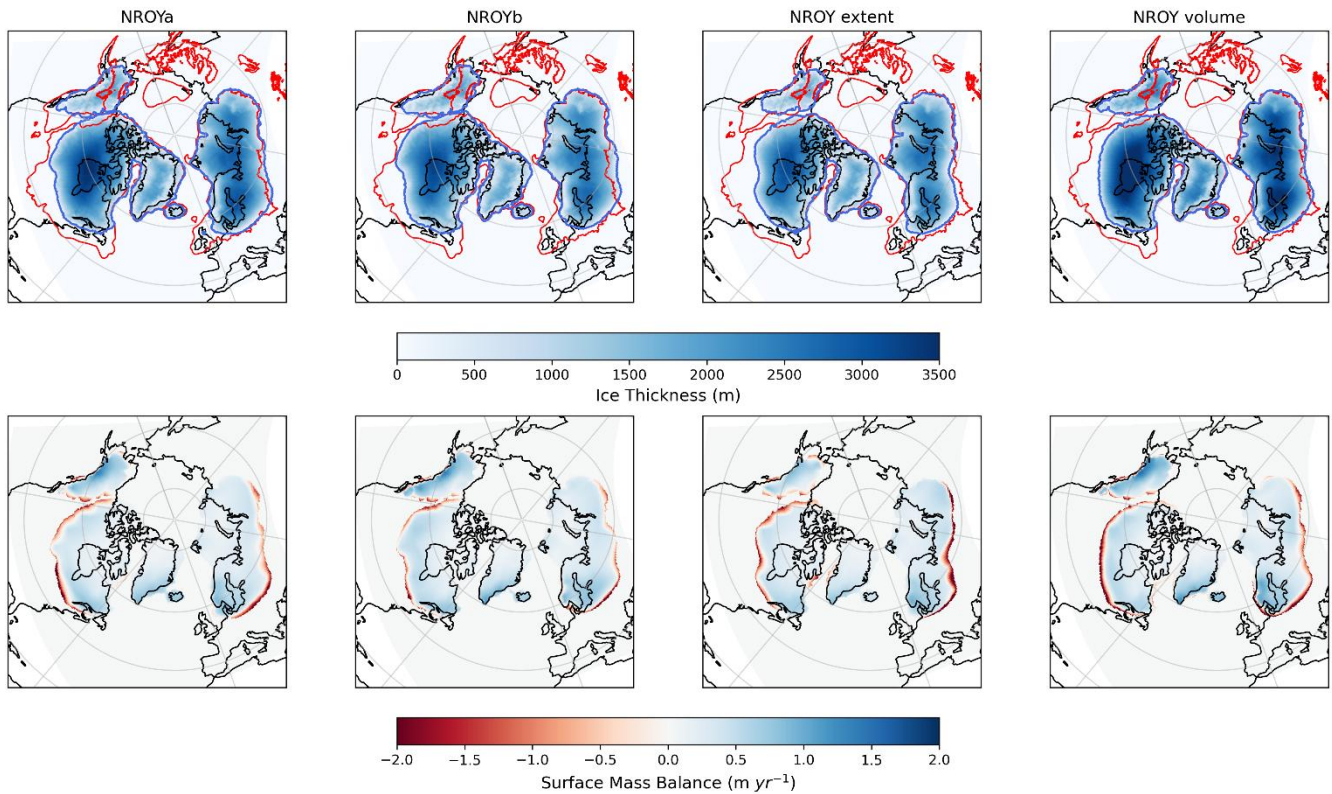
688 ~~All NROY simulations still lack a BIIS, however, which suggests that biases in the climate model are the cause rather than~~  
 689 ~~model parameter values.~~ All NROY simulations lack a BIIS suggesting this feature is due to our modelling setup rather than  
 690 parameter uncertainty. The BRITICE-CHRONO comprehensive reconstruction of the BIIS deglaciation revealed that the ice  
 691 sheet reached its maximum extent around 26 ka (or before in some sectors) and had initiated a rapid collapse at 22 ka which  
 692 saw most of the ice sheet disintegrate by 16 ka (Clark et al., 2022). We can infer that the BIIS was at disequilibrium with the  
 693 21 ka climate and had significantly negative surface mass balance leading to the collapse of the ice sheet within ~5000 years.  
 694 The full deglaciation of the BIIS during our 5000-year long equilibrium simulations under 21 ka forcing is thus in agreement  
 695 with the BRITICE-CRHONO reconstruction. Transient coupled climate-ice sheet simulations would be required to simulate  
 696 the rapid growth and retreat of the BIIS around the LGM.

697 Due to high rates of sub-shelf melt ( $\sim 60\text{-}75 \text{ m yr}^{-1}$ ), the NROY simulations also lack ice shelves by the end of the 5000 ice  
 698 sheet years, which could also have contributed to the underestimation of the eastern margin of the NAIS and the deglaciation  
 699 of the BIIS (Scherrenberg et al., 2023b). However, there are not many constraints on the extent of ice shelves during the LGM  
 700 or PGM since they leave few glaciological traces behind. There is some evidence that a large, thick ice shelf extended into the  
 701 Arctic Ocean during the MIS 6 glaciation (Jakobsson et al., 2016; Svendsen et al., 2004) and during the last glaciation a thick

702 ice shelf may have covered Baffin Bay (Couette et al., 2022). Similarly, the rate of sub-shelf melt is poorly constrained during  
703 past periods, however, since some studies have shown ocean driven melt to be important for the evolution of the marine based  
704 sectors of the NH ice sheets (Alvarez-Solas et al., 2019; Clark et al., 2020; Petrini et al., 2020), it may be useful to implement  
705 a more complex parameterisation or perform some additional sensitivity tests to explore this process further in future studies.

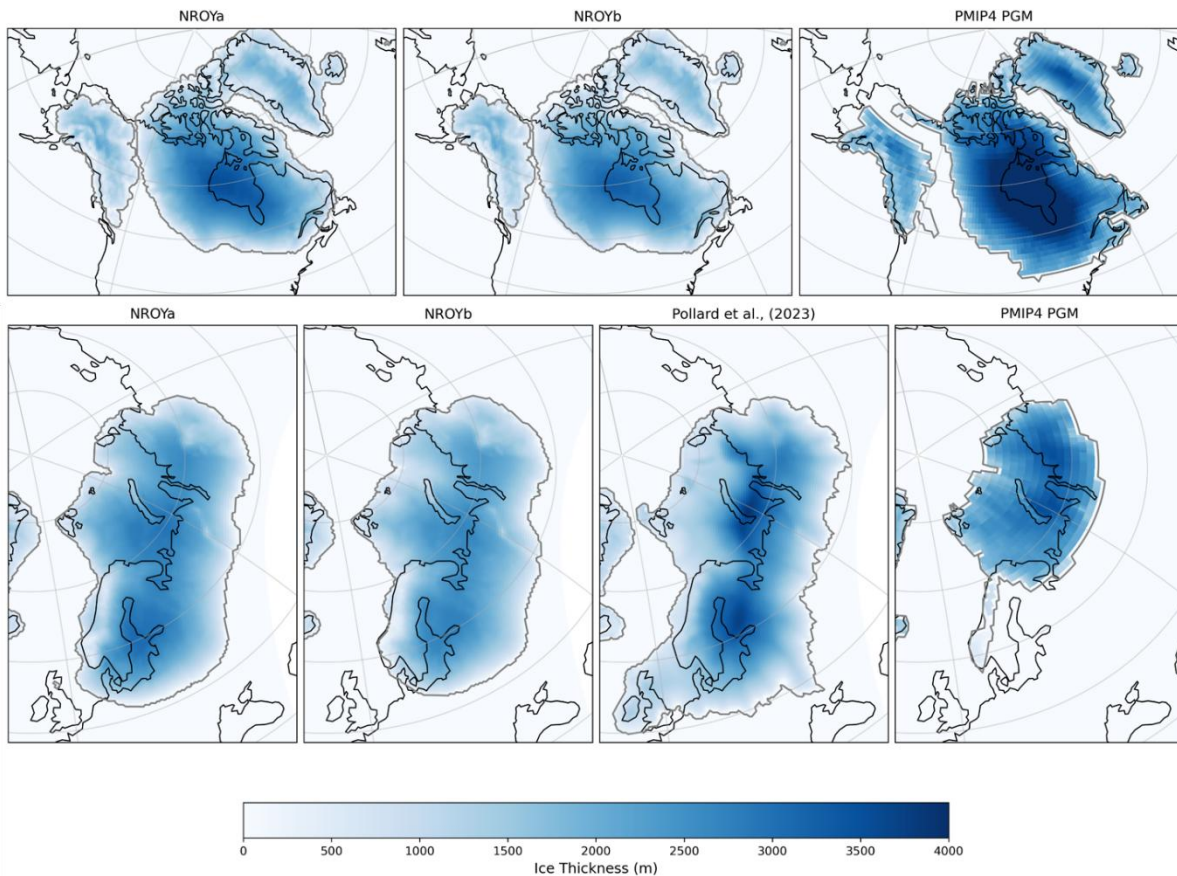


706



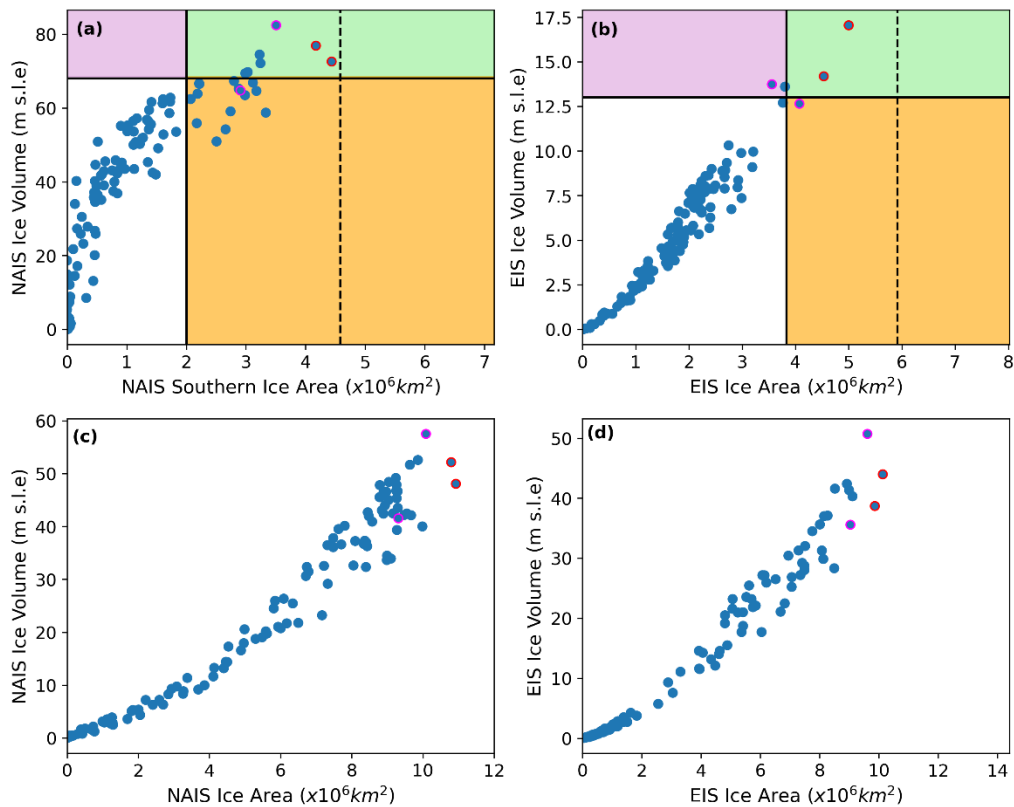
707  
 708 **Figure 7: Final ice thickness and surface mass balance for the four NROY PGM simulations. The red contours indicate the**  
 709 **reconstructed MIS 6 ice sheet extents of Batchelor et al. (2019) and the blue contours indicate the extent of the modelled ice sheets**  
 710 **displayed in the figure.**

711 Despite difficulties in the past in obtaining a sufficient southern extent of the NAIS in lower resolution models, ~~the NROYa~~  
 712 ~~and NROYb simulations do a relatively good job.~~ (Gandy et al., 2023; Sherriff-Tadano et al., 2024; Ziemen et al., 2014), the  
 713 NROYa and NROYb simulations do a relatively good job, with the southern ice sheet area only falling short of the Dalton et  
 714 al., (2020) reconstruction by 3 % and 9 %, respectively. The two additional NROY simulations are less close to the  
 715 reconstructed extent, however, and all four still fail to capture the ice lobe structures. This is because they are formed by  
 716 extensions of terrestrial ice streams as a result of complex ice dynamics and subglacial processes (Jennings, 2006; Margold et  
 717 al., 2018). They are also highly asynchronous, dynamic features resulting in their glacial maximum limits being very uncertain  
 718 (Dalton et al., 2020; Margold et al., 2018). Therefore, it is not surprising that a relatively low resolution climate and ice sheet  
 719 model with ~~highly idealised~~ simple representation of subglacial ~~environments~~ processes is unable to resolve such features  
 720 (Gandy et al., 2019; Zweck and Huybrechts, 2005).



721  
722 **Figure 8: Comparison of the two NROY PGM simulations to other model reconstructions (Abe-Ouchi et al., 2013; Pollard et al.,**  
723 **2023)**

724 The parameter values used in the two NROYa and NROYb simulations are in a similar [areas-region](#) of the parameter space for  
725 all parameters except *tgrad* ([lapse rate](#)) and *drain<sub>r</sub>* ([till water drainage rate](#)), suggesting the ice sheets are fairly insensitive to  
726 these two parameters (Supplementary Fig. S1). Interestingly, Figs. 9a and 9b show that, if considering the NAIS and EIS  
727 separately, there are five simulations that produce only a plausible NAIS but do not meet constraints for the EIS. Furthermore,  
728 as we have already seen, there are also simulations that produce plausible ice sheet extents but fall short on the volume and  
729 vice versa. Many of these simulations are situated in different areas of the parameters space than the two NROY simulations  
730 for most of the parameters (Supplementary Fig. S1). Figures 9c and 9d show that the NROYa and NROYb parameter sets also  
731 produce the largest PGM ice sheet extents in the ensemble but there are additional simulations that produce similar or larger  
732 volume ice sheets, which, in relation to the EIS, was not the case for the LGM. These results all suggest that both ice sheets  
733 and both time periods display different sensitivities to model parameters.



734  
 735 **Figure 9: Results from the full ensembles of simulations showing (a) LGM North American ice sheet southern area versus volume and**  
 736 **(b) LGM Eurasian ice sheet area versus volume. The solid lines show the minimum values used in the implausibility metric for**  
 737 **area and extent and the dotted line shows the actual extent of the ice sheet reconstructions. Simulations that fall within the green**  
 738 **box satisfy area and volume constraints for each individual ice sheet, the orange box indicates they satisfy the area constraints only**  
 739 **and purple only the volume constraints. The points outlined in red are the two NROY simulations (i.e. fall into the green box for**  
 740 **both ice sheets) and the points outlined in pink are the additional NROY extent and NROY volume simulations. Panels (c) and (d)**  
 741 **show the equivalent results for the PGM ensembles without the constraints.**

742 **3.3 Sensitivity to parameters**

743 ~~To examine and quantify these different sensitivities we perform the~~ We used Gaussian Process emulation and Sobol Sensitivity  
 744 analysis ~~described in~~ (Sect. 2.5. ~~Due~~) to quantify the ~~performance~~ sensitivity of the ~~emulators leading to some uncertainty in~~  
 745 ~~the predicted ice extent and volume to the model parameters we varied. Given emulator uncertainties, we focus on the largest~~  
 746 values and ~~therefore the values of the Sobol indices, we are careful to not over interpret the results and only analyse the highest~~  
 747 ~~values and largest differences. We also use emulation to isolate the relationship~~ between ~~certain influential~~ the Sobol indices.  
 748 We encourage the reader not to over-interpret the relative importance of the less significant parameters ~~and~~. Emulation was  
 749 also used to isolate the effect of individual parameters on ice sheet volume in which the emulator predicts the model output  
 750 across a sample of the range of ~~by varying~~ one parameter whilst all other parameters are held ~~while holding others~~ at their  
 751 ~~midpoint values~~ midpoints.

752 The first and second order sensitivity indices for the NAIS and EIS volumes for the LGM and PGM are shown in Fig. 10a and  
753 10b and the difference in sensitivities between the two ice sheets in Fig. 10c. The analysis indicates that the ice sheets were  
754 relatively insensitive to the parameters *vfl*, *drain*, *ct*, *rhcrit* and *c*. The insensitivity to the value of the sub-shelf melt is  
755 unsurprising despite previous studies reporting a high sensitivity of the Antarctic and Eurasian ice sheets (Alvarez Solas et al.,  
756 2019; Berdahl et al., 2023; Berends et al., 2023). This is because the simulations lost their ice shelves fairly soon into the  
757 model run due to either high rates of sub-shelf melt resulting from the large values of *c*, or large ablation rates as a result of  
758 other climate model parameter values.

759 The most influential parameters in all aspects are *fsnow* and *av\_gr*, which control the albedo of the ice sheet, with larger values  
760 of *fsnow* and smaller values of *av\_gr* leading to larger ice sheets. The third albedo parameter, *daice*, is also important,  
761 particularly for the NAIS, having a positive correlation with ice sheet size. However, as in the case of NROY extent, the value  
762 of *daice* is less important provided that *fsnow* is high and *av\_gr* is low since these produce a high enough albedo to maintain  
763 an extensive ice sheet on their own (Fig. F1). These three parameters also have important interactions with other parameters  
764 and each other. This importance of the albedo parameters is consistent with previous studies investigating the sensitivity of the  
765 NAIS to uncertain parameters (Gandy et al., 2023; Patterson et al., 2024; Sherriff-Tadano et al., 2024), but our detailed Sobol  
766 sensitivity analysis is able to not only identify the most important parameters but also quantify the importance of all the other  
767 parameters. Furthermore, the inclusion of the EIS in our analysis reveals the importance of some other parameters for the  
768 configuration of the EIS. This includes *beta*, *cw* at the LGM, and, despite the value of *tgrad* being in different areas of the  
769 parameter space for the NROY simulations, this analysis shows that the EIS is highly sensitive to this parameter, especially  
770 for the PGM. The NAIS is also sensitive to new parameters introduced in this study that weren't tested in Gandy et al., (2023)  
771 or Patterson et al., (2024). This includes *beta*, and for the LGM the volume is also impacted by the value of *elevation*.

772 Here Figure 10 shows the first and second order sensitivity indices for the NAIS and EIS volumes during the LGM and PGM.  
773 The ice sheets were relatively insensitive to the parameters *vfl* (precipitating ice fall out speed), *drain* (till water drainage rate),  
774 *ct* (cloud liquid water conversion rate), *rhcrit* (relative humidity threshold) and *c* (sub-shelf melt constant). The low sensitivity  
775 to *c* (sub-shelf melt constant) is expected, as ice shelves were lost early in the simulations due to high sub-shelf melt or ablation  
776 from other climate parameters. We expect that the sub-shelf melt constant *c* would have much more influence in the context  
777 of deglaciations than in the equilibrium simulations we ran here. Similarly, *drain* (till water drainage rate) is more important  
778 for the characteristics of ice flow than for ice volume and extent.

779 The most influential parameters are *fsnow* (surface snow density threshold) and *av\_gr* (sensitivity to grain size), which control  
780 the albedo of the ice sheet, with larger values of *fsnow* and smaller values of *av\_gr* leading to larger ice sheets. *Daice* (bare ice  
781 albedo sensitivity) also played a role, especially for the NAIS, though its effect was secondary when *fsnow* and *av\_gr* already  
782 produced high albedo (Fig. F1). These three albedo parameters also showed strong interactions with each other and other  
783 parameters. Our Sobol analysis not only confirms the importance of albedo parameters, consistent with previous studies  
784 (Gandy et al., 2023; Patterson et al., 2024; Sherriff-Tadano et al., 2024), but also quantifies the influence of other parameters,  
785 particularly for the EIS.

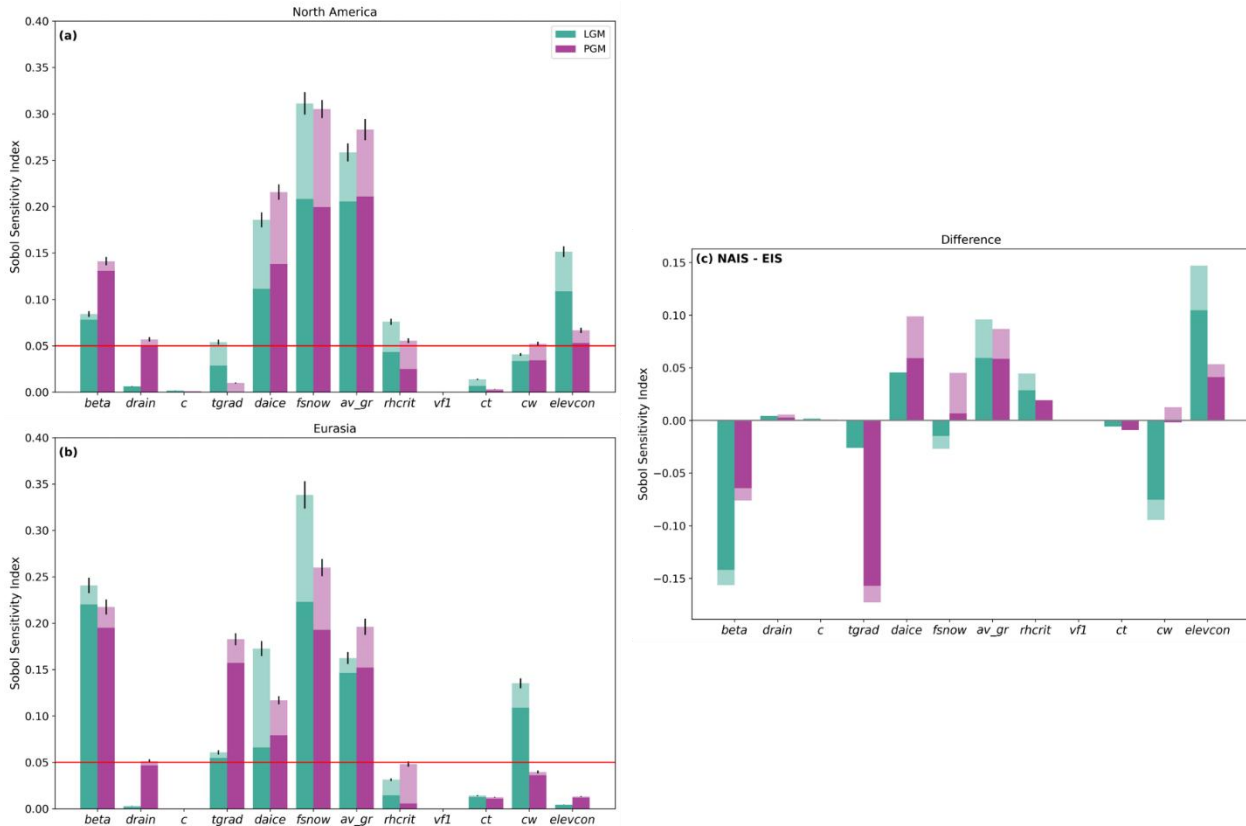
786 [For the EIS, the other important parameters are  \$\beta\$  \(Weertman friction coefficient\),  \$c\_w\$  \(cloud liquid water threshold\) at the](#)  
787 [LGM, and  \$t\_{grad}\$  \(lapse rate\), especially for the PGM. The NAIS is also sensitive to new parameters introduced in this study](#)  
788 [that were not tested in Gandy et al., \(2023\) or Patterson et al., \(2024\), including  \$\beta\$ , and  \$elevcon\$  \(height correction; which](#)  
789 [the LGM volume is sensitive to\).](#)

790 [Here,](#) we discuss some of the possible reasons these four parameters ( $elevcon$ ,  $c_w$ ,  $t_{grad}$  and  $\beta$ ) could have an effect on the  
791 various ice sheets. ~~However, further simulations and testing would need to be carried out to come to any conclusions. One~~  
792 ~~reason that the LGM NAIS shows a particular~~[The sensitivity of the LGM NAIS to  \$elevcon\$  could be related to the size of the](#)  
793 [ice sheets since it affects higher ice elevations more](#) ~~and, indeed,~~ [Indeed we find](#) the value of the [elevcon](#) Sobol index ~~for this~~  
794 ~~parameter is in line with~~[proportional to](#) the average thickness of each ice sheet. The fact that a larger value of  $elevcon$  leads to  
795 a larger NAIS (Fig. 11a) but ~~doesn't~~[does not](#) impact the size of the EIS could explain why the ensemble produced more  
796 plausible North American ice sheets at the LGM but did not perform as well for the Eurasian ice sheet (Fig. 9). ~~It may also~~  
797 ~~explain some of the difference in NAIS size between the LGM and PGM.~~[9\).](#)

798 ~~Similarly, the~~

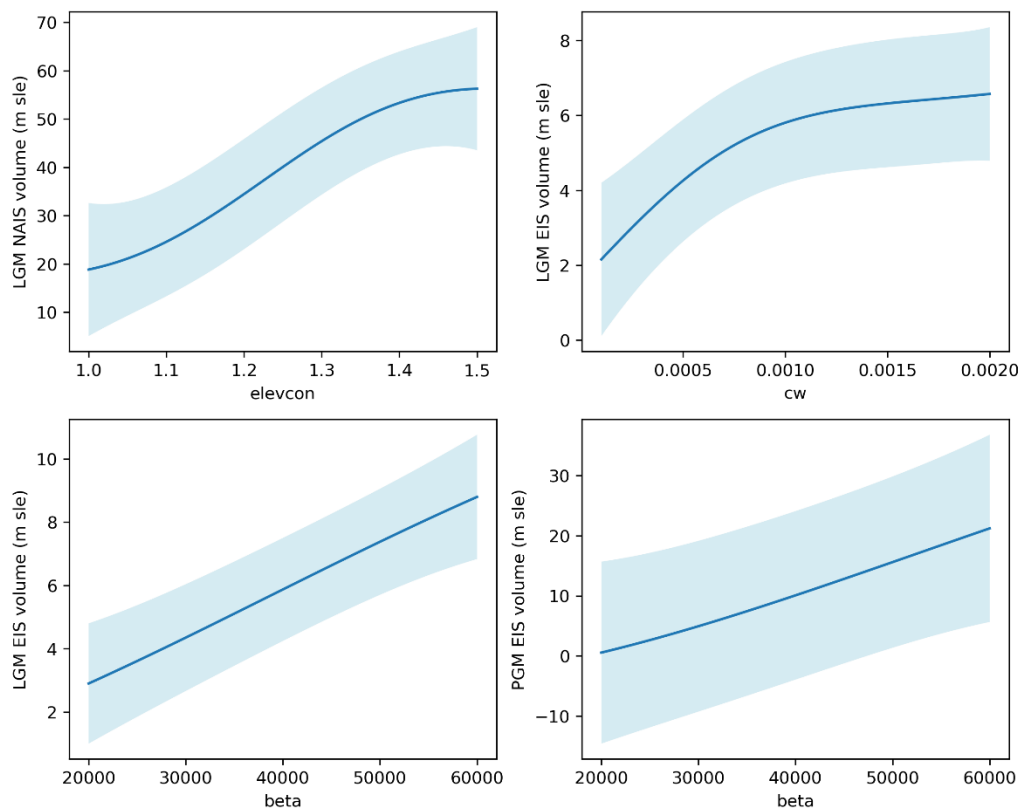
799 [The sensitivity of LGM EIS being to  \$c\_w\$  \(cloud liquid water threshold\) suggests that the EIS is more sensitive to the value of](#)  
800  ~~$c_w$  differences in precipitation than the NAIS or either PGM ice sheet could explain why there are more simulations that~~  
801 ~~produced larger volume Eurasian.~~[This likely reflects differences in the climatic regimes of both ice sheets at the PGM imposed](#)  
802 [by their geographical locations. Indeed the EIS is subject to a more maritime climate than the LGM, but the NAIS behaved](#)  
803 ~~similarly between both periods (Fig. 9),~~[with higher precipitation rates and cloudiness sensitive to  \$c\_w\$ . Interestingly at the PGM,](#)  
804 [the EIS is less sensitive to this parameter, likely because its larger size puts its southern margins in a more continental climatic](#)  
805 [regime less sensitive to precipitation rates or cloud cover.](#)  $C_w$  has a positive correlation with EIS volume up to a value of  
806 around  $0.0012 \text{ kg m}^{-3}$  (Fig. 11b). ~~Any increase~~ above ~~this does not appear to increase the ice~~[which](#) volume ~~much~~  
807 ~~further~~[plateaus](#). This could be because lower values of  $c_w$  cause increased precipitation due to decreasing the threshold of  
808 cloud liquid water above which precipitation forms. This ~~has a particular effect in~~[leads to higher](#) summer ~~leading to higher~~  
809 rainfall ~~rates over the Northern Hemisphere continents which contributes~~[contributing](#) to the surface melting ~~of the ice sheets~~  
810 through the [heat](#) flux ~~of heat from the rain to the ice. One reason the~~[The](#) LGM EIS is particularly susceptible to this effect  
811 ~~could be~~ due to its smaller size. Precipitation is not downscaled onto elevation tiles in the coupling, rather the coarse  
812 atmospheric output is applied to the ice sheet model which leads to rainfall being spread across relatively large areas of the ice  
813 sheet, therefore affecting a large proportion of the LGM EIS (Smith et al., 2021). ~~Another reason~~[Therefore, the use of a higher](#)  
814 [resolution atmospheric model or an improvement to the coupling scheme may reduce the sensitivity to this parameter \(Dong](#)  
815 [and Valdes, 2000; van Kampenhout et al., 2019; Lofverstrom and Liakka, 2018\).](#) Another reason the LGM EIS is [positively](#)  
816 [correlated with  \$c\_w\$](#)  could be related to the change in liquid cloud cover and its effect on the energy balance. The increased  
817 precipitation leads to a decrease in the fraction of cloud cover which would allow a higher receipt of incoming shortwave  
818 radiation, thus increasing the surface melt. However, the downwelling longwave radiation may also be decreased which would  
819 have the opposite effect, decreasing the absorbed energy. Since the accumulation zone usually has a high albedo, reflecting

820 much of the incoming solar radiation, the SMB of this area is mostly controlled by changes in the longwave fluxes. In contrast,  
 821 the low albedo ablation zone is largely impacted by the shortwave radiation budget in the summer melt season. This latter  
 822 process has been found to be dominant in studies of the Greenland Ice Sheet, with reduced cloudiness contributing to its mass  
 823 loss and increasing its sensitivity to warming (Hofer et al., 2017; Izeboud et al., 2020; Mostue et al., 2024; Ryan et al., 2022).  
 824 Again, due to its smaller size, a large proportion of the LGM EIS is under ablation (54 % compared to around 35 % for the  
 825 other ice sheets in Fig. 5), potentially explaining why it is so sensitive to changes in cloud cover.



826  
 827 **Figure 10: The Sobol sensitivity index of the ice volume for each parameter for (a) the North American Ice Sheet and (b) the Eurasian**  
 828 **Ice Sheet. (c) The difference in sensitivity indices between the North American and Eurasian ice sheets. The darker colour represents**  
 829 **the first order index and the lighter colour the second order index (together showing the total sensitivity). The variance of the Sobol**  
 830 **indices plus the mean emulator variance is indicated by the black error bars. The red line indicates the index value of 0.05, above**  
 831 **which the sensitivity is significant.**

832 PGM EIS is much more sensitive to the value of *tgrad* than the other ice sheets. More negative values of *tgrad* cause a stronger  
 833 temperature-elevation feedback, resulting in warmer temperatures at lower elevations. This ~~is going to have~~ has the largest  
 834 impact on ice sheets with larger ablation areas. Many of the simulated PGM Eurasian ice sheets collapse (Fig. 3) as a result of  
 835 the larger ice sheet being more unstable due to the larger GIA feedback. Therefore, many of these simulations ~~will~~ have strong  
 836 ablation over the Eurasian ice sheet that increases throughout the run, making it more sensitive to *tgrad* and the temperature-  
 837 elevation feedback.



838

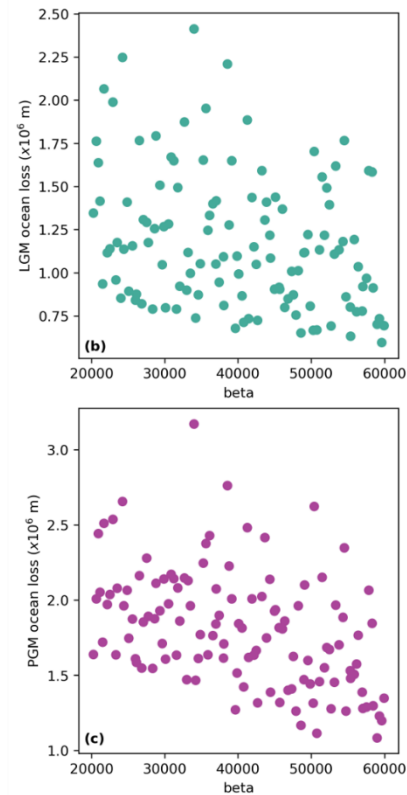
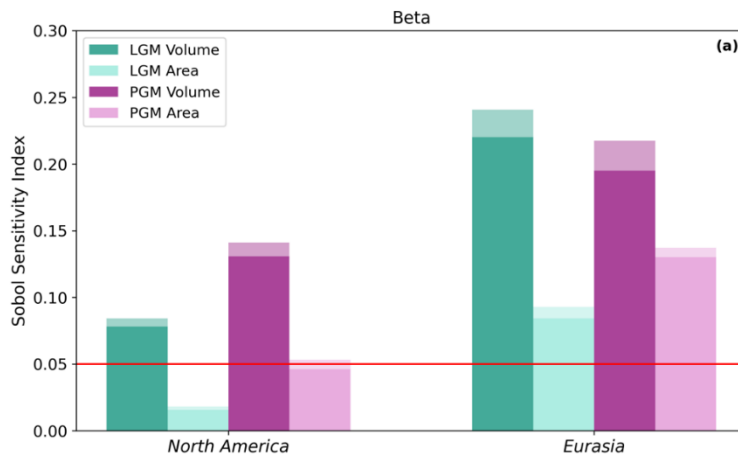
839 **Figure 11: The relationship between emulated mean ice sheet volumes and (a) *elevcon* , (b) *cw* , (c) and (d) *beta* a The 95<sup>th</sup> percentiles**  
 840 **are shown by the blue shaded region.**

841 ~~In addition, The parameter *beta* has a positive correlation to the size of the Eurasian ice sheet at both the LGM and PGM (Fig. 11c and 11d).~~  
 842 ~~but does not have as much of an impact on the NAIS which could also explain some of the different behaviours~~  
 843 ~~seen between both ice sheets. *Beta* is also the only parameter that causes a large difference in the sensitivity indexes~~  
 844 ~~of volume and versus extent, with the ice volume being much more sensitive to *Beta* than extent is (Fig. 12a). This could explain why the~~  
 845 ~~NROY extent simulation falls short of the volume constraints since it has a relatively low *beta* value (Fig. F1). This also~~  
 846 ~~supports the idea Our interpretation is that reduced basal friction results in more ice mass loss from the Eurasian ice sheet~~  
 847 ~~compared to North America since because faster flow from the interior of the ice sheet to the more extensive marine margins~~  
 848 ~~causes a larger discharge of ice across the grounding line where it is calved or lost by sub-shelf melting (Fig. 12b and 12c).~~  
 849 ~~This therefore affects the volume and thickness of the ice sheet but not so much the extent since ice already reaches the edge~~  
 850 ~~of the continental shelf (Blasco et al., 2021; Scherrenberg et al., 2023a; Sherriff-Tadano et al., 2024). Scherrenberg et al.,~~  
 851 ~~(2023a) and Quiquet et al., (2021) show a similar impact of basal friction on ice sheet volume compared to extent at the LGM~~  
 852 ~~but also show that the thinner ice sheets, larger ablation area and increased ice velocities, caused by lower basal friction led to~~  
 853 ~~a faster deglaciation. Interestingly, both of the NROYa and NROYb simulations have lower values of *beta* than the five~~  
 854 ~~additional simulations that produce a plausible NAIS but not EIS. This suggests that the right combination of parameters,~~

855 especially in regard to the albedo parameters  $f_{snow}$ ,  $av_{gr}$  and  $da_{ice}$ , and the interactions between parameters, can compensate  
856 for the faster flow and are thus more important for the size of Eurasia (Fig. F1).

857

858 The sensitivity of LGM and PGM volume and extent to model parameters is likely model dependent. However, the relative  
859 importance of the processes controlled by these parameters are likely to hold for other models. Overall, we find that the EIS  
860 size is more sensitive to parameters controlling cloudiness/precipitation and ice flow than the NAIS which is more sensitive  
861 to parameters controlling surface melt due to the geographical locations of the ice sheets controlling the continentality of  
862 climate and the marine margins. Furthermore, the relative importance of key processes is significantly different between the  
863 LGM and PGM despite the strong climatic similarities, because of the major difference in ice sheet sizes between the two  
864 periods.



865

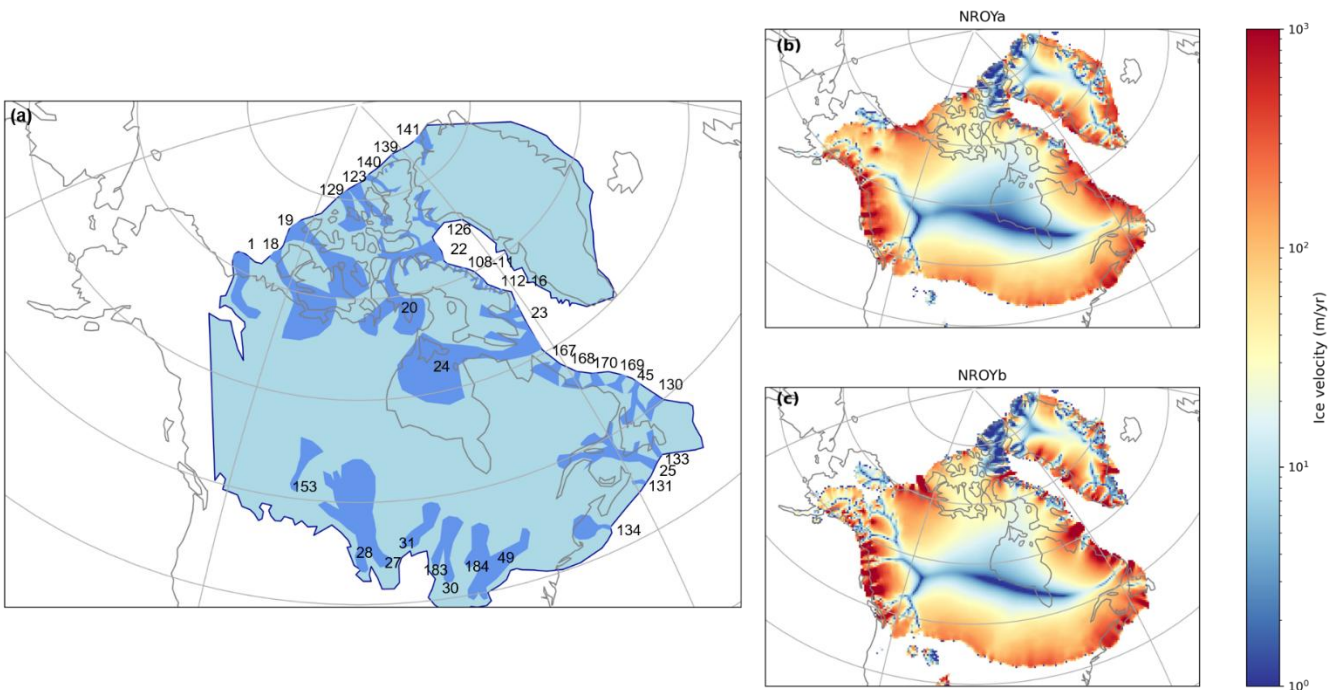
866 **Figure 12: (a) Sobol Sensitivity Indices for the ice volume and extent at the LGM and PGM for the parameter  $\beta$  and (b) LGM**  
867 **and (c) PGM total ice loss to the ocean (calving + sub-shelf melt) versus the value of  $\beta$ .**

### 868 3.4 Ice dynamics

869 The representation of ice streams in the simulations was updated from the previous FAMOUS-BISICLES simulations of the  
870 NAIS (Sherriff-Tadano et al., 2024) by performing the sensitivity tests and internal temperature spin up detailed in Sect. 2.2.  
871 The velocity of areas of ice streaming in the NROY simulations range from a few hundred  $\text{m yr}^{-1}$  to  $5000 \text{ m yr}^{-1}$  which is a

872 ~~similar range to what has been observed on present day~~By performing an internal temperature spin-up and sensitivity tests  
 873 (Sect. 2.2 and Appendices B and C), we have improved ice streaming in our simulations compared with FAMOUS-BISICLES  
 874 simulations of the NAIS Ice stream velocity in the NROY simulations ranges from a few hundred  $\text{m yr}^{-1}$  to  $5000 \text{ m yr}^{-1}$ , in  
 875 agreement with present day observations of Antarctica and Greenland (Joughin et al., 2010; Rignot et al., 2011). We asses to  
 876 what extent the modelled ice streams in the ~~NROYa and NROYb~~simulations match empirical reconstructions by performing  
 877 a qualitative comparison of NROYa and NROYb to LGM reconstructions of the Laurentide ~~ice streams~~ (Fig.13a; Margold et  
 878 al., 2018) and ~~the~~ Eurasian ice streams (Fig.14a; Patton et al., 2017).

879 For the Laurentide Ice Sheet, the locations of many of the ice streams show good agreement, particularly in NROYb (Fig. ~~13b~~  
 880 ~~and 13c~~). ~~Using the numbers and names used in Margold et al., (2018) this 13.~~ This includes; (1) Mackenzie Trough, (18)  
 881 Amundsen Gulf, (123) Massey Sound, (129) Prince Gustaf Adolf Sea, (126) Smith Sound/Nares Strait, (22) Lancaster Sound,  
 882 (23) Cumberland Sound, (24) Hudson Strait, (45) Notre Dame Channel, (133) Placentia Bay-Halibut Channel, (25) Laurentian  
 883 Channel, (131) The Gully and (134) Northeast Channel IS: (see labels in Margold et al., 2018). There are also areas of general  
 884 streaming where many smaller ice streams are found (numbers 108-116 and 167-170). One major ice stream that is not very  
 885 very active in these simulations is (19) M'Clure Strait and there is a poor representation of ice streaming along the southern margin  
 886 of the Laurentide Ice Sheet.

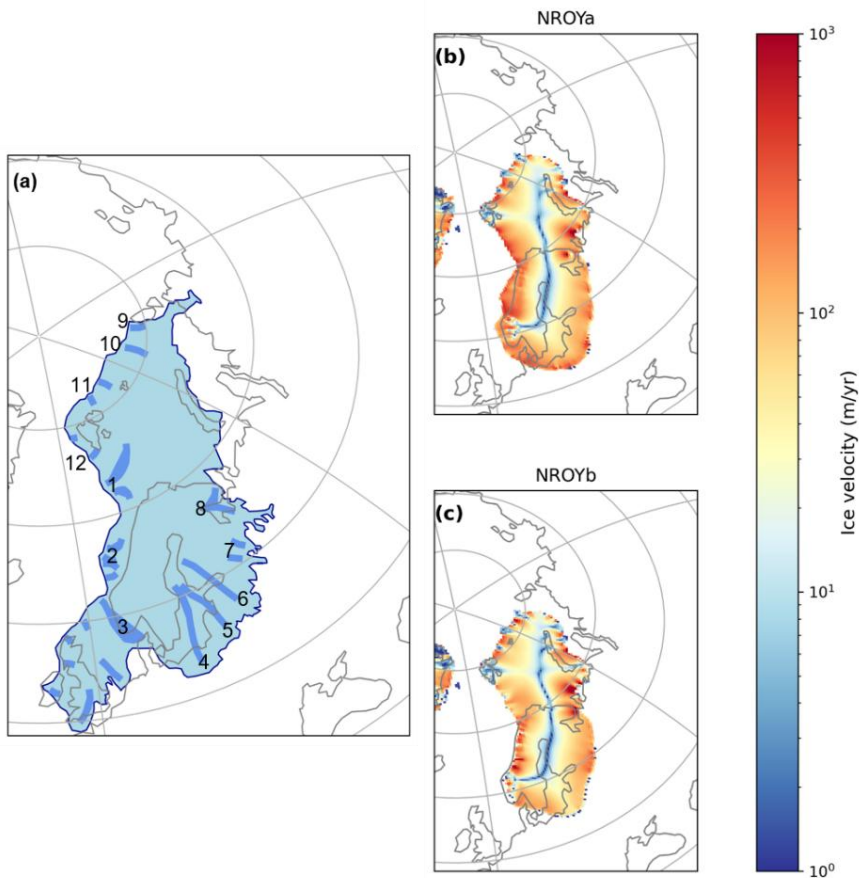


887  
 888 **Figure 13: (a) Empirical reconstruction of the active LGM Laurentide ice sheet ice streams (adapted from Margold et al., (2018),**  
 889 **and (b) NROYa and (c) NROYb ice velocities at the end of the 5000 year simulations.**

890 The Eurasian Ice Sheet does not have as defined areas of ice streaming, nevertheless, some of the major ice stream features  
891 can be picked out (Fig. 14b and 14c). ~~The following numbers relate to those in Fig. 14a and names are taken from van Aalderen~~  
892 ~~et al., (2023) and Stokes and Clark, (2001). There is some streaming activity in the location of one of the major ice streams;~~  
893 ~~(1) Bjornoyrenna ice stream~~14). There is some streaming activity in the location of one of the major ice streams. (1)  
894 Bjornoyrenna ice stream, and (10) Svyataya Anna ice stream is relatively well represented. Some of the smaller ice streams  
895 are also modelled including; (2) Mid Norwegian, (8), (9), (11) and (12). However, other major and minor ice streams are not  
896 active in these simulations; (3) Norwegian Channel, (4) and (5) Baltic Sea, (6) Gulf of Bothnia and (7-~~7~~) (see labels in van  
897 Aalderen et al., 2024 and Stokes and Clark, 2001). In addition, since the BIIS is not present, neither are the ice streams in this  
898 region. Interestingly, there are active areas of ice streaming to the south of the Barents Sea that are not present in the  
899 reconstruction. This could be due to the formation of a pro-glacial lake in this region allowing the formation of ice shelves  
900 which have zero basal friction and therefore increase ice velocity (Sutherland et al., 2020).

901 There are no comparable reconstructions of PGM ice streaming due to difficulties in dating and the erasure of glaciological  
902 evidence following the Last Glacial advance. However, due to extent and topographic constraints on ice streaming, it is likely  
903 that ice stream location was similar across the marine margins of the ice sheets (Pollard et al., 2023). The simulated PGM  
904 NAIS velocity behaves similarly to the LGM but there is a lack of (1) Mackenzie Trough and a less pronounced (18) Amundsen  
905 Gulf as a result of the different configuration of the ice sheets in this area (i.e. the location of the ice free corridor between the  
906 Laurentide and Cordilleran ice sheets). However, there is more evidence of (19) M'Clure Strait in NROYa and more activity  
907 on the southern Laurentide margin (Fig. G1). The PGM EIS velocity shows a more defined (3) Norwegian Channel ice stream  
908 and NROYb has a better representation of (10) Svyataya Anna, (11) and (1) Bjornoyrenna ice stream than the LGM. There is  
909 still no streaming in the Baltic Sea but the PGM also shows activity in the South Barents Sea. There is also additional ice  
910 streaming in the Northeast where the PGM ice sheet extent further then at the LGM (Fig. G2).

911 Whilst the value of *drain* does not affect the volume or area of the ice sheets (Sect. 3.3) it has a significant effect on the ice  
912 streaming/velocity of the simulations. The two NROY simulations display very different levels of ice streaming despite having  
913 similar configurations largely as a result of having different values of *drain*. NROYa has a higher value of 0.04 causing  
914 relatively quick drainage of the till water compared to NROYb which has a value of 0.01. Therefore, NROYb allows more  
915 sliding since the effective pressure is lower and thus so is the basal shear stress. The value of *drain* may become more important  
916 in simulations of deglaciations as ice streaming affects the stability of ice sheets and rate of retreat.



919

920 **Figure 14:** (a) Empirical reconstruction of the location of active LGM Eurasian ice sheet ice streams (adapted from Patton et al.,  
 921 (2017), and (b) and (c) ice velocities at the end of the 5000 year NROY simulations.

922 **4 Conclusions**

923 We ran ensembles of simulations using a coupled atmosphere-ice sheet model under LGM and PGM boundary conditions,  
 924 varying uncertain climate and ice sheet model parameters. The model ~~simulates~~ simulated plausible Northern Hemisphere ice  
 925 sheets compared to empirical reconstructions and previous modelling studies, capturing the different configurations between  
 926 the LGM and PGM. Through Gaussian Process emulation and a Sobol sensitivity analysis, we ~~find~~ found that the volume and  
 927 extent of both the simulated Northern Hemisphere ice sheets are sensitive to the parameters that control their albedo. However,  
 928 the North American ice sheet and the Eurasian ice sheet, and the two glacial maxima, ~~display~~ displayed different sensitivities  
 929 to ~~certain~~ other parameters. The size of the Eurasian ice sheet is more sensitive to parameters controlling basal sliding and  
 930 clouds/precipitation than for the North American ice sheet ~~at the LGM is sensitive to the value of the height correction~~  
 931 ~~parameter (*elevcon*), the~~ We also find that the sensitivity to parameters controlling sliding and surface mass balance can  
 932 depend on the size of the ~~Eurasian ice sheet is sensitive to the value of the lapse rate parameter (*tgrad*) at the PGM and to the~~

933 basal friction parameter (*beta*) at both ice sheet at each glacial maxima. This result highlights that, as well as the use of different  
934 initial conditions for the LGM and PGM, the difference in final ice volume and extent between both periods may also be  
935 impacted by the choice of

936 We described two sets of Not Ruled Out Yet (NROY) parameter values. However, after applying an implausibility metric we  
937 find two sets of NROY parameter values that are plausible compatible with reconstructed extent and volumes for both periods  
938 and both ice sheets, and we highlight ~~an~~two additional ~~two~~ simulations that we deem NROY depending on the criteria used.  
939 ~~We also do some work to improve the representation of ice streaming in the glacial ice sheets and find that~~ Improvements in  
940 ~~our simulations~~model setup produce a good match to empirical reconstructions of LGM ice streams, especially in simulations  
941 with lower values of till water drainage rate (*drain*).

942 The four NROY simulations produced in this study provide a ~~good starting point~~means for other studies to evaluate the effect  
943 of ice sheet uncertainty on climate and sea levels. They also provide new and improved initial conditions that can be used for  
944 simulating and comparing the Last and the Penultimate deglaciations, which will be the focus of future work. However, since  
945 it has been shown in the past that models can be overturned to certain climate conditions, it is not guaranteed that these parameter  
946 values will be conducive to the deglaciation of the ice sheets in line with empirical reconstructions and work will need to be  
947 done to test this and calibrate the model for both past and present conditions which will likely involve the use of emulators. In  
948 addition, there are some factors that were not considered or not well represented in this work that may become more important  
949 for the deglaciation. These include; the ice shelf melt parameterisation (Berends et al., 2023), the resolution at the grounding  
950 line (Gandy et al., 2021) and the representation of proglacial lakes (Sutherland et al., 2020). This study was also limited by the  
951 use of prescribed surface ocean conditions and pre-industrial vegetation and the absence of dust, all of which have been shown  
952 to initiate important feedbacks for ice sheet evolution (Ganopolski et al., 2010; Obase et al., 2021; Willeit et al., 2024). Current  
953 modelling capabilities prevented the use of a fully coupled atmosphere-ocean-ice sheet model with dynamic vegetation and  
954 dust for the large number of simulations run in this study, however as technological advances are made to enable this in the  
955 future, running similar simulations will provide useful information of the role of these other feedbacks on the evolution of the  
956 LGM and PGM ice sheets.

957 By performing a systematic calibration of our coupled climate-ice sheet model to reconstructed LGM ice extent and volume  
958 and simultaneously applying it to the PGM, we produced new reconstructions of the North American and Eurasian ice sheets  
959 at the Penultimate Glacial Maximum, greatly improved compared to previous work and informed by climate and ice sheet  
960 physics and geological data. Our PGM reconstructions can be used to model or study the climate, ice sheet dynamics, the solid  
961 earth and sea levels.

## 962 **Appendices**

### 963 **Appendix A: Implementation of the *elevcon* parameter**

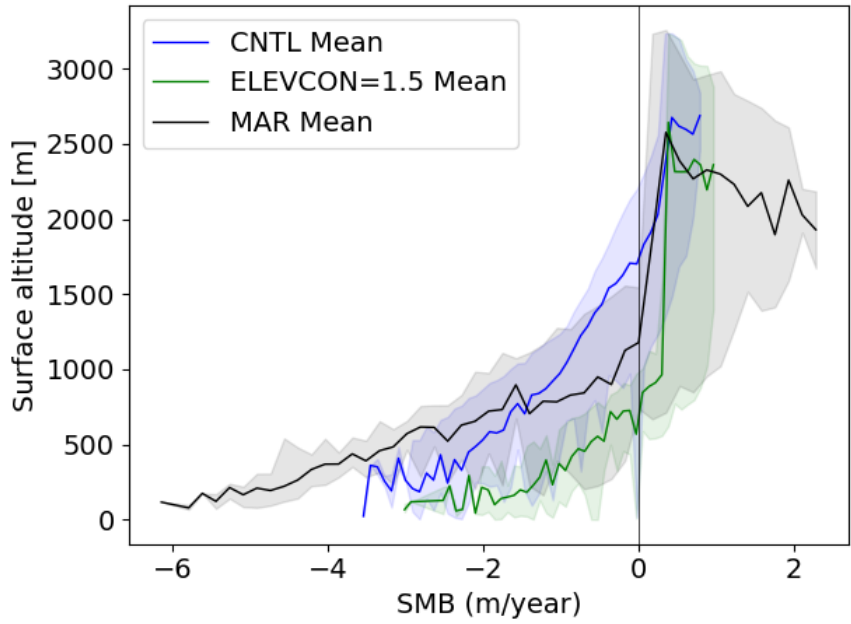
964 *elevcon* affects the surface temperature and SMB during the height adjustment to ice sheet tiles in the following manner;

- The effective elevation of each tile is multiplied by the value of *elevcon*. A value of 1.10 (10 %) means that the elevation of an 1800 m tile has been increased to 1980 m.
- Surface air temperatures and longwave radiation are downscaled to each increased elevation tile.
- Surface fluxes and SMB are calculated based on the downscaled variables and other variables from the original FAMOUS grid.
- The SMB and fluxes are then passed to the ice sheet and atmospheric models, but taken to represent the original tile elevation, not the increased elevation to which the surface temperature was actually downscaled. For example, the surface air temperature and SMB could be calculated on a 1980 m elevation tile, but they will be passed to the ice sheet and atmospheric models as outputs from an 1800 m elevation tile.

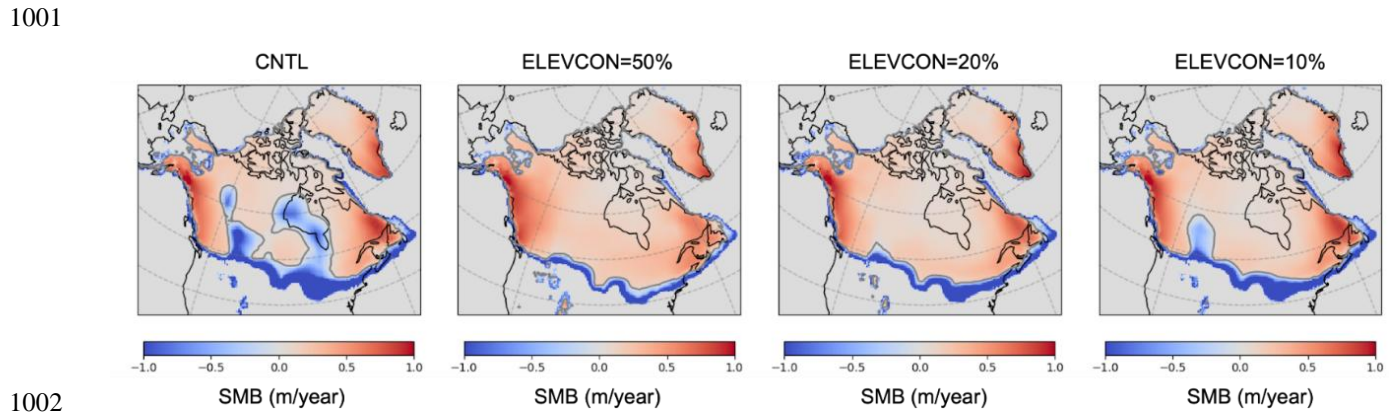
Therefore, the increase in the tile elevation is only accounted for during the downscaling of surface temperature but is not reflected when passing it to the ice sheet model or elsewhere in FAMOUS. In this way, additional cooling is applied over the ice sheet interior by *elevcon*, which can be regarded as elevation-dependent height adjustment over ice sheets. This crudely mimics the effect of the stable boundary layer in maintaining the cold surface condition in that area.

Two types of sensitivity experiments are performed with FAMOUS-BISICLES to validate the effect of *elevcon* on the modern and LGM ice sheets and climates. The first sensitivity experiment is conducted under modern climate and the Greenland ice sheet based on a control simulation performed by Lang et al. (in prep) and focuses on the effect of *elevcon* on the SMB. As shown in Smith et al., (2021), the model simulates a mean ELA of approximately 1.8 km over the Greenland ice sheet, whereas high resolution regional atmospheric models (e.g. [MAR; Fettweis et al., 2013](#)) suggest 1.2 km, meaning that the model overestimates the ELA by 50 % (Fig. A1). Here, we applied an *elevcon* value of 50% and rerun the simulation. The inclusion of the *elevcon* adjustment strongly suppresses the negative SMB seen around the elevation of 1 km to 2 km, and the ELA drops from 1.8 km to approximately 900 m height (Fig. A1). Given that the ELA is now underestimated compared with the high-resolution models, the value of 50 % appears to be too large and can be regarded as the upper limit. However, this sensitivity experiment clarifies the substantial effect of *elevcon* on the SMB at the interior of the ice sheet. It further shows that *elevcon* can be used to explore the effect of uncertainties in the SMB at the interior of the ice sheet arising from underestimating the role of the stable boundary layer.

The second type of sensitivity experiments are performed under the LGM climate for the North American ice sheet. Here, values of 10 %, 20 % and 50 % are tested with one of the ensemble members from Sherriff-Tadano et al., (2024) that exhibits a strong local melting of the ice sheet from parts of the interior. Results are shown in Fig. A2. The strong local melting observed around the Hudson Bay region in the control simulation is removed in all the sensitivity experiments. Also, depending on the magnitude of the value of *elevcon*, the negative SMB seen at the eastern part of the Rocky Mountains is reduced and pushes the ELA southwards.



996  
 997 **Figure A1: Relation of SMB and surface altitude over the Greenland ice sheet in the modern climate simulations with FAMOUS-**  
 998 **BISICLES.** The blue line (shading) shows the mean result (range) from the control experiments, and the green shows those from the  
 999 sensitivity experiments that include *elevcon* with a value of 1.5 (50 %). Also shown in black are the results from simulations using  
 1000 the MAR regional climate model (Fettweis et al., 2013).

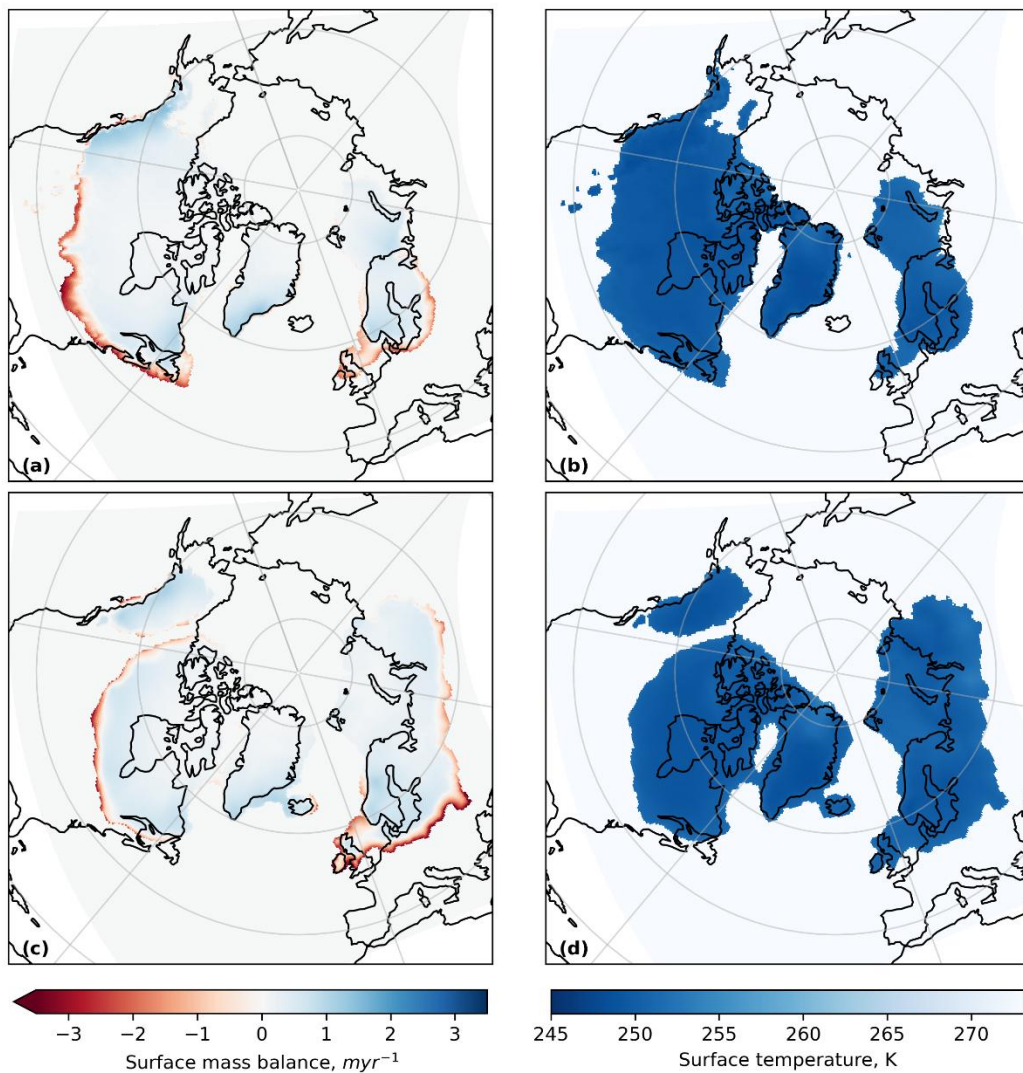


1005  
**Figure A2: Effects of different magnitudes of *elevcon* on the spatial pattern of SMB over the North American ice sheet at the LGM.** CNTL corresponds to one of the ensemble members (xppma) in Sherriff-Tadano et al. (2024).

## 1006 **Appendix B: BISICLES spin-up**

1007 The internal temperature of ice sheets is an important factor in controlling the deformation, rheology and velocity of the ice  
1008 due to the temperature dependence of the sliding law and enthalpy scheme (Blatter et al., 2010). The ice sheets start with a  
1009 uniform internal temperature of 268 K and it can take tens of thousands of years for the process of cold ice advection from the  
1010 interior and heat conduction from the bed to occur and reach an equilibrium, which is important for the formation of ice streams  
1011 (Fyke et al., 2014; Heine and Mctigue, 1996). Thus, we perform ice sheet model only spin-ups for the LGM and the PGM to  
1012 allow the ice sheet internal temperatures to reach close to equilibrium. This temperature profile is then used as the internal ice  
1013 sheet temperature in the initial condition for the sensitivity tests ([Appendix C](#)) and coupled simulations.

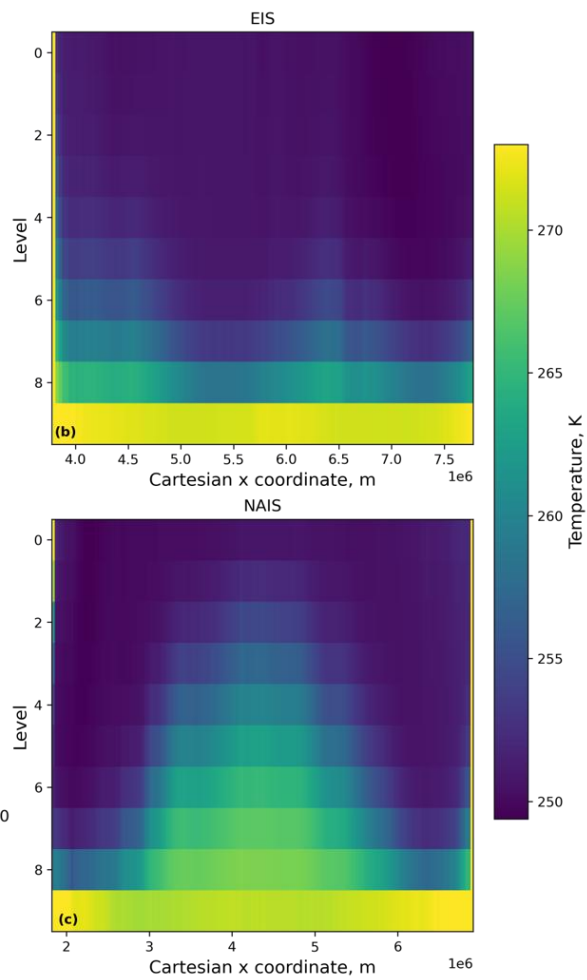
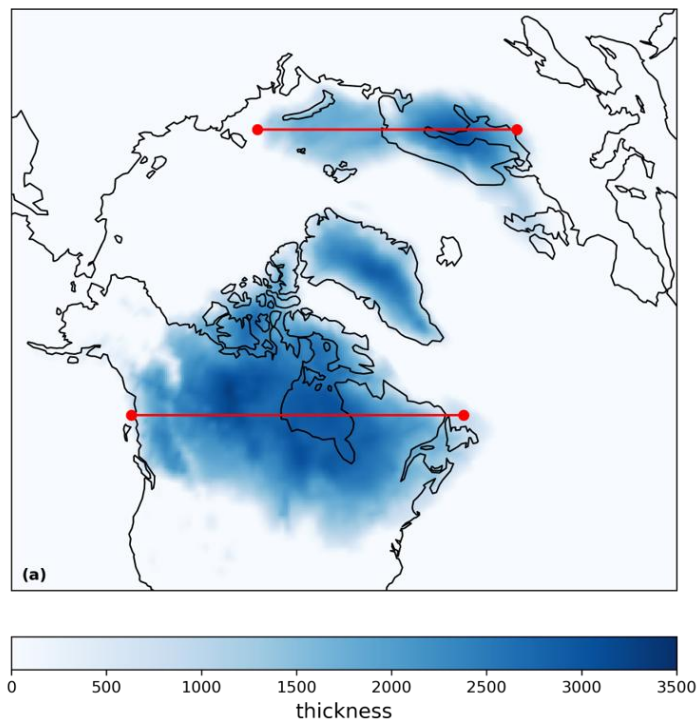
1014 The spin ups were run at 32 km resolution for 20,000 years using single surface mass balance and surface temperature fields  
1015 taken from a FAMOUS-BISICLES equilibrium simulation that used climate model parameters identified to be NROY in  
1016 simulations of the NAIS by Patterson et al., (2024), default ice sheet model parameters and an *elevcon* value of 1.2 (Fig. B1).  
1017 The initial ice sheet configurations were the same as used in the coupled simulations (described in Sect. 2.3.1; Fig. 1). The  
1018 sliding law was set to a temperature dependent Weertman sliding without till water dependent Coulomb sliding enabled since  
1019 the bulk of the temperature field is not affected much by Coulomb sliding near the coast. The resulting temperature profiles  
1020 are shown in [Figs. B2 and B3](#).



1022

1023

**Figure B1:** Surface mass balance and ice surface temperature fields used in the (a), (b) LGM and (c), (d) PGM spin ups.

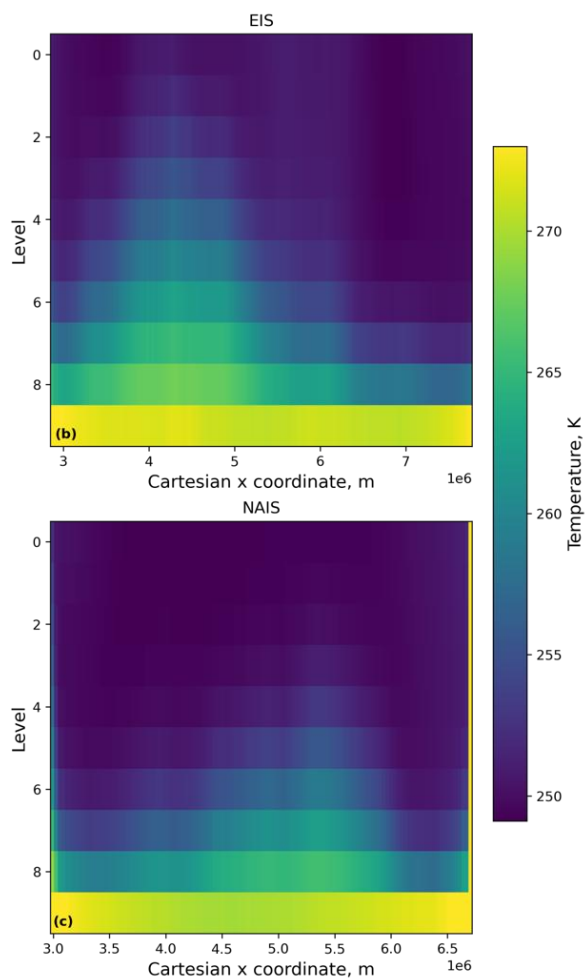
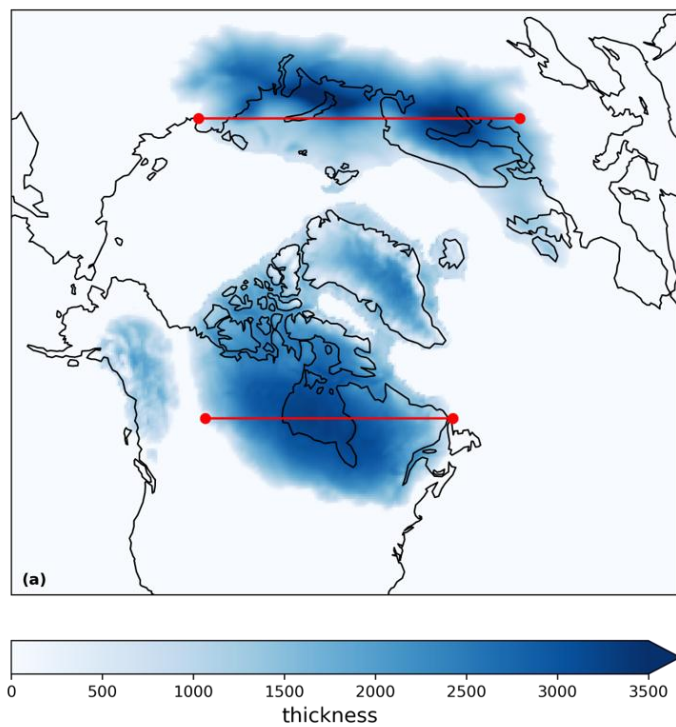


1024

1025

1026

**Figure B2: Cross section of LGM ice temperature at the end of the 20,000 year spin-up for the transects indicated by the red lines in (a), for the Eurasian ice sheet (b) and the North American ice sheet (c).**



1027

1028

1029

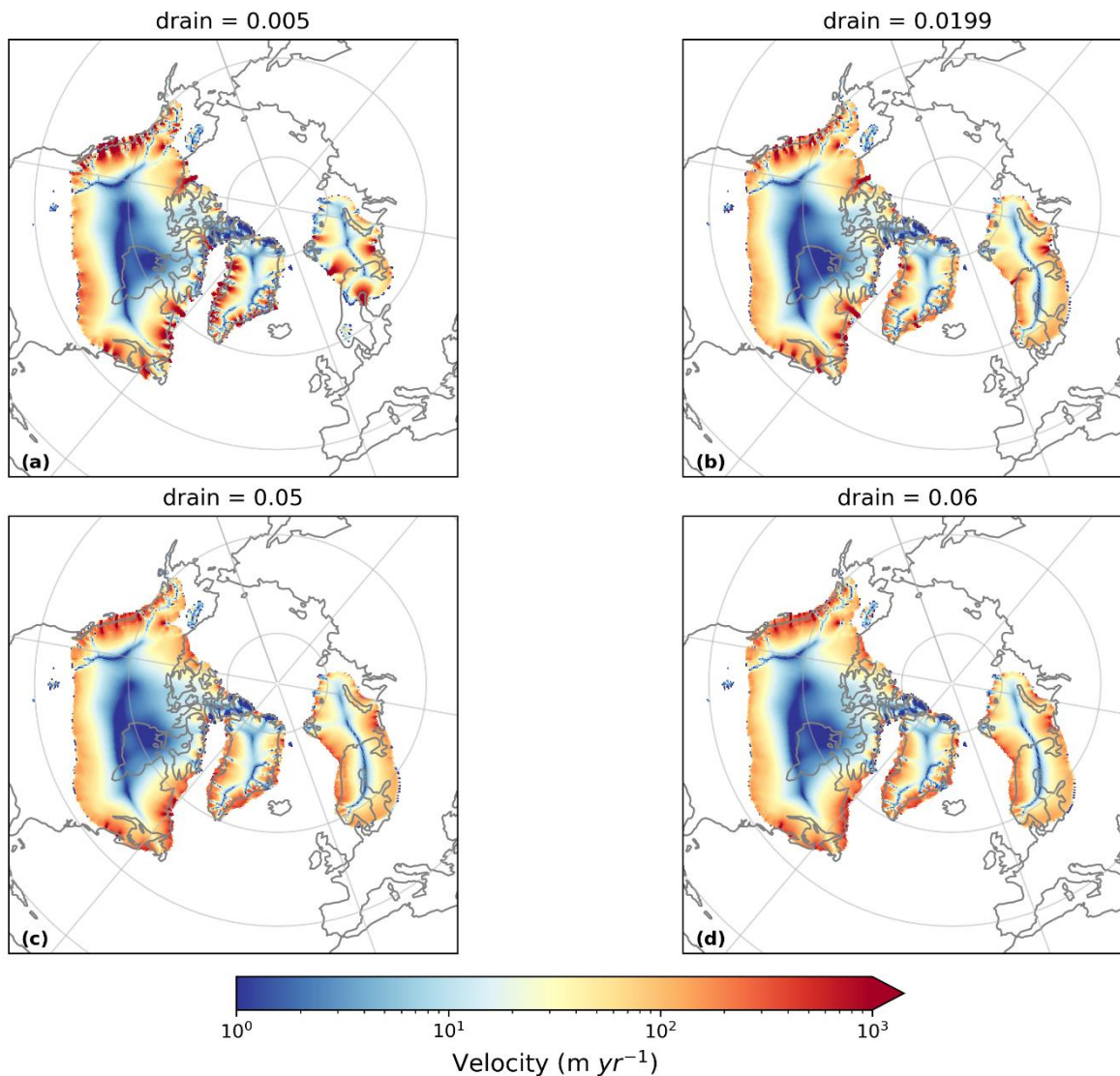
1030

**Figure B3: Cross section of PGM ice temperature at the end of the 20,000 year spin up for the transects indicated by the red lines in (a), for the Eurasian ice sheet (b) and the North American ice sheet (c).**

## Appendix C: Sensitivity tests

In their study, Sherriff-Tadano et al., (2024) used much higher values of *drain* (0.2-0.6 m yr<sup>-1</sup>) than has typically been used in previous studies (0.001-0.005 m yr<sup>-1</sup>; Gandy et al., 2019; Kazmierczak et al., 2022; Moreno-Parada et al., 2023). This was to prevent large till water depths leading to too large velocities across the entire ice sheet and long simulation times, as high velocities require more iterations and smaller timesteps to solve. This resulted in the till water drainage outpacing the supply and thus very small till water depths, leading to mostly Weertman sliding across the whole ice sheet.

Slow till drainage (low values of *drain*) can lead to isolated regions of fast flow, > 50 km yr<sup>-1</sup>, which have a disproportionate effect on simulation time. To prevent this we introduce an artificial drag term rising with the fourth power of ice speed and calibrated to be negligible for ice speeds below 1 km yr<sup>-1</sup>. This drag factor is also used in the coupled simulations throughout the rest of this study. We then perform sensitivity tests with different values of *drain* spanning the range 0.001-0.06 m yr<sup>-1</sup> but all other factors kept constant. The results of some of these tests are shown in Fig. C1. Values of *drain* above 0.05 prevent much of the coulomb sliding at the coasts and the representation of some of the major ice streams, particularly the Hudson Strait Ice Stream, is poor. Low values usually used in ice sheet models (0.001-0.005) cause too large velocities and ice streams that remove much of the ice sheet, especially in Eurasia. Therefore, in this study, we implement a range of 0.01-0.05 to cover values just below the default till water supply rate of 0.02, to where no coulomb sliding occurs. For studies that seek to examine ice streaming of the glacial maximum ice sheets, we would recommend performing additional sensitivity tests that vary ice shelf basal melt parameterisation and geothermal heat flux, but this is beyond the scope of the present study.



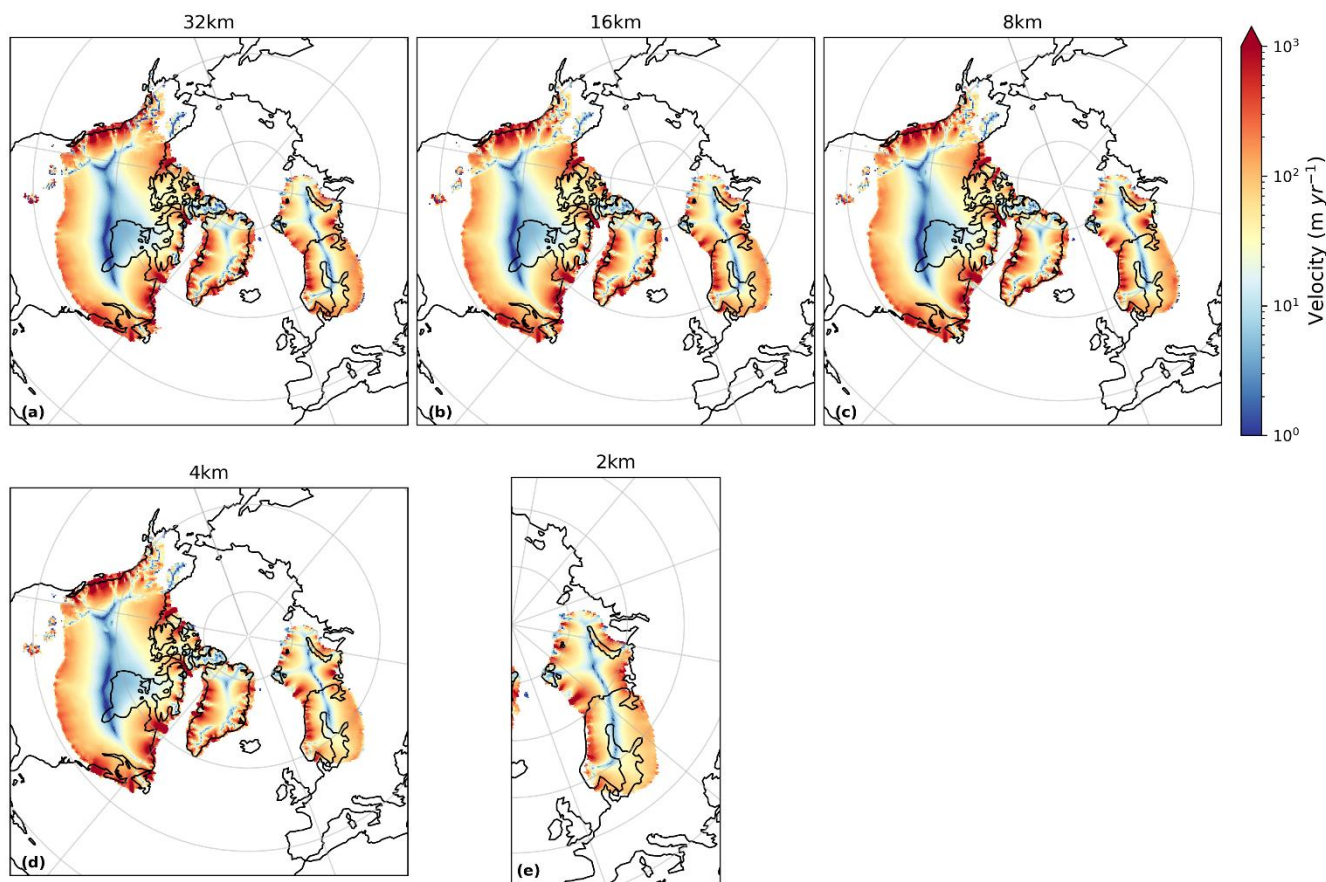
1049

1050 **Figure C1: Ice velocity after 5000 ice sheet years in simulations using till water drainage rates of (a) 0.005 m yr<sup>-1</sup>, (b) 0.0199 m yr<sup>-1</sup>,**  
 1051 **(c) 0.05 m yr<sup>-1</sup> and (d) 0.06 m yr<sup>-1</sup>. All other parameters and initial conditions were kept the same.**

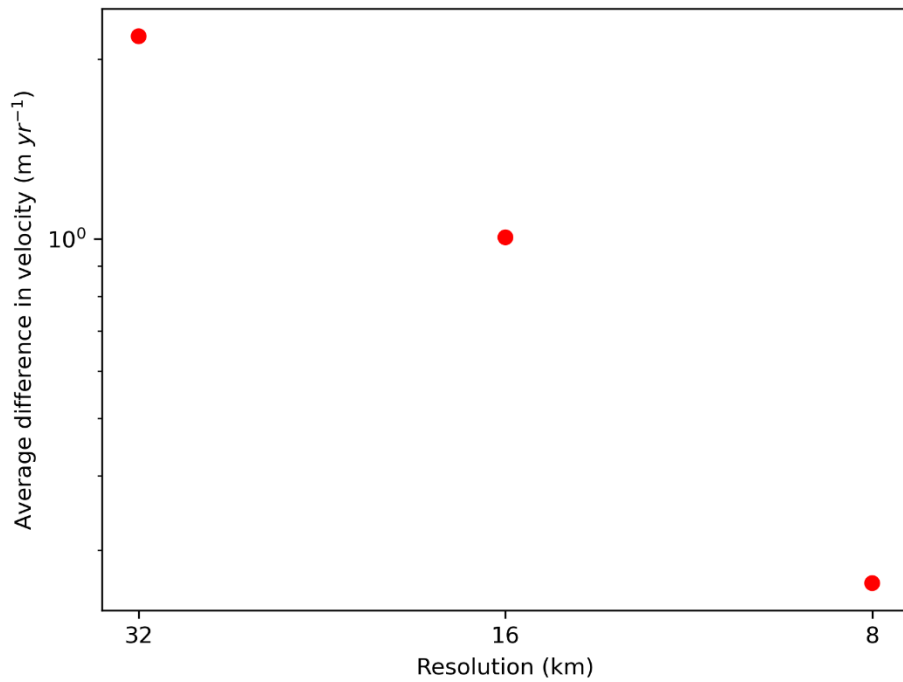
1052 The base resolution of the ice sheet model is 32 km. The AMR allows the areas covered by ice to be refined once to 16 km,  
 1053 which shows some improvement to the simulated ice streams, although the difference is only about 1.2 m yr<sup>-1</sup> on average over  
 1054 the whole ice sheet (Figs. C2a and C2b). Additional sensitivity simulations were performed refining only the areas of ice  
 1055 streaming up to 8 km and up to 4 km (Figs. C2c and C2d). These tests showed that after refining the entire ice sheet to 16km,  
 1056 the difference in average ice velocity for any further refinement of the ice streams converges to zero (Fig. C3) and the pattern  
 1057 of major ice stream features (Fig C2), the position of the marine margins and the ice volume across the NH ice sheets is not  
 1058 significantly changed, except across the southern area of the Eurasian ice sheet (Fig. C4). However, computational costs are

1059 quadrupled with each level of refinement. Thus, we determine one level of refinement (16 km) to be sufficient for this study  
1060 in which we are focussing more on the large-scale geometry of the ice sheet rather than the finer details of the ice streams.  
1061 This is a similar conclusion to that drawn from the simulations presented by Albrecht et al., (2020) and Gandy et al., (2019),  
1062 the latter further showing anything finer than 4 km does not improve the match of simulated ice streams to empirical data [over](#)  
1063 [the British Isles.](#)

1064 There is an increase in the velocity of up to around 3000 m yr<sup>-1</sup> at the centre of some of the ice streams at the higher resolutions,  
1065 which could be important during simulations of the deglaciation (Robel and Tziperman, 2016). We performed an additional  
1066 simulation refining the ice streams across the marine section of the Eurasian ice sheet to 2 km to see if any marine processes  
1067 would be captured that could not have been resolved at lower resolutions. This did not lead to any significant difference in the  
1068 ice velocity in this region compared to the 4 km simulation (Fig. C2e), but again could be important in deglaciation simulations  
1069 when MISI could be triggered (Gandy et al., 2020; Patton et al., 2015; Petrini et al., 2020; van Aalderen et al., 2024).



1071  
1072 **Figure C2: Ice velocity averaged over the 5000 year simulations using different levels of ice stream refinement. All areas covered by**  
1073 **ice were refined to 16 km in panel (b); the ice sheet remains at 16 km and only areas of ice streaming are refined to the finer**  
1074 **resolutions indicated in panels (c)-(e). Only the ice streaming across the marine section (BKIS) was refined on panel (e).**

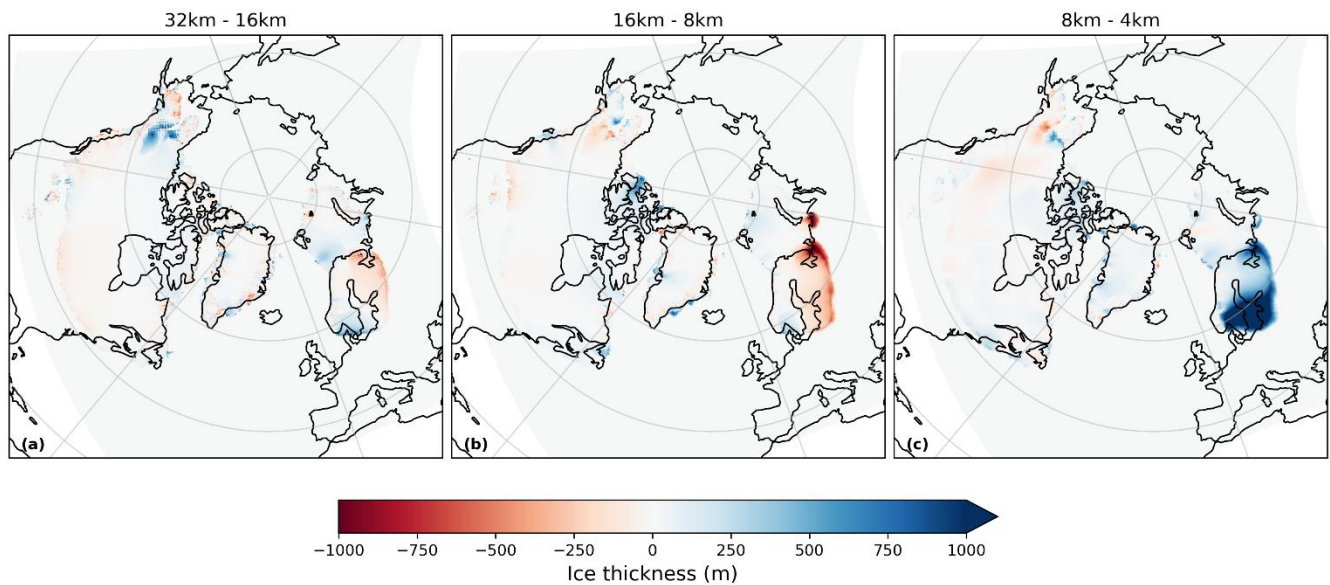


1075

1076

1077

**Figure C3: Difference in ice velocity averaged over the whole ice sheet and 5000 year simulations between the 4km resolution simulation and higher resolutions (8 km, 16 km and 32 km).**



1078

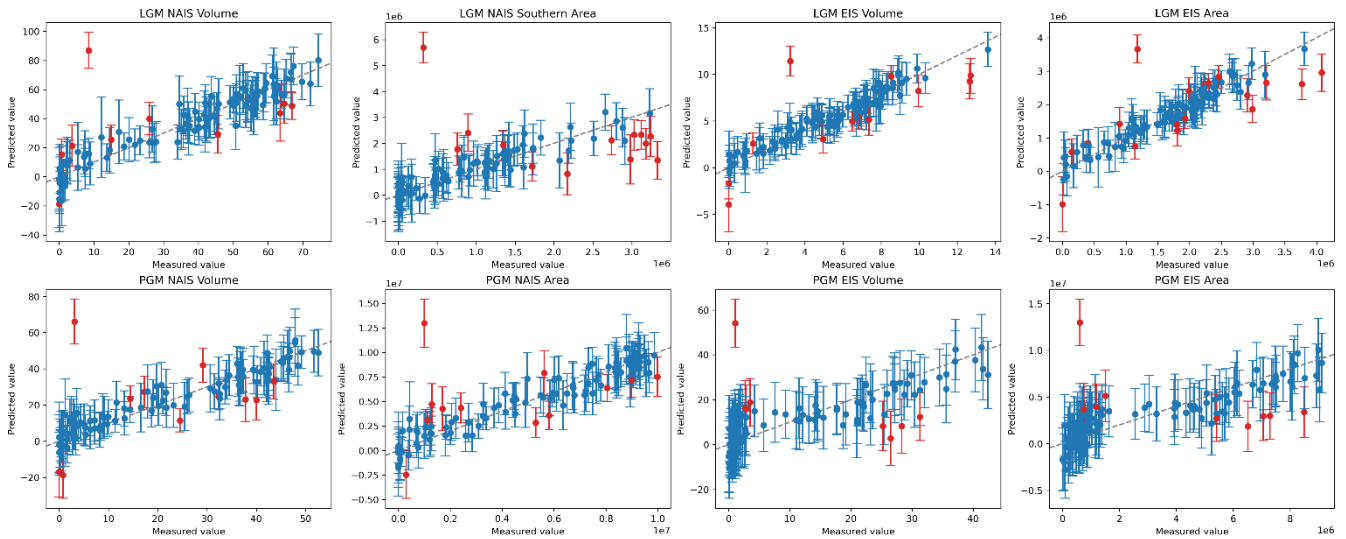
1079

1080

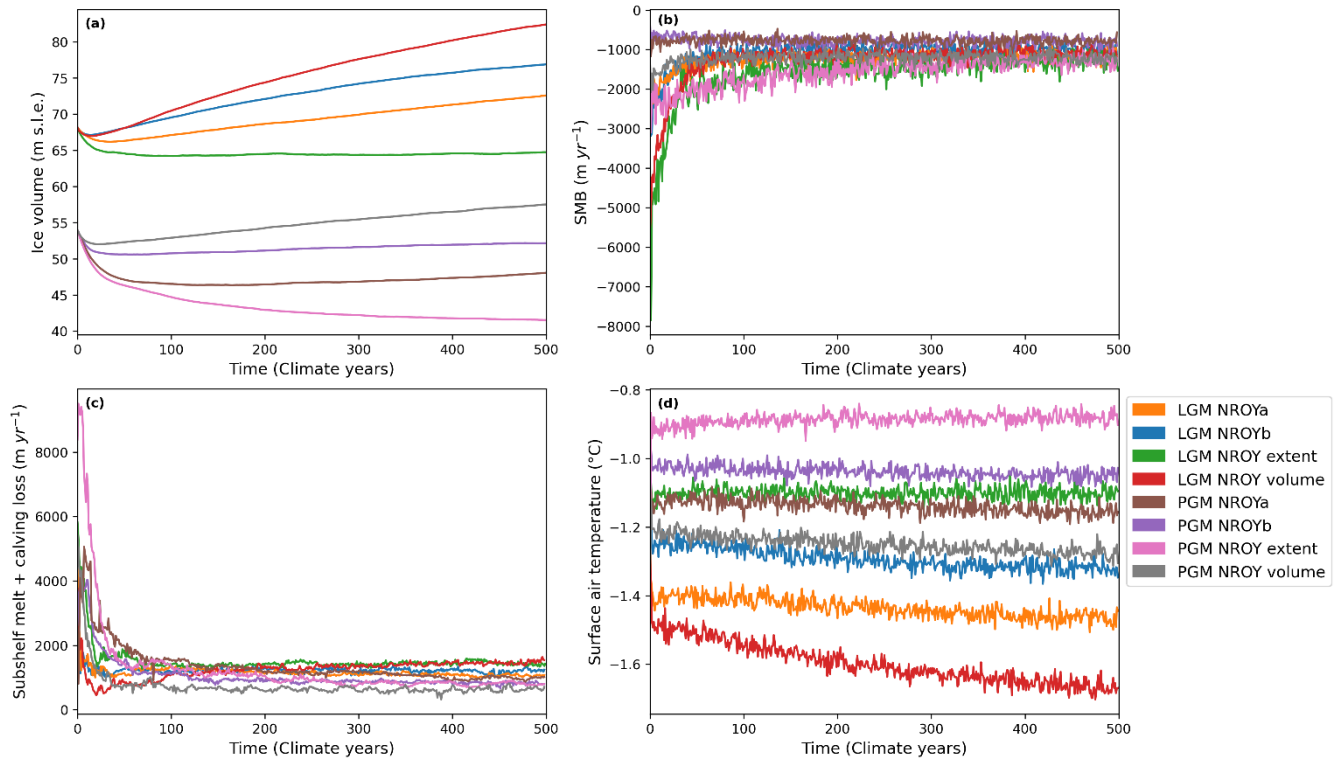
**Figure C4: Difference in final ice sheet thickness between simulations with different levels of refinement**

1081 **Appendix D: Leave-one-out-cross-validation (LOOCV)**

1082 Whilst a large proportion of the predicted diagnostics matched the modelled values within the 95 % credible interval, the  
1083 LOOCV reveals that the Gaussian Process emulator struggled the most with predicting smaller ice sheet volumes and areas.  
1084 This was especially the case for the PGM Eurasian ice sheet where many of the simulations collapsed due to GIA feedbacks  
1085 and non-linearities in ice sheet-climate interactions. There is also one obvious outlier in all eight of the diagnostics where the  
1086 emulator predicted a much higher value than what was actually modelled. This is the same parameter set (xprk/xpruk) for  
1087 each.

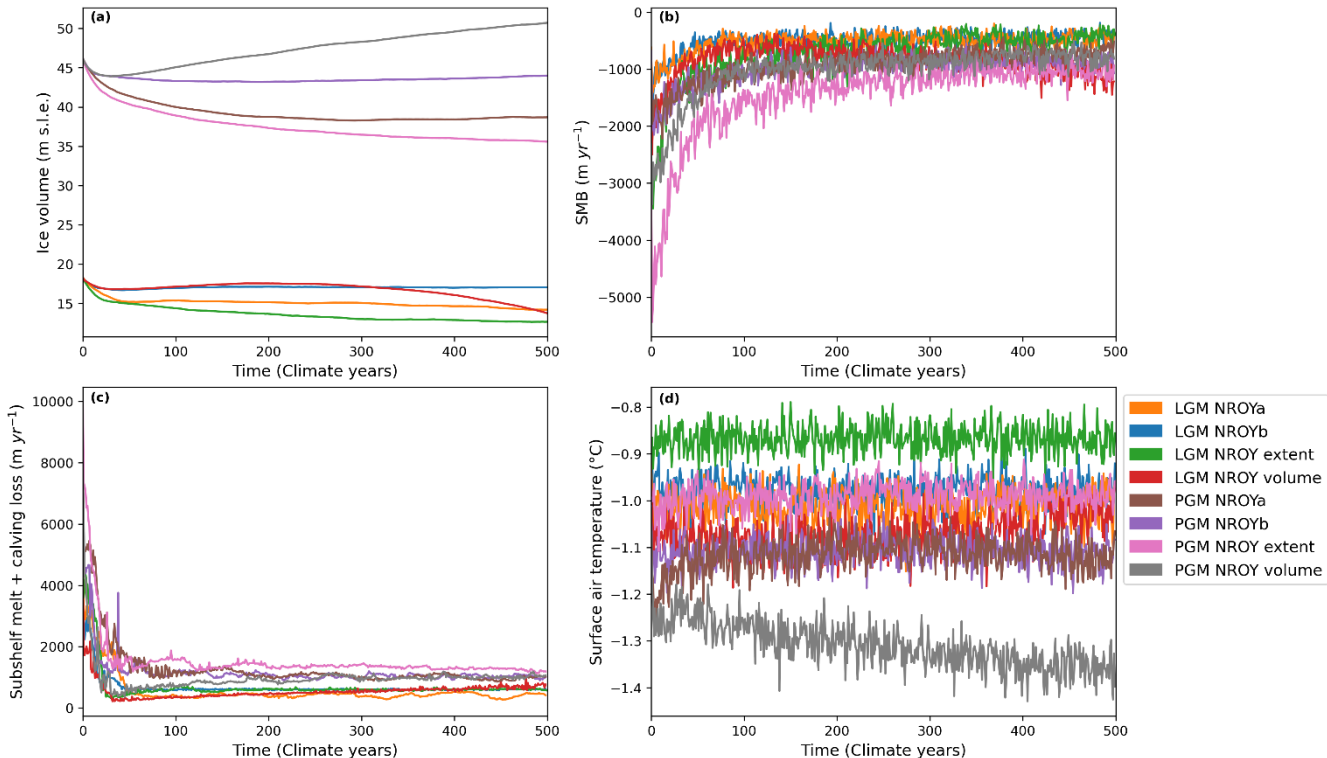


1088  
1089 **Figure D1: The results of the Leave-One-Out Cross Validation performed on emulators for the eight diagnostics. The points show**  
1090 **the value produced by the numerical model against the value predicted by the emulator for the same sets of input parameters. The**  
1091 **line through the centre is the 1:1 line and the error bars show the 95 % credible interval for each point. The points for which the**  
1092 **measured value does not fall within the error bars are highlighted in red.**



1094

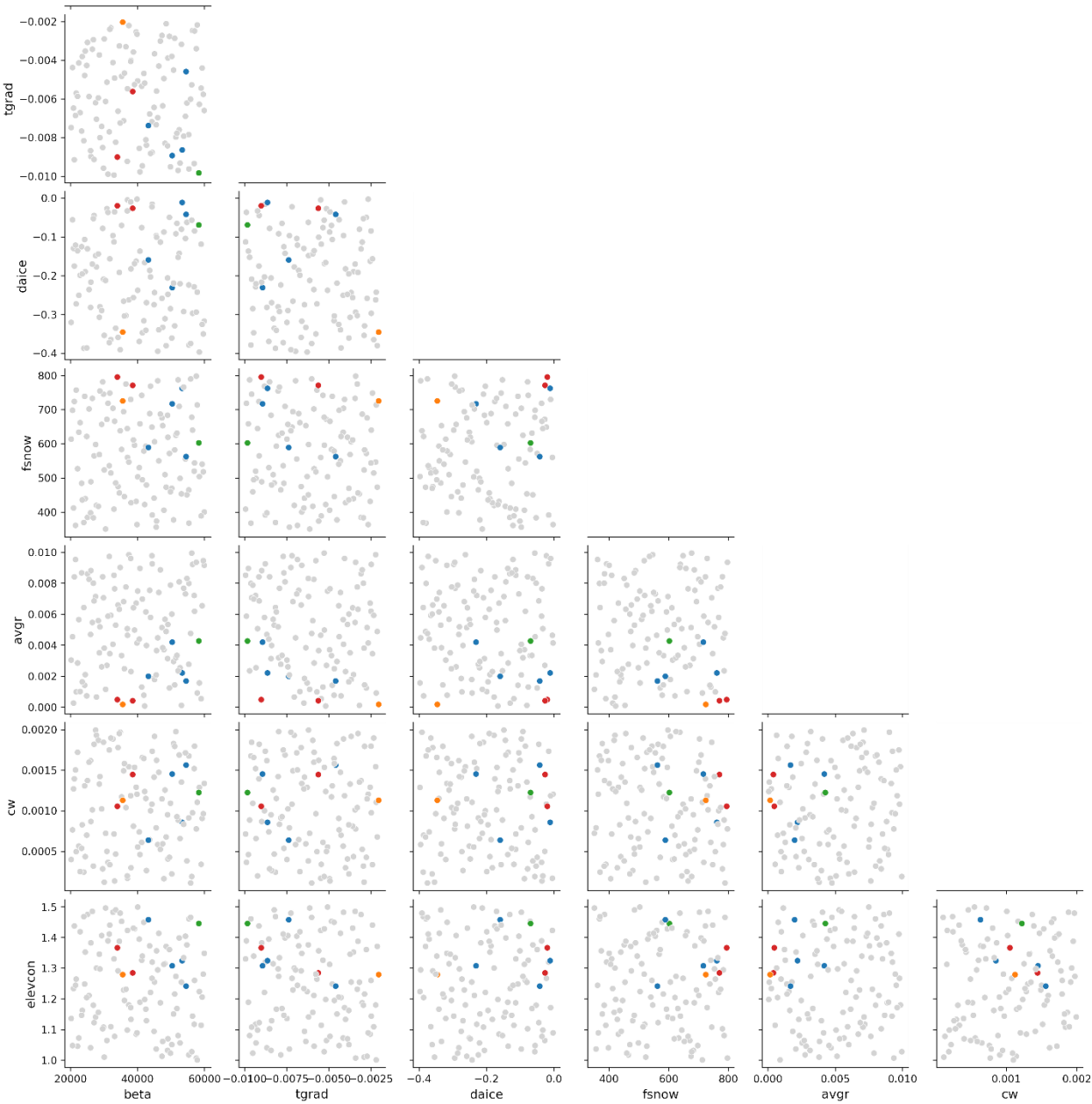
1095 **Figure E1: Time series of variables averaged over North America for the NROY simulations; (a) ice volume; (b) surface mass**  
 1096 **balance; (c) total sub-shelf melt plus calving mass loss; and (d) surface air temperature.**



1098

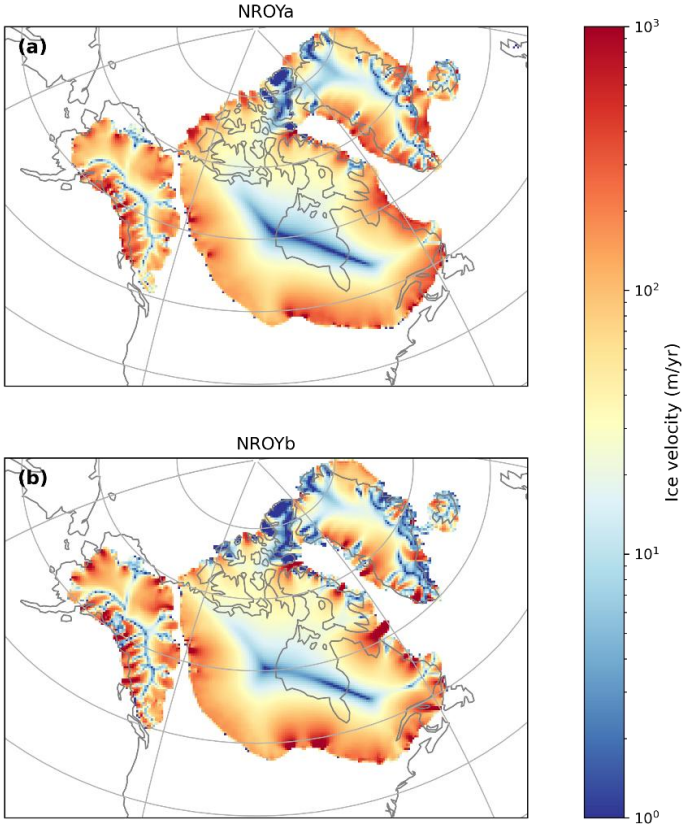
1099 **Figure E2: Time series of variables averaged over Eurasia for the NROY simulations; (a) ice volume; (b) surface mass balance; (c)**  
1100 **total sub-shelf melt plus calving mass loss; and (d) surface air temperature.**

1101



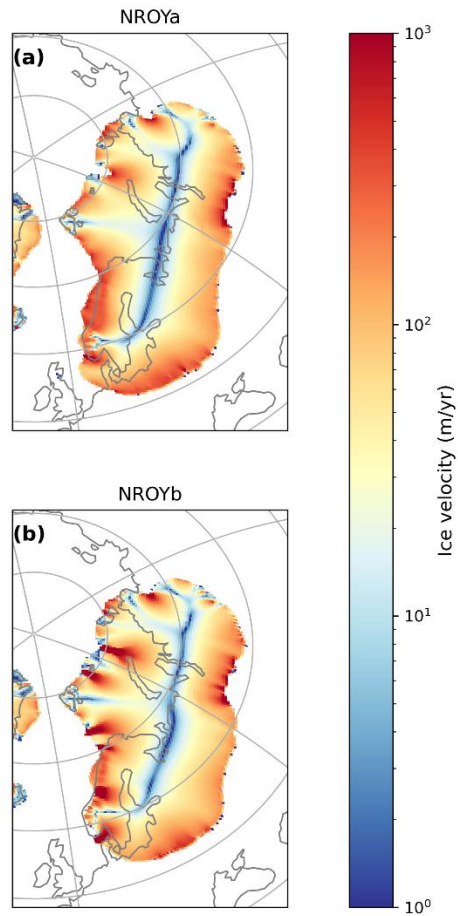
1103

1104 **Figure F1: Parameter pair plot of the most influential parameters with the NROYa and NROYb simulations in red, NROY extent**  
 1105 **simulation in orange, NROY volume simulation in green and the four other simulations that meet the North American ice sheet**  
 1106 **constraints but not the Eurasian in blue.**



1108

1109 Figure G1. North American ice sheet ice velocity at the end of the 5000 ice sheet years for the two equivalent PGM NROY simulations



1110

1111 **Figure G2. Eurasian ice sheet ice velocities at the end of the 5000 ice sheet years for the two equivalent PGM NROY simulations**

1112 **Data availability**

1113 ~~For this pre print, the~~The boundary and initial conditions used in this study as well as the full ensemble final year ice sheet  
 1114 model output and volume and extent metrics, climate timeseries for the NROY simulations and final ice sheet model output  
 1115 from the sensitivity tests ~~have been made available to reviewers.~~are available at  
 1116 <https://dx.doi.org/10.5285/4ce75927eab444b89b5439e33ecf1a80> (Patterson et al., 2025). All other model output data are  
 1117 available on request.

1118 **Supplement link**

1119 **Author contribution**

1120 VLP lead the project and performed the majority of the work. VLP, LJG, RFI, and NG designed the simulations, and VLP  
1121 prepared the initial and boundary conditions, ran the simulations and analysed the results. SC provided technical and scientific  
1122 support in the set-up and updating of BISICLES. SST and RSS implemented and tested the elevcon height adjustment  
1123 parameter. JO provided support on statistical methods including the Sobol analysis and emulation. VLP wrote the manuscript  
1124 with comments and contributions from all co-authors, with particular contribution from SST on the FAMOUS-ice coupling  
1125 and elevcon description. LJG, RFI, and NG supervised the project, and LJG acquired the funding.

1126 **Competing interests**

1127 The authors declare that they have no conflict of interest.

1128 **Acknowledgments**

1129 Violet Patterson would like to thank their supervisors and co-authors for their time, support and valuable input on this study.  
1130 The simulations were run on the high-performance research computing facilities of the University of Leeds, and technical  
1131 support was provided by Richard Rigby from the Centre for Environmental Modelling and Computation (CEMAC). The  
1132 authors would also like to thank Oliver Pollard for his help in creating the PGM ice sheet boundary conditions used in this  
1133 study and his support on the Sobol analysis and GP emulation methodology. Also thank you to Jonathan Gregory for his  
1134 contribution to developing the elevcon height adjustment parameter.

1135 **Financial support**

1136 This research is primarily supported by the “SMB-Gen” UK Research and Innovation Future Leaders Fellowship (grant no.  
1137 MR/S016961/1), with Lauren J. Gregoire, Jonathan Owen, and Niall Gandy supported by the award, and Violet L. Patterson’s  
1138 PhD studentship funded by the University of Leeds. Ruza F. Ivanovic and Robin S. Smith’s contributions were supported by  
1139 the RISICMAP19 NERC standard grant NE/T007443/1. Sam Sherriff-Tadano was funded by JSPS Overseas Research  
1140 Fellowships 202260537.

1141 **References**

1142 van Aalderen, V., Charbit, S., Dumas, C., and Quiquet, A.: Relative importance of the mechanisms triggering the Eurasian ice  
1143 sheet deglaciation, *EGUsphere*, 1–30, <https://doi.org/10.5194/egusphere-2023-34>, 2023.

1144 [van Aalderen, V., Charbit, S., Dumas, C., and Quiquet, A.: Relative importance of the mechanisms triggering the Eurasian ice](https://doi.org/10.5194/cp-20-187-2024)  
1145 [sheet deglaciation in the GRISLI2.0 ice sheet model, \*Clim. Past\*, 20, 187–209, <https://doi.org/10.5194/cp-20-187-2024>, 2024.](https://doi.org/10.5194/cp-20-187-2024)

- 1146 Abe-Ouchi, A., Segawa, T., and Saito, F.: Climatic Conditions for modelling the Northern Hemisphere ice sheets throughout  
1147 the ice age cycle, *Clim. Past*, 3, 423–438, <https://doi.org/10.5194/cp-3-423-2007>, 2007.
- 1148 Abe-Ouchi, A., Saito, F., Kawamura, K., Raymo, M. E., Okuno, J., Takahashi, K., and Blatter, H.: Insolation-driven 100,000-  
1149 year glacial cycles and hysteresis of ice-sheet volume, *Nature*, 500, 190–193, <https://doi.org/10.1038/nature12374>, 2013.
- 1150 Abe-Ouchi, A., Saito, F., Kageyama, M., Braconnot, P., Harrison, S. P., Lambeck, K., Otto-Bliesner, B. L., Peltier, W. R.,  
1151 Tarasov, L., Peterschmitt, J.-Y., and Takahashi, K.: Ice-sheet configuration in the CMIP5/PMIP3 Last Glacial Maximum  
1152 experiments, *Geosci. Model Dev.*, 8, 3621–3637, <https://doi.org/10.5194/gmd-8-3621-2015>, 2015.
- 1153 Albrecht, T., Winkelmann, R., and Levermann, A.: Glacial-cycle simulations of the Antarctic Ice Sheet with the Parallel Ice  
1154 Sheet Model (PISM) – Part 1: Boundary conditions and climatic forcing, *The Cryosphere*, 14, 599–632,  
1155 <https://doi.org/10.5194/tc-14-599-2020>, 2020.
- 1156 Alder, J. R. and Hostetler, S. W.: Applying the Community Ice Sheet Model to evaluate PMIP3 LGM climatologies over the  
1157 North American ice sheets, *Clim. Dyn.*, 53, 2807–2824, <https://doi.org/10.1007/s00382-019-04663-x>, 2019.
- 1158 Alvarez-Solas, J., Banderas, R., Robinson, A., and Montoya, M.: Ocean-driven millennial-scale variability of the Eurasian ice  
1159 sheet during the last glacial period simulated with a hybrid ice-sheet–shelf model, *Clim. Past*, 15, 957–979,  
1160 <https://doi.org/10.5194/cp-15-957-2019>, 2019.
- 1161 Annan, J. D. and Hargreaves, J. C.: A new global reconstruction of temperature changes at the Last Glacial Maximum, *Clim.*  
1162 *Past*, 9, 367–376, <https://doi.org/10.5194/cp-9-367-2013>, 2013.
- 1163 Annan, J. D., Hargreaves, J. C., and Mauritsen, T.: A new global surface temperature reconstruction for the Last Glacial  
1164 Maximum, *Clim. Past*, 18, 1883–1896, <https://doi.org/10.5194/cp-18-1883-2022>, 2022.
- 1165 [Barnett, R. L., Austermann, J., Dyer, B., Telfer, M. W., Barlow, N. L. M., Boulton, S. J., Carr, A. S., and Creel, R. C.:  
1166 Constraining the contribution of the Antarctic Ice Sheet to Last Interglacial sea level, \*Sci. Adv.\*, 9, eadf0198,  
1167 <https://doi.org/10.1126/sciadv.adf0198>, 2023.](https://doi.org/10.1126/sciadv.adf0198)
- 1168 Bastos, L. S. and O’Hagan, A.: Diagnostics for Gaussian Process Emulators, *Technometrics*, 51, 425–438,  
1169 <https://doi.org/10.1198/TECH.2009.08019>, 2009.
- 1170 Batchelor, C. L., Margold, M., Krapp, M., Murton, D. K., Dalton, A. S., Gibbard, P. L., Stokes, C. R., Murton, J. B., and  
1171 Manica, A.: The configuration of Northern Hemisphere ice sheets through the Quaternary, *Nat. Commun.*, 10, 3713,  
1172 <https://doi.org/10.1038/s41467-019-11601-2>, 2019.
- 1173 Beckmann, A. and Goosse, H.: A parameterization of ice shelf–ocean interaction for climate models, *Ocean Model.*, 5, 157–  
1174 170, [https://doi.org/10.1016/S1463-5003\(02\)00019-7](https://doi.org/10.1016/S1463-5003(02)00019-7), 2003.
- 1175 ~~Beghin, P., Charbit, S., Dumas, C., Kageyama, M., Roche, D. M., and Ritz, C.: Interdependence of the growth of the Northern  
1176 Hemisphere ice sheets during the last glaciation: the role of atmospheric circulation, *Clim. Past*, 10, 345–358,  
1177 <https://doi.org/10.5194/cp-10-345-2014>, 2014.~~
- 1178 ~~Beghin, P., Charbit, S., Dumas, C., Kageyama, M., and Ritz, C.: How might the North American ice sheet influence the  
1179 northwestern Eurasian climate?, *Clim. Past*, 11, 1467–1490, <https://doi.org/10.5194/cp-11-1467-2015>, 2015.~~

- 1180 ~~Berdahl, M., Leguy, G., Lipscomb, W. H., Urban, N. M., and Hoffman, M. J.: Exploring ice sheet model sensitivity to ocean~~  
1181 ~~thermal forcing and basal sliding using the Community Ice Sheet Model (CISM), *The Cryosphere*, 17, 1513–1543,~~  
1182 ~~<https://doi.org/10.5194/tc-17-1513-2023>, 2023.~~
- 1183 ~~Bereiter, B., Eggleston, S., Schmitt, J., Nehrbass-Ahles, C., Stocker, T. F., Fischer, H., Kipfstuhl, S., and Chappellaz, J.:~~  
1184 ~~Revision of the EPICA Dome C CO<sub>2</sub> record from 800 to 600 kyr before present, *Geophys. Res. Lett.*, 42, 542–549,~~  
1185 ~~<https://doi.org/10.1002/2014GL061957>, 2015.~~
- 1186 Berends, C. J., Stap, L. B., and Wal, R. S. W. van de: Strong impact of sub-shelf melt parameterisation on ice-sheet retreat in  
1187 idealised and realistic Antarctic topography, *J. Glaciol.*, 69, 1434–1448, <https://doi.org/10.1017/jog.2023.33>, 2023.
- 1188 ~~Berger, A.: Long Term Variations of Daily Insolation and Quaternary Climatic Changes, *J. Atmospheric Sci.*, 35, 2362–2367,~~  
1189 ~~[https://doi.org/10.1175/1520-0469\(1978\)035<2362:LTVODI>2.0.CO;2](https://doi.org/10.1175/1520-0469(1978)035<2362:LTVODI>2.0.CO;2), 1978.~~
- 1190 ~~Berger, A. and Loutre, M. F.: Insolation values for the climate of the last 10 million years, *Quat. Sci. Rev.*, 10, 297–317,~~  
1191 ~~[https://doi.org/10.1016/0277-3791\(91\)90033-Q](https://doi.org/10.1016/0277-3791(91)90033-Q), 1991.~~
- 1192 ~~Bintanja, R., van de Wal, R. S. W., and Oerlemans, J.: Modelled atmospheric temperatures and global sea-levels over the past~~  
1193 ~~million years, *Nature*, 437, 125–128, <https://doi.org/10.1038/nature03975>, 2005.~~
- 1194 Blasco, J., Alvarez-Solas, J., Robinson, A., and Montoya, M.: Exploring the impact of atmospheric forcing and basal drag on  
1195 the Antarctic Ice Sheet under Last Glacial Maximum conditions, *The Cryosphere*, 15, 215–231, [https://doi.org/10.5194/tc-15-](https://doi.org/10.5194/tc-15-215-2021)  
1196 [215-2021](https://doi.org/10.5194/tc-15-215-2021), 2021.
- 1197 Blatter, H., Greve, R., and Abe-Ouchi, A.: A short history of the thermomechanical theory and modeling of glaciers and ice  
1198 sheets, *J. Glaciol.*, 56, 1087–1094, <https://doi.org/10.3189/002214311796406059>, 2010.
- 1199 ~~Braconnot, P., Harrison, S. P., Kageyama, M., Bartlein, P. J., Masson Delmotte, V., Abe Ouchi, A., Otto-Bliesner, B., and~~  
1200 ~~Zhao, Y.: Evaluation of climate models using palaeoclimatic data, *Nat. Clim. Change*, 2, 417–424,~~  
1201 ~~<https://doi.org/10.1038/nclimate1456>, 2012.~~
- 1202 Bradley, S. L., Sellevold, R., Petrini, M., Vizcaino, M., Georgiou, S., Zhu, J., Otto-Bliesner, B. L., and Lofverstrom, M.:  
1203 Surface mass balance and climate of the Last Glacial Maximum Northern Hemisphere ice sheets: simulations with CESM2.1,  
1204 *Clim. Past*, 20, 211–235, <https://doi.org/10.5194/cp-20-211-2024>, 2024.
- 1205 Briggs, R. D., Pollard, D., and Tarasov, L.: A data-constrained large ensemble analysis of Antarctic evolution since the Eemian,  
1206 *Quat. Sci. Rev.*, 103, 91–115, <https://doi.org/10.1016/j.quascirev.2014.09.003>, 2014.
- 1207 Bueler, E. and van Pelt, W.: Mass-conserving subglacial hydrology in the Parallel Ice Sheet Model version 0.6, *Geosci. Model*  
1208 *Dev.*, 8, 1613–1635, <https://doi.org/10.5194/gmd-8-1613-2015>, 2015.
- 1209 ~~[Capron, É., Govin, A., and Stone, E. J.: Recent advances on the dynamical representation and our understanding of the](https://doi.org/10.4000/quarternaire.8029)~~  
1210 ~~[warmer-than-present last interglacial climate, \*Quat. Rev. Assoc. Fr. Pour L'étude Quat.\*, 185–193,](https://doi.org/10.4000/quarternaire.8029)~~  
1211 ~~<https://doi.org/10.4000/quarternaire.8029>, 2017.~~
- 1212 Charbit, S., Ritz, C., Philippon, G., Peyaud, V., and Kageyama, M.: Numerical reconstructions of the Northern Hemisphere  
1213 ice sheets through the last glacial-interglacial cycle, *Clim. Past*, 3, 15–37, <https://doi.org/10.5194/cp-3-15-2007>, 2007.
- 1214 Clark, C. D., Ely, J. C., Hindmarsh, R. C. A., Bradley, S., Ignéczi, A., Fabel, D., Ó Cofaigh, C., Chiverrell, R. C., Scourse, J.,  
1215 Benetti, S., Bradwell, T., Evans, D. J. A., Roberts, D. H., Burke, M., Callard, S. L., Medialdea, A., Saher, M., Small, D.,

- 1216 Smedley, R. K., Gasson, E., Gregoire, L., Gandy, N., Hughes, A. L. C., Ballantyne, C., Bateman, M. D., Bigg, G. R., Doole,  
1217 J., Dove, D., Duller, G. A. T., Jenkins, G. T. H., Livingstone, S. L., McCarron, S., Moreton, S., Pollard, D., Praeg, D., Sejrup,  
1218 H. P., Van Landeghem, K. J. J., and Wilson, P.: Growth and retreat of the last British–Irish Ice Sheet, 31 000 to 15 000 years  
1219 ago: the BRITICE-CHRONO reconstruction, *Boreas*, 51, 699–758, <https://doi.org/10.1111/bor.12594>, 2022.
- 1220 Clark, P. U., ~~Dyke, A. S., Shakun, J. D., Carlson, A. E., Clark, J., Wohlfarth, B., Mitrovica, J. X., Hostetler, S. W., and McCabe,~~  
1221 ~~A. M.: The Last Glacial Maximum, *Science*, 325, 710–714, <https://doi.org/10.1126/science.1172873>, 2009.~~
- 1222 ~~Clark, P. U.,~~ He, F., Golledge, N. R., Mitrovica, J. X., Dutton, A., Hoffman, J. S., and Dendy, S.: Oceanic forcing of penultimate  
1223 deglacial and last interglacial sea-level rise, *Nature*, 577, 660–664, <https://doi.org/10.1038/s41586-020-1931-7>, 2020.
- 1224 ~~Colleoni, F., Krinner, G., Jakobsson, M., Peyaud, V., and Ritz, C.: Influence of regional parameters on the surface mass balance~~  
1225 ~~of the Eurasian ice sheet during the peak Saalian (140 kya), *Glob. Planet. Change*, 68, 132–148,~~  
1226 ~~<https://doi.org/10.1016/j.gloplacha.2009.03.021>, 2009a.~~
- 1227 ~~Colleoni, F., Krinner, G.,~~ and Jakobsson, M.: Sensitivity of the Late Saalian (140 kyrs BP) and LGM (21 kyrs BP) Eurasian  
1228 ice sheet surface mass balance to vegetation feedbacks, *Geophys. Res. Lett.*, 36, <https://doi.org/10.1029/2009GL037200>,  
1229 [2009b](https://doi.org/10.1029/2009GL037200) [2009](https://doi.org/10.1029/2009GL037200).
- 1230 ~~Colleoni, F., Liakka, J., Krinner, G., Jakobsson, M., Masina, S., and Peyaud, V.: The sensitivity of the Late Saalian (140 ka)~~  
1231 ~~and LGM (21 ka) Eurasian ice sheets to sea surface conditions, *Clim. Dyn.*, 37, 531–553, [https://doi.org/10.1007/s00382-010-](https://doi.org/10.1007/s00382-010-0870-7)  
1232 [0870-7](https://doi.org/10.1007/s00382-010-0870-7), 2011.~~
- 1233 Colleoni, F., Wekerle, C., Näslund, J.-O., Brandefelt, J., and Masina, S.: Constraint on the penultimate glacial maximum  
1234 Northern Hemisphere ice topography ( $\approx$ 140 kyrs BP), *Quat. Sci. Rev.*, 137, 97–112,  
1235 <https://doi.org/10.1016/j.quascirev.2016.01.024>, 2016.
- 1236 Cornford, S. L., Martin, D. F., Graves, D. T., Ranken, D. F., Le Brocq, A. M., Gladstone, R. M., Payne, A. J., Ng, E. G., and  
1237 Lipscomb, W. H.: Adaptive mesh, finite volume modeling of marine ice sheets, *J. Comput. Phys.*, 232, 529–549,  
1238 <https://doi.org/10.1016/j.jcp.2012.08.037>, 2013.
- 1239 Cornford, S. L., Martin, D. F., Payne, A. J., Ng, E. G., Le Brocq, A. M., Gladstone, R. M., Edwards, T. L., Shannon, S. R.,  
1240 Agosta, C., van den Broeke, M. R., Hellmer, H. H., Krinner, G., Ligtenberg, S. R. M., Timmermann, R., and Vaughan, D. G.:  
1241 Century-scale simulations of the response of the West Antarctic Ice Sheet to a warming climate, *The Cryosphere*, 9, 1579–  
1242 1600, <https://doi.org/10.5194/tc-9-1579-2015>, 2015.
- 1243 Couette, P.-O., Lajeunesse, P., Ghienne, J.-F., Dorschel, B., Gebhardt, C., Hebbeln, D., and Brouard, E.: Evidence for an  
1244 extensive ice shelf in northern Baffin Bay during the Last Glacial Maximum, *Commun. Earth Environ.*, 3, 1–12,  
1245 <https://doi.org/10.1038/s43247-022-00559-7>, 2022.
- 1246 Crucifix, M. and Hewitt, C. D.: Impact of vegetation changes on the dynamics of the atmosphere at the Last Glacial Maximum,  
1247 *Clim. Dyn.*, 25, 447–459, <https://doi.org/10.1007/s00382-005-0013-8>, 2005.
- 1248 Dalton, A. S., Margold, M., Stokes, C. R., Tarasov, L., Dyke, A. S., Adams, R. S., Allard, S., Arends, H. E., Atkinson, N.,  
1249 Attig, J. W., Barnett, P. J., Barnett, R. L., Batterson, M., Bernatchez, P., Borns, H. W., Breckenridge, A., Briner, J. P., Brouard,  
1250 E., Campbell, J. E., Carlson, A. E., Clague, J. J., Curry, B. B., Daigneault, R.-A., Dubé-Loubert, H., Easterbrook, D. J., Franzi,  
1251 D. A., Friedrich, H. G., Funder, S., Gauthier, M. S., Gowan, A. S., Harris, K. L., Héту, B., Hooyer, T. S., Jennings, C. E.,  
1252 Johnson, M. D., Kehew, A. E., Kelley, S. E., Kerr, D., King, E. L., Kjeldsen, K. K., Knaeble, A. R., Lajeunesse, P., Lakeman,  
1253 T. R., Lamothe, M., Larson, P., Lavoie, M., Loope, H. M., Lowell, T. V., Lusardi, B. A., Manz, L., McMartin, I., Nixon, F.  
1254 C., Occhietti, S., Parkhill, M. A., Piper, D. J. W., Pronk, A. G., Richard, P. J. H., Ridge, J. C., Ross, M., Roy, M., Seaman, A.,

- 1255 Shaw, J., Stea, R. R., Teller, J. T., Thompson, W. B., Thorleifson, L. H., Utting, D. J., Veillette, J. J., Ward, B. C., Weddle, T.  
 1256 K., and Wright, H. E.: An updated radiocarbon-based ice margin chronology for the last deglaciation of the North American  
 1257 Ice Sheet Complex, *Quat. Sci. Rev.*, 234, 106223, <https://doi.org/10.1016/j.quascirev.2020.106223>, 2020.
- 1258 Dalton, A. S., Stokes, C. R., and Batchelor, C. L.: Evolution of the Laurentide and Innuitian ice sheets prior to the Last Glacial  
 1259 Maximum (115 ka to 25 ka), *Earth-Sci. Rev.*, 224, 103875, <https://doi.org/10.1016/j.earscirev.2021.103875>, 2022.
- 1260 Dalton, A. S., Dulfer, H. E., Margold, M., Heyman, J., Clague, J. J., Froese, D. G., Gauthier, M. S., Hughes, A. L. C., Jennings,  
 1261 C. E., Norris, S. L., and Stoker, B. J.: Deglaciation of the north American ice sheet complex in calendar years based on a  
 1262 comprehensive database of chronological data: NADI-1, *Quat. Sci. Rev.*, 321, 108345,  
 1263 <https://doi.org/10.1016/j.quascirev.2023.108345>, 2023.
- 1264 DeConto, R. M. and Pollard, D.: Contribution of Antarctica to past and future sea-level rise, *Nature*, 531, 591–597,  
 1265 <https://doi.org/10.1038/nature17145>, 2016.
- 1266 Dentith, J. E., Ivanovic, R. F., Gregoire, L. J., Tindall, J. C., and Robinson, L. F.: Simulating stable carbon isotopes in the  
 1267 ocean component of the FAMOUS general circulation model with MOSES1 (XOAVI), *Geosci. Model Dev.*, 13, 3529–3552,  
 1268 <https://doi.org/10.5194/gmd-13-3529-2020>, 2020.
- 1269 Depoorter, M. A., Bamber, J. L., Griggs, J. A., Lenaerts, J. T. M., Ligtenberg, S. R. M., van den Broeke, M. R., and Moholdt,  
 1270 G.: Calving fluxes and basal melt rates of Antarctic ice shelves, *Nature*, 502, 89–92, <https://doi.org/10.1038/nature12567>,  
 1271 2013.
- 1272 [Dong, B. and Valdes, P. J.: \*Climates at the Last Glacial Maximum: Influence of Model Horizontal Resolution\*, 2000.](#)
- 1273 Drew, M. and Tarasov, L.: Surging of a Hudson Strait-scale ice stream: subglacial hydrology matters but the process details  
 1274 mostly do not, *The Cryosphere*, 17, 5391–5415, <https://doi.org/10.5194/tc-17-5391-2023>, 2023.
- 1275 [Dutton, A. and Lambeck, K.: \*Ice Volume and Sea Level During the Last Interglacial\*, \*Science\*, 337, 216–219,](#)  
 1276 <https://doi.org/10.1126/science.1205749>, 2012.
- 1277 [Dutton, A., Carlson, A. E., Long, A. J., Milne, G. A., Clark, P. U., DeConto, R., Horton, B. P., Rahmstorf, S., and Raymo, M.](#)  
 1278 [E.: \*Sea-level rise due to polar ice-sheet mass loss during past warm periods\*, \*Science\*, 349, aaa4019,](#)  
 1279 <https://doi.org/10.1126/science.aaa4019>, 2015.
- 1280 Dyer, B., Austermann, J., D’Andrea, W. J., Creel, R. C., Sandstrom, M. R., Cashman, M., Rovere, A., and Raymo, M. E.: Sea-  
 1281 level trends across The Bahamas constrain peak last interglacial ice melt, *Proc. Natl. Acad. Sci.*, 118, e2026839118,  
 1282 <https://doi.org/10.1073/pnas.2026839118>, 2021.
- 1283 Dyke, A. S., Andrews, J. T., Clark, P. U., England, J. H., Miller, G. H., Shaw, J., and Veillette, J. J.: The Laurentide and  
 1284 Innuitian ice sheets during the Last Glacial Maximum, *Quat. Sci. Rev.*, 21, 9–31, [https://doi.org/10.1016/S0277-](https://doi.org/10.1016/S0277-3791(01)00095-6)  
 1285 [3791\(01\)00095-6](https://doi.org/10.1016/S0277-3791(01)00095-6), 2002.
- 1286 Edwards, T. L., Brandon, M. A., Durand, G., Edwards, N. R., Golledge, N. R., Holden, P. B., Nias, I. J., Payne, A. J., Ritz, C.,  
 1287 and Wernecke, A.: Revisiting Antarctic ice loss due to marine ice-cliff instability, *Nature*, 566, 58–64,  
 1288 <https://doi.org/10.1038/s41586-019-0901-4>, 2019.
- 1289 [Edwards, T. L., Nowicki, S., Marzeion, B., Hock, R., Goelzer, H., Seroussi, H., Jourdain, N. C., Slater, D. A., Turner, F. E.,](#)  
 1290 [Smith, C. J., McKenna, C. M., Simon, E., Abe Ouchi, A., Gregory, J. M., Larour, E., Lipscomb, W. H., Payne, A. J., Shepherd,](#)  
 1291 [A., Agosta, C., Alexander, P., Albrecht, T., Anderson, B., Asay Davis, X., Aschwanden, A., Barthel, A., Bliss, A., Calov, R.,](#)

- 1292 Chambers, C., Champollion, N., Choi, Y., Cullather, R., Cuzzone, J., Dumas, C., Felikson, D., Fettweis, X., Fujita, K., Galton-  
1293 Fenzi, B. K., Gladstone, R., Golledge, N. R., Greve, R., Hattermann, T., Hoffman, M. J., Humbert, A., Huss, M., Huybrechts,  
1294 P., Immerzeel, W., Kleiner, T., Kraaijenbrink, P., Le clec'h, S., Lee, V., Leguy, G. R., Little, C. M., Lowry, D. P., Malles, J.,  
1295 H., Martin, D. F., Maussion, F., Morlighem, M., O'Neill, J. F., Nias, I., Pattyn, F., Pelle, T., Price, S. F., Quiquet, A., Radić,  
1296 V., Reese, R., Rounce, D. R., Rückamp, M., Sakai, A., Shafer, C., Schlegel, N. J., Shannon, S., Smith, R. S., Straneo, F., Sun,  
1297 S., Tarasov, L., Trusel, L. D., Van Breedam, J., van de Wal, R., van den Broeke, M., Winkelmann, R., Zekollari, H., Zhao, C.,  
1298 Zhang, T., and Zwinger, T.: Projected land ice contributions to twenty first century sea level rise, *Nature*, 593, 74–82,  
1299 <https://doi.org/10.1038/s41586-021-03302-y>, 2021.
- 1300 Ehlers, J., Gibbard, P. L., and Hughes, P. D.: Chapter 4 - Quaternary Glaciations and Chronology, in: *Past Glacial*  
1301 *Environments (Second Edition)*, edited by: Menzies, J. and van der Meer, J. J. M., Elsevier, 77–101,  
1302 <https://doi.org/10.1016/B978-0-08-100524-8.00003-8>, 2018.
- 1303 Essery, R. L. H., Best, M. J., Betts, R. A., Cox, P. M., and Taylor, C. M.: Explicit Representation of Subgrid Heterogeneity in  
1304 a GCM Land Surface Scheme, *J. Hydrometeorol.*, 4, 530–543, [https://doi.org/10.1175/1525-](https://doi.org/10.1175/1525-7541(2003)004<0530:EROSHI>2.0.CO;2)  
1305 [7541\(2003\)004<0530:EROSHI>2.0.CO;2](https://doi.org/10.1175/1525-7541(2003)004<0530:EROSHI>2.0.CO;2), 2003.
- 1306 Favier, L., Jourdain, N. C., Jenkins, A., Merino, N., Durand, G., Gagliardini, O., Gillet-Chaulet, F., and Mathiot, P.:  
1307 Assessment of sub-shelf melting parameterisations using the ocean–ice-sheet coupled model NEMO(v3.6)–Elmer/Ice(v8.3),  
1308 *Geosci. Model Dev.*, 12, 2255–2283, <https://doi.org/10.5194/gmd-12-2255-2019>, 2019.
- 1309 Fettweis, X., Franco, B., Tedesco, M., van Angelen, J. H., Lenaerts, J. T. M., van den Broeke, M. R., and Gallée, H.: Estimating  
1310 the Greenland ice sheet surface mass balance contribution to future sea level rise using the regional atmospheric climate model  
1311 MAR, *The Cryosphere*, 7, 469–489, <https://doi.org/10.5194/tc-7-469-2013>, 2013.
- 1312 [Fyke, J., Sergienko, O., Löffverström, M., Price, S., and Lenaerts, J. T. M.: An Overview of Interactions and Feedbacks Between](https://doi.org/10.1029/2018RG000600)  
1313 [Ice Sheets and the Earth System, \*Rev. Geophys.\*, 56, 361–408, <https://doi.org/10.1029/2018RG000600>, 2018.](https://doi.org/10.1029/2018RG000600)
- 1314 [Fyke, J. G., Sacks, W. J., and Lipscomb, W. H.: A technique for generating consistent ice sheet initial conditions for coupled](https://doi.org/10.5194/gmd-7-1183-2014)  
1315 [ice sheet/climate models, \*Geosci. Model Dev.\*, 7, 1183–1195, <https://doi.org/10.5194/gmd-7-1183-2014>, 2014.](https://doi.org/10.5194/gmd-7-1183-2014)
- 1316 Gandy, N., Gregoire, L. J., Ely, J. C., Clark, C. D., Hodgson, D. M., Lee, V., Bradwell, T., and Ivanovic, R. F.: Marine ice  
1317 sheet instability and ice shelf buttressing of the Minch Ice Stream, northwest Scotland, *The Cryosphere*, 12, 3635–3651,  
1318 <https://doi.org/10.5194/tc-12-3635-2018>, 2018.
- 1319 Gandy, N., Gregoire, L. J., Ely, J. C., Cornford, S. L., Clark, C. D., and Hodgson, D. M.: Exploring the ingredients required  
1320 to successfully model the placement, generation, and evolution of ice streams in the British-Irish Ice Sheet, *Quat. Sci. Rev.*,  
1321 223, 105915, <https://doi.org/10.1016/j.quascirev.2019.105915>, 2019.
- 1322 Gandy, N., Gregoire, L. J., Ely, J. C., Cornford, S. L., Clark, C. D., and Hodgson, D. M.: Collapse of the Last Eurasian Ice  
1323 Sheet in the North Sea Modulated by Combined Processes of Ice Flow, Surface Melt, and Marine Ice Sheet Instabilities, *J.*  
1324 *Geophys. Res. Earth Surf.*, 126, e2020JF005755, <https://doi.org/10.1029/2020JF005755>, 2021.
- 1325 Gandy, N., Astfalck, L. C., Gregoire, L. J., Ivanovic, R. F., Patterson, V. L., Sherriff-Tadano, S., Smith, R. S., Williamson, D.,  
1326 and Rigby, R.: De-Tuning Albedo Parameters in a Coupled Climate Ice Sheet Model to Simulate the North American Ice Sheet  
1327 at the Last Glacial Maximum, *J. Geophys. Res. Earth Surf.*, 128, e2023JF007250, <https://doi.org/10.1029/2023JF007250>,  
1328 2023.
- 1329 Ganopolski, A., Calov, R., and Claussen, M.: Simulation of the last glacial cycle with a coupled climate ice-sheet model of  
1330 intermediate complexity, *Clim. Past*, 6, 229–244, <https://doi.org/10.5194/cp-6-229-2010>, 2010.

- 1331 ~~Golledge, N. R., Keller, E. D., Gomez, N., Naughten, K. A., Bernales, J., Trusel, L. D., and Edwards, T. L.: Global~~  
1332 ~~environmental consequences of twenty first century ice sheet melt, *Nature*, 566, 65–72, [https://doi.org/10.1038/s41586-019-](https://doi.org/10.1038/s41586-019-0889-9)~~  
1333 ~~0889-9, 2019.~~
- 1334 Gomez, N., Mitrovica, J. X., Huybers, P., and Clark, P. U.: Sea level as a stabilizing factor for marine-ice-sheet grounding  
1335 lines, *Nat. Geosci.*, 3, 850–853, <https://doi.org/10.1038/ngeo1012>, 2010.
- 1336 ~~Gordon, C., Cooper, C., Senior, C. A., Banks, H., Gregory, J. M., Johns, T. C., Mitchell, J. F. B., and Wood, R. A.: The~~  
1337 ~~simulation of SST, sea ice extents and ocean heat transports in a version of the Hadley Centre coupled model without flux~~  
1338 ~~adjustments, *Clim. Dyn.*, 16, 147–168, <https://doi.org/10.1007/s003820050010>, 2000.~~
- 1339 [Govin, A., Capron, E., Tzedakis, P. C., Verheyden, S., Ghaleb, B., Hillaire-Marcel, C., St-Onge, G., Stoner, J. S., Bassinot, F.,](#)  
1340 [Bazin, L., Blunier, T., Combourieu-Nebout, N., El Ouahabi, A., Genty, D., Gersonde, R., Jimenez-Amat, P., Landais, A.,](#)  
1341 [Martrat, B., Masson-Delmotte, V., Parrenin, F., Seidenkrantz, M.-S., Veres, D., Waelbroeck, C., and Zahn, R.: Sequence of](#)  
1342 [events from the onset to the demise of the Last Interglacial: Evaluating strengths and limitations of chronologies used in](#)  
1343 [climatic archives, \*Quat. Sci. Rev.\*, 129, 1–36, <https://doi.org/10.1016/j.quascirev.2015.09.018>, 2015.](#)
- 1344 Gregoire, L. J., Valdes, P. J., Payne, A. J., and Kahana, R.: Optimal tuning of a GCM using modern and glacial constraints,  
1345 *Clim. Dyn.*, 37, 705–719, <https://doi.org/10.1007/s00382-010-0934-8>, 2011.
- 1346 Gregoire, L. J., Payne, A. J., and Valdes, P. J.: Deglacial rapid sea level rises caused by ice-sheet saddle collapses, *Nature*,  
1347 487, 219–222, <https://doi.org/10.1038/nature11257>, 2012.
- 1348 Gregoire, L. J., Otto-Bliesner, B., Valdes, P. J., and Ivanovic, R.: Abrupt Bølling warming and ice saddle collapse contributions  
1349 to the Meltwater Pulse 1a rapid sea level rise, *Geophys. Res. Lett.*, 43, 9130–9137, <https://doi.org/10.1002/2016GL070356>,  
1350 2016.
- 1351 [Gregoire, L. J., Ivanovic, R. F., Maycock, A. C., Valdes, P. J., and Stevenson, S.: Holocene lowering of the Laurentide ice](#)  
1352 [sheet affects North Atlantic gyre circulation and climate, \*Clim. Dyn.\*, 51, 3797–3813, \[https://doi.org/10.1007/s00382-018-\]\(https://doi.org/10.1007/s00382-018-4111-9\)](#)  
1353 [4111-9, 2018.](#)
- 1354 Gregory, J. M., Browne, O. J. H., Payne, A. J., Ridley, J. K., and Rutt, I. C.: Modelling large-scale ice-sheet–climate  
1355 interactions following glacial inception, *Clim. Past*, 8, 1565–1580, <https://doi.org/10.5194/cp-8-1565-2012>, 2012.
- 1356 Gregory, J. M., George, S. E., and Smith, R. S.: Large and irreversible future decline of the Greenland ice sheet, *The*  
1357 *Cryosphere*, 14, 4299–4322, <https://doi.org/10.5194/tc-14-4299-2020>, 2020.
- 1358 ~~Harrison, S. P., Bartlein, P. J., and Prentice, I. C.: What have we learnt from palaeoclimate simulations?, *J. Quat. Sci.*, 31, 363–~~  
1359 ~~385, <https://doi.org/10.1002/jqs.2842>, 2016.~~
- 1360 Heine, J. T. and Mctigue, D. F.: A case for cold-based continental ice sheets — a transient thermal model, *J. Glaciol.*, 42, 37–  
1361 42, <https://doi.org/10.3189/S0022143000030513>, 1996.
- 1362 Hemming, S. R.: Heinrich events: Massive late Pleistocene detritus layers of the North Atlantic and their global climate  
1363 imprint, *Rev. Geophys.*, 42, <https://doi.org/10.1029/2003RG000128>, 2004.
- 1364 ~~Heymsfield, A.: Precipitation Development in Stratiform Ice Clouds: A Microphysical and Dynamical Study, *J. Atmos. Sci.*,~~  
1365 ~~<https://journals.ametsoc.org/view/journals/atsc/34,> ~~367–381,~~ ~~[https://doi.org/10.1175/1520-](https://doi.org/10.1175/1520-0469(1977)034<0367:PDISIC>2.0.CO;2)~~~~  
1366 ~~[0469\(1977\)034<0367:PDISIC>2.0.CO;2,](https://doi.org/10.1175/1520-0469(1977)034<0367:PDISIC>2.0.CO;2) ~~1977/2/1520-0469~~ ~~1977 034 0367~~ ~~pdisc 2 0 co 2.xml~~, last access: 7 February~~  
1367 ~~2024.~~

- 1368 Hindmarsh, R. C. A.: Consistent generation of ice-streams via thermo-viscous instabilities modulated by membrane stresses,  
1369 *Geophys. Res. Lett.*, 36, <https://doi.org/10.1029/2008GL036877>, 2009.
- 1370 ~~Hofer, D., Raible, C. C., Dehnert, A., and Kuhlemann, J.: The impact of different glacial boundary conditions on atmospheric~~  
1371 ~~dynamics and precipitation in the North Atlantic region, *Clim. Past*, 8, 935–949, <https://doi.org/10.5194/ep-8-935-2012>, 2012.~~
- 1372 ~~Hofer, S., Tedstone, A. J., Fettweis, X., and Bamber, J. L.: Decreasing cloud cover drives the recent mass loss on the Greenland~~  
1373 ~~Ice Sheet, *Sci. Adv.*, 3, e1700584, <https://doi.org/10.1126/sciadv.1700584>, 2017.~~
- 1374 Holden, P. B., Edwards, N. R., Oliver, K. I. C., Lenton, T. M., and Wilkinson, R. D.: A probabilistic calibration of climate  
1375 sensitivity and terrestrial carbon change in GENIE-1, *Clim. Dyn.*, 35, 785–806, <https://doi.org/10.1007/s00382-009-0630-8>,  
1376 2010.
- 1377 Holland, P. R., Jenkins, A., and Holland, D. M.: The Response of Ice Shelf Basal Melting to Variations in Ocean Temperature,  
1378 *J. Clim.*, 21, 2558–2572, <https://doi.org/10.1175/2007JCLI1909.1>, 2008.
- 1379 Hubbard, A., Bradwell, T., Golledge, N., Hall, A., Patton, H., Sugden, D., Cooper, R., and Stoker, M.: Dynamic cycles, ice  
1380 streams and their impact on the extent, chronology and deglaciation of the British–Irish ice sheet, *Quat. Sci. Rev.*, 28, 758–  
1381 776, <https://doi.org/10.1016/j.quascirev.2008.12.026>, 2009.
- 1382 Hughes, A. L. C., Gyllencreutz, R., Lohne, Ø. S., Mangerud, J., and Svendsen, J. I.: The last Eurasian ice sheets – a  
1383 chronological database and time-slice reconstruction, *DATED-1, Boreas*, 45, 1–45, <https://doi.org/10.1111/bor.12142>, 2016.
- 1384 Hughes, P. D. and Gibbard, P. L.: Global glacier dynamics during 100 ka Pleistocene glacial cycles, *Quat. Res.*, 90, 222–243,  
1385 <https://doi.org/10.1017/qua.2018.37>, 2018.
- 1386 ~~Intergovernmental Panel On Climate Change: Climate Change 2021 – The Physical Science Basis: Working Group I~~  
1387 ~~Contribution to the Sixth Assessment Report of the Intergovernmental Panel on Climate Change, 1st ed., Cambridge University~~  
1388 ~~Press, <https://doi.org/10.1017/9781009157896>, 2021.~~
- 1389 Ivanovic, R. F., Gregoire, L. J., Kageyama, M., Roche, D. M., Valdes, P. J., Burke, A., Drummond, R., Peltier, W. R., and  
1390 Tarasov, L.: Transient climate simulations of the deglaciation 21–9 thousand years before present (version 1) – PMIP4 Core  
1391 experiment design and boundary conditions, *Geosci. Model Dev.*, 9, 2563–2587, <https://doi.org/10.5194/gmd-9-2563-2016>,  
1392 2016.
- 1393 Izeboud, M., Lhermitte, S., Van Tricht, K., Lenaerts, J. T. M., Van Lipzig, N. P. M., and Wever, N.: The Spatiotemporal  
1394 Variability of Cloud Radiative Effects on the Greenland Ice Sheet Surface Mass Balance, *Geophys. Res. Lett.*, 47,  
1395 e2020GL087315, <https://doi.org/10.1029/2020GL087315>, 2020.
- 1396 [Izumi, K., Valdes, P., Ivanovic, R., and Gregoire, L.: Impacts of the PMIP4 ice sheets on Northern Hemisphere climate during](https://doi.org/10.1007/s00382-022-06456-1)  
1397 [the last glacial period, \*Clim. Dyn.\*, 60, 2481–2499, <https://doi.org/10.1007/s00382-022-06456-1>, 2023.](https://doi.org/10.1007/s00382-022-06456-1)
- 1398 Jakobsson, M., Nilsson, J., Anderson, L., Backman, J., Björk, G., Cronin, T. M., Kirchner, N., Koshurnikov, A., Mayer, L.,  
1399 Noormets, R., O’Regan, M., Stranne, C., Ananiev, R., Barrientos Macho, N., Cherniykh, D., Coxall, H., Eriksson, B., Flodén,  
1400 T., Gemery, L., Gustafsson, Ö., Jerram, K., Johansson, C., Khortov, A., Mohammad, R., and Semiletov, I.: Evidence for an  
1401 ice shelf covering the central Arctic Ocean during the penultimate glaciation, *Nat. Commun.*, 7, 10365,  
1402 <https://doi.org/10.1038/ncomms10365>, 2016.
- 1403 Jennings, C. E.: Terrestrial ice streams—a view from the lobe, *Geomorphology*, 75, 100–124,  
1404 <https://doi.org/10.1016/j.geomorph.2005.05.016>, 2006.

- 1405 Joughin, I., Smith, B. E., Howat, I. M., Scambos, T., and Moon, T.: Greenland flow variability from ice-sheet-wide velocity  
1406 mapping, *J. Glaciol.*, 56, 415–430, <https://doi.org/10.3189/002214310792447734>, 2010.
- 1407 Jourdain, N. C., Mathiot, P., Burgard, C., Caillet, J., and Kittel, C.: Ice Shelf Basal Melt Rates in the Amundsen Sea at the End  
1408 of the 21st Century, *Geophys. Res. Lett.*, 49, e2022GL100629, <https://doi.org/10.1029/2022GL100629>, 2022.
- 1409 Kachuck, S. B., Martin, D. F., Bassis, J. N., and Price, S. F.: Rapid Viscoelastic Deformation Slows Marine Ice Sheet Instability  
1410 at Pine Island Glacier, *Geophys. Res. Lett.*, 47, e2019GL086446, <https://doi.org/10.1029/2019GL086446>, 2020.
- 1411 ~~Kageyama, M. and Valdes, P. J.: Impact of the North American ice sheet orography on the Last Glacial Maximum eddies and  
1412 snowfall, *Geophys. Res. Lett.*, 27, 1515–1518, <https://doi.org/10.1029/1999GL011274>, 2000.~~
- 1413 ~~Kageyama, M., Valdes, P. J., Ramstein, G., Hewitt, C., and Wyputta, U.: Northern Hemisphere Storm Tracks in Present Day  
1414 and Last Glacial Maximum Climate Simulations: A Comparison of the European PMIP Models, *J. Clim.*, 12, 742–760,  
1415 [https://doi.org/10.1175/1520-0442\(1999\)012<0742:NHSTIP>2.0.CO;2](https://doi.org/10.1175/1520-0442(1999)012<0742:NHSTIP>2.0.CO;2), 1999.~~
- 1416 ~~Kageyama, M., Charbit, S., Ritz, C., Khodri, M., and Ramstein, G.: Quantifying ice sheet feedbacks during the last glacial  
1417 inception, *Geophys. Res. Lett.*, 31, <https://doi.org/10.1029/2004GL021339>, 2004.~~
- 1418 ~~Kageyama, M., Albani, S., Braconnot, P., Harrison, S. P., Hopcroft, P. O., Ivanovic, R. F., Lambert, F., Marti, O., Peltier, W.  
1419 R., Peterschmitt, J.-Y., Roche, D. M., Tarasov, L., Zhang, X., Brady, E. C., Haywood, A. M., LeGrande, A. N., Lunt, D. J.,  
1420 Mahowald, N. M., Mikolajewicz, U., Nisancioglu, K. H., Otto-Blietsner, B. L., Renssen, H., Tomas, R. A., Zhang, Q., Abe-  
1421 Ouchi, A., Bartlein, P. J., Cao, J., Li, Q., Lohmann, G., Ohgaito, R., Shi, X., Volodin, E., Yoshida, K., Zhang, X., and Zheng,  
1422 W.: The PMIP4 contribution to CMIP6 – Part 4: Scientific objectives and experimental design of the PMIP4-CMIP6 Last  
1423 Glacial Maximum experiments and PMIP4 sensitivity experiments, *Geosci. Model Dev.*, 10, 4035–4055,  
1424 <https://doi.org/10.5194/gmd-10-4035-2017>, 2017.~~
- 1425 ~~[van Kampenhout, L., Rhoades, A. M., Herrington, A. R., Zarzycki, C. M., Lenaerts, J. T. M., Sacks, W. J., and van den Broeke,  
1426 M. R.: Regional grid refinement in an Earth system model: impacts on the simulated Greenland surface mass balance, \*The  
1427 Cryosphere\*, 13, 1547–1564, <https://doi.org/10.5194/tc-13-1547-2019>, 2019.](https://doi.org/10.5194/tc-13-1547-2019)~~
- 1428 Kazmierczak, E., Sun, S., Coulon, V., and Pattyn, F.: Subglacial hydrology modulates basal sliding response of the Antarctic  
1429 ice sheet to climate forcing, *The Cryosphere*, 16, 4537–4552, <https://doi.org/10.5194/tc-16-4537-2022>, 2022.
- 1430 Kennedy, M. C. and O’Hagan, A.: Bayesian Calibration of Computer Models, *J. R. Stat. Soc. Ser. B Stat. Methodol.*, 63, 425–  
1431 464, <https://doi.org/10.1111/1467-9868.00294>, 2001.
- 1432 Knies, J., Kleiber, H.-P., Matthiessen, J., Müller, C., and Nowaczyk, N.: Marine ice-rafted debris records constrain maximum  
1433 extent of Saalian and Weichselian ice-sheets along the northern Eurasian margin, *Glob. Planet. Change*, 31, 45–64,  
1434 [https://doi.org/10.1016/S0921-8181\(01\)00112-6](https://doi.org/10.1016/S0921-8181(01)00112-6), 2001.
- 1435 Kopp, R. E., DeConto, R. M., Bader, D. A., Hay, C. C., Horton, R. M., Kulp, S., Oppenheimer, M., Pollard, D., and Strauss,  
1436 B. H.: Evolving Understanding of Antarctic Ice-Sheet Physics and Ambiguity in Probabilistic Sea-Level Projections, *Earths  
1437 Future*, 5, 1217–1233, <https://doi.org/10.1002/2017EF000663>, 2017.
- 1438 ~~Krinner, G., Mangerud, J., Jakobsson, M., Crucifix, M., Ritz, C., and Svendsen, J. I.: Enhanced ice sheet growth in Eurasia  
1439 owing to adjacent ice-dammed lakes, *Nature*, 427, 429–432, <https://doi.org/10.1038/nature02233>, 2004.~~
- 1440 ~~Krinner, G., Boucher, O., and Balkanski, Y.: Ice-free glacial northern Asia due to dust deposition on snow, *Clim. Dyn.*, 27,  
1441 613–625, <https://doi.org/10.1007/s00382-006-0159-z>, 2006.~~

- 1442 Krinner, G., Diekmann, B., Colleoni, F., and Stauch, G.: Global, regional and local scale factors determining glaciation extent  
1443 in Eastern Siberia over the last 140,000 years, *Quat. Sci. Rev.*, 30, 821–831, <https://doi.org/10.1016/j.quascirev.2011.01.001>,  
1444 2011.
- 1445 Lambeck, K., Purcell, A., Funder, S., Kjær, K. H., Larsen, E., and Moller, P.: Constraints on the Late Saalian to early Middle  
1446 Weichselian ice sheet of Eurasia from field data and rebound modelling, *Boreas*, 35, 539–575,  
1447 <https://doi.org/10.1080/03009480600781875>, 2006.
- 1448 Lambeck, K., Rouby, H., Purcell, A., Sun, Y., and Sambridge, M.: Sea level and global ice volumes from the Last Glacial  
1449 Maximum to the Holocene, *Proc. Natl. Acad. Sci.*, 111, 15296–15303, <https://doi.org/10.1073/pnas.1411762111>, 2014.
- 1450 ~~Lambeck, K.,~~ Purcell, A., and Zhao, S.: The North American Late Wisconsin ice sheet and mantle viscosity from glacial  
1451 rebound analyses, *Quat. Sci. Rev.*, 158, 172–210, <https://doi.org/10.1016/j.quascirev.2016.11.033>, 2017.
- 1452 Lee, V., Cornford, S. L., and Payne, A. J.: Initialization of an ice-sheet model for present-day Greenland, *Ann. Glaciol.*, 56,  
1453 129–140, <https://doi.org/10.3189/2015AoG70A121>, 2015.
- 1454 Liakka, J., Nilsson, J., and Löfverström, M.: Interactions between stationary waves and ice sheets: linear versus nonlinear  
1455 atmospheric response, *Clim. Dyn.*, 38, 1249–1262, <https://doi.org/10.1007/s00382-011-1004-6>, 2012.
- 1456 ~~Liakka, J., Löfverström, M., and Colleoni, F.: The impact of the North American glacial topography on the evolution of the~~  
1457 ~~Eurasian ice sheet over the last glacial cycle, *Clim. Past*, 12, 1225–1241, <https://doi.org/10.5194/cp-12-1225-2016>, 2016.~~
- 1458 Liu, Z., Bao, Y., Thompson, L. G., Mosley-Thompson, E., Tabor, C., Zhang, G. J., Yan, M., Lofverstrom, M., Montanez, I.,  
1459 and Oster, J.: Tropical mountain ice core  $\delta^{18}O$ : A Goldilocks indicator for global temperature change, *Sci. Adv.*, 9, eadi6725,  
1460 <https://doi.org/10.1126/sciadv.adi6725>, 2023.
- 1461 ~~Loulergue, L., Schilt, A., Spahni, R., Masson-Delmotte, V., Blunier, T., Lemieux, B., Barnola, J., Lofverstrom, M., Raynaud,~~  
1462 ~~D., Stocker, T. F., and Chappellaz, J.: Orbital and millennial scale features~~ Liakka, J.: The influence of atmospheric CH<sub>4</sub> over  
1463 the past 800,000 years, *Nature*, 453, 383–386 ~~grid resolution in a climate model-forced ice sheet simulation, *The Cryosphere*,~~  
1464 ~~12, 1499–1510, <https://doi.org/10.1038/nature06950>, 2008~~ [5194/tc-12-1499-2018](https://doi.org/10.5194/tc-12-1499-2018), 2018.
- 1465 Margari, V., Skinner, L. C., Hodell, D. A., Martrat, B., Toucanne, S., Grimalt, J. O., Gibbard, P. L., Lunkka, J. P., and Tzedakis,  
1466 P. C.: Land-ocean changes on orbital and millennial time scales and the penultimate glaciation, *Geology*, 42, 183–186,  
1467 <https://doi.org/10.1130/G35070.1>, 2014.
- 1468 Margold, M., Stokes, C. R., and Clark, C. D.: Reconciling records of ice streaming and ice margin retreat to produce a  
1469 palaeogeographic reconstruction of the deglaciation of the Laurentide Ice Sheet, *Quat. Sci. Rev.*, 189, 1–30,  
1470 <https://doi.org/10.1016/j.quascirev.2018.03.013>, 2018.
- 1471 Martin, M. A., Winkelmann, R., Haseloff, M., Albrecht, T., Bueller, E., Khroulev, C., and Levermann, A.: The Potsdam Parallel  
1472 Ice Sheet Model (PISM-PIK) – Part 2: Dynamic equilibrium simulation of the Antarctic ice sheet, *The Cryosphere*, 5, 727–  
1473 740, <https://doi.org/10.5194/tc-5-727-2011>, 2011.
- 1474 ~~Masson-Delmotte, V., Stenni, B., Pol, K., Braconnot, P., Cattani, O., Falourd, S., Kageyama, M., Jouzel, J., Landais, A.,~~  
1475 ~~Minster, B., Barnola, J. M., Chappellaz, J., Krinner, G., Johnsen, S., Röthlisberger, R., Hansen, J., Mikolajewicz, U., and Otto-~~  
1476 ~~Bliesner, B.: EPICA Dome C record of glacial and interglacial intensities, *Quat. Sci. Rev.*, 29, 113–128,~~  
1477 ~~<https://doi.org/10.1016/j.quascirev.2009.09.030>, 2010.~~

- 1478 ~~Masson Delmotte, V., Schulz, M., Abe-Ouchi, A., Beer, J., Ganopolski, A., Fidel, J., Rouco, G., Jansen, E., Lambeck, K.,~~  
1479 ~~Luterbacher, J., Naish, T., Ramesh, R., Rojas, M., Shao, X., Anchukaitis, K., Arblaster, J., Bartlein, P. J., Benito, G., Clark,~~  
1480 ~~P., Comiso, J. C., Crowley, T., Deckker, P. D., de Vernal, A., Delmonte, B., DiNezio, P., Dowsett, H. J., Edwards, R. L.,~~  
1481 ~~Fischer, H., Fleitmann, D., Foster, G., Fröhlich, C., Hall, A., Hargreaves, J., Haywood, A., Hollis, C., Krinner, G., Landais,~~  
1482 ~~A., Li, C., Lunt, D., Mahowald, N., McGregor, S., Meehl, G., Mitrovica, J. X., Moberg, A., Mudelsee, M., Muhs, D. R.,~~  
1483 ~~Mulitza, S., Müller, S., Overland, J., Parrenin, F., Pearson, P., Robock, A., Rohling, E., Salzmann, U., Savarino, J., Sedláček,~~  
1484 ~~J., Shindell, D., Smerdon, J., Solomina, O., Tarasov, P., Vinther, B., Waelbroeck, C., Wolf, D., Yokoyama, Y., Yoshimori,~~  
1485 ~~M., Zachos, J., Zwartz, D., Gupta, A. K., Rahimzadeh, F., Raynaud, D., and Wanner, H.: Information from Paleoclimate~~  
1486 ~~Archives, 2013.~~
- 1487 [Matero, I. S. O., Gregoire, L. J., Ivanovic, R. F., Tindall, J. C., and Haywood, A. M.: The 8.2 ka cooling event caused by](#)  
1488 [Laurentide ice saddle collapse. \*Earth Planet. Sci. Lett.\*, 473, 205–214, <https://doi.org/10.1016/j.epsl.2017.06.011>, 2017.](#)
- 1489 Matero, I. S. O., Gregoire, L. J., and Ivanovic, R. F.: Simulating the Early Holocene demise of the Laurentide Ice Sheet with  
1490 BISICLES (public trunk revision 3298), *Geosci. Model Dev.*, 13, 4555–4577, <https://doi.org/10.5194/gmd-13-4555-2020>,  
1491 2020.
- 1492 Menviel, L., Capron, E., Govin, A., Dutton, A., Tarasov, L., Abe-Ouchi, A., Drysdale, R. N., Gibbard, P. L., Gregoire, L., He,  
1493 F., Ivanovic, R. F., Kageyama, M., Kawamura, K., Landais, A., Otto-Bliesner, B. L., Oyabu, I., Tzedakis, P. C., Wolff, E., and  
1494 Zhang, X.: The penultimate deglaciation: protocol for Paleoclimate Modelling Intercomparison Project (PMIP) phase 4  
1495 transient numerical simulations between 140 and 127&thinsp;ka, version 1.0, *Geosci. Model Dev.*, 12, 3649–3685,  
1496 <https://doi.org/10.5194/gmd-12-3649-2019>, 2019.
- 1497 ~~Merz, N., Raible, C. C., and Woollings, T.: North Atlantic Eddy Driven Jet in Interglacial and Glacial Winter Climates, *J.*~~  
1498 ~~*Clim.*, 28, 3977–3997, <https://doi.org/10.1175/JCLI-D-14-00525.1>, 2015.~~
- 1499 Moreno-Parada, D., Alvarez-Solas, J., Blasco, J., Montoya, M., and Robinson, A.: Simulating the Laurentide Ice Sheet of the  
1500 Last Glacial Maximum, *The Cryosphere*, 17, 2139–2156, <https://doi.org/10.5194/tc-17-2139-2023>, 2023.
- 1501 Mostue, I. A., Hofer, S., Storelymo, T., and Fettweis, X.: Cloud- and ice-albedo feedbacks drive greater Greenland Ice Sheet  
1502 sensitivity to warming in CMIP6 than in CMIP5, *The Cryosphere*, 18, 475–488, <https://doi.org/10.5194/tc-18-475-2024>, 2024.
- 1503 ~~Naafs, B. D. A., Hefter, J., Acton, G., Haug, G. H., Martínez Garcia, A., Pancost, R., and Stein, R.: Strengthening of North~~  
1504 ~~American dust sources during the late Pliocene (2.7 Ma), *Earth Planet. Sci. Lett.*, 317–318, 8–19,~~  
1505 ~~<https://doi.org/10.1016/j.epsl.2011.11.026>, 2012.~~
- 1506 ~~Naafs, B. D. A., Hefter, J., and Stein, R.: Millennial-scale ice rafting events and Hudson Strait Heinrich(-like) Events during~~  
1507 ~~the late Pliocene and Pleistocene: a review, *Quat. Sci. Rev.*, 80, 1–28, <https://doi.org/10.1016/j.quascirev.2013.08.014>, 2013.~~
- 1508 Nias, I. J., Cornford, S. L., and Payne, A. J.: New Mass-Conserving Bedrock Topography for Pine Island Glacier Impacts  
1509 Simulated Decadal Rates of Mass Loss, *Geophys. Res. Lett.*, 45, 3173–3181, <https://doi.org/10.1002/2017GL076493>, 2018.
- 1510 Niu, L., Lohmann, G., Hinck, S., Gowan, E. J., and Krebs-Kanzow, U.: The sensitivity of Northern Hemisphere ice sheets to  
1511 atmospheric forcing during the last glacial cycle using PMIP3 models, *J. Glaciol.*, 65, 645–661,  
1512 <https://doi.org/10.1017/jog.2019.42>, 2019.
- 1513 Oakley, J. E. and O’Hagan, A.: Probabilistic Sensitivity Analysis of Complex Models: A Bayesian Approach, *J. R. Stat. Soc.*  
1514 *Ser. B Stat. Methodol.*, 66, 751–769, <https://doi.org/10.1111/j.1467-9868.2004.05304.x>, 2004.

- 1515 Obase, T., Abe-Ouchi, A., and Saito, F.: Abrupt climate changes in the last two deglaciations simulated with different Northern  
1516 ice sheet discharge and insolation, *Sci. Rep.*, 11, 22359, <https://doi.org/10.1038/s41598-021-01651-2>, 2021.
- 1517 Obrochta, S. P., Crowley, T. J., Channell, J. E. T., Hodell, D. A., Baker, P. A., Seki, A., and Yokoyama, Y.: Climate variability  
1518 and ice-sheet dynamics during the last three glaciations, *Earth Planet. Sci. Lett.*, 406, 198–212,  
1519 <https://doi.org/10.1016/j.epsl.2014.09.004>, 2014.
- 1520 Osman, M. B., Tierney, J. E., Zhu, J., Tardif, R., Hakim, G. J., King, J., and Poulsen, C. J.: Globally resolved surface  
1521 temperatures since the Last Glacial Maximum, *Nature*, 599, 239–244, <https://doi.org/10.1038/s41586-021-03984-4>, 2021.
- 1522 [Parker, R. L., Foster, G. L., Gutjahr, M., Wilson, P. A., Littler, K. L., Cooper, M. J., Michalik, A., Milton, J. A., Crockett, K.  
1523 C., and Bailey, I.: Laurentide Ice Sheet extent over the last 130 thousand years traced by the Pb isotope signature of weathering  
1524 inputs to the Labrador Sea, \*Quat. Sci. Rev.\*, 287, 107564, <https://doi.org/10.1016/j.quascirev.2022.107564>, 2022.](#)
- 1525 [Patterson, V., Gregoire, L., Ivanovic, R., Gandy, N., Cornford, S., Owen, J., Sherriff-Tadano, S., and Smith, R.: FAMOUS-  
1526 BISICLES simulation data with interactive Northern Hemisphere ice sheets \(21ka and 140ka\), NERC](#)
- 1527 [EDS Centre for Environmental Data Analysis \[data set\], <https://doi.org/10.5285/4CE75927EAB444B89B5439E33ECF1A80>,  
1528 2025.](#)
- 1529 Patterson, V. L., Gregoire, L. J., Ivanovic, R., Gandy, N., Owen, J., Smith, R. S., Pollard, O. G., and Astfalck, L. C.: Contrasting  
1530 the Penultimate and Last Glacial Maxima (140 and 21 ka BP) using coupled climate-ice sheet modelling, *Clim. Past Discuss.*,  
1531 1–37, <https://doi.org/10.5194/cp-2024-10>, 2024.
- 1532 Patton, H., Andreassen, K., Bjarnadóttir, L. R., Dowdeswell, J. A., Winsborrow, M. C. M., Noormets, R., Polyak, L., Auriac,  
1533 A., and Hubbard, A.: Geophysical constraints on the dynamics and retreat of the Barents Sea ice sheet as a paleobenchmark  
1534 for models of marine ice sheet deglaciation, *Rev. Geophys.*, 53, 1051–1098, <https://doi.org/10.1002/2015RG000495>, 2015.
- 1535 Patton, H., Hubbard, A., Andreassen, K., Winsborrow, M., and Stroeven, A. P.: The build-up, configuration, and dynamical  
1536 sensitivity of the Eurasian ice-sheet complex to Late Weichselian climatic and oceanic forcing, *Quat. Sci. Rev.*, 153, 97–121,  
1537 <https://doi.org/10.1016/j.quascirev.2016.10.009>, 2016.
- 1538 Patton, H., Hubbard, A., Andreassen, K., Auriac, A., Whitehouse, P. L., Stroeven, A. P., Shackleton, C., Winsborrow, M.,  
1539 Heyman, J., and Hall, A. M.: Deglaciation of the Eurasian ice sheet complex, *Quat. Sci. Rev.*, 169, 148–172,  
1540 <https://doi.org/10.1016/j.quascirev.2017.05.019>, 2017.
- 1541 Pattyn, F., Schoof, C., Perichon, L., Hindmarsh, R. C. A., Bueler, E., de Fleurian, B., Durand, G., Gagliardini, O., Gladstone,  
1542 R., Goldberg, D., Gudmundsson, G. H., Huybrechts, P., Lee, V., Nick, F. M., Payne, A. J., Pollard, D., Rybak, O., Saito, F.,  
1543 and Vieli, A.: Results of the Marine Ice Sheet Model Intercomparison Project, MISMIP, *The Cryosphere*, 6, 573–588,  
1544 <https://doi.org/10.5194/tc-6-573-2012>, 2012.
- 1545 Pelt, W. J. J. V. and Oerlemans, J.: Numerical simulations of cyclic behaviour in the Parallel Ice Sheet Model (PISM), *J.  
1546 Glaciol.*, 58, 347–360, <https://doi.org/10.3189/2012JoG11J217>, 2012.
- 1547 Peltier, W. R., Argus, D. F., and Drummond, R.: Space geodesy constrains ice age terminal deglaciation: The global ICE-  
1548 6G\_C (VM5a) model, *J. Geophys. Res. Solid Earth*, 120, 450–487, <https://doi.org/10.1002/2014JB011176>, 2015.
- 1549 Petrini, M., Colleoni, F., Kirchner, N., Hughes, A. L. C., Camerlenghi, A., Rebesco, M., Lucchi, R. G., Forte, E., Colucci, R.  
1550 R., Noormets, R., and Mangerud, J.: Simulated last deglaciation of the Barents Sea Ice Sheet primarily driven by oceanic  
1551 conditions, *Quat. Sci. Rev.*, 238, 106314, <https://doi.org/10.1016/j.quascirev.2020.106314>, 2020.

- 1552 Peyaud, V.: Rôle de la dynamique des calottes glaciaires dans les grands changements climatiques des périodes glaciaires-  
1553 interglaciaires., phdthesis, Université Joseph-Fourier - Grenoble I, 2006.
- 1554 Pollard, D. and DeConto, R. M.: Description of a hybrid ice sheet-shelf model, and application to Antarctica, *Geosci. Model*  
1555 *Dev.*, 5, 1273–1295, <https://doi.org/10.5194/gmd-5-1273-2012>, 2012.
- 1556 Pollard, O. G., Barlow, N. L. M., Gregoire, L. J., Gomez, N., Cartelle, V., Ely, J. C., and Astfalck, L. C.: Quantifying the  
1557 uncertainty in the Eurasian ice-sheet geometry at the Penultimate Glacial Maximum (Marine Isotope Stage 6), *The Cryosphere*,  
1558 17, 4751–4777, <https://doi.org/10.5194/tc-17-4751-2023>, 2023.
- 1559 ~~Pope, V. D., Gallani, M. L., Rowntree, P. R., and Stratton, R. A.: The impact of new physical parametrizations in the Hadley  
1560 Centre climate model: HadAM3, *Clim. Dyn.*, 16, 123–146, <https://doi.org/10.1007/s003820050009>, 2000.~~
- 1561 [Pollard, O. G., Barlow, N. L. M., Gregoire, L. J., and Gomez, N.: Relative sea-level sensitivity in the Eurasian region to Earth  
1562 and ice-sheet model uncertainty during the Last Interglacial, \*Quat. Sci. Rev.\*, 343, 108908,  
1563 <https://doi.org/10.1016/j.quascirev.2024.108908>, 2024.](https://doi.org/10.1016/j.quascirev.2024.108908)
- 1564 [Quiquet, A. and Roche, D. M.: Investigating similarities and differences of the penultimate and last glacial terminations with  
1565 a coupled ice sheet–climate model, \*Clim. Past\*, 20, 1365–1385, <https://doi.org/10.5194/cp-20-1365-2024>, 2024.](https://doi.org/10.5194/cp-20-1365-2024)
- 1566 Quiquet, A., Roche, D. M., Dumas, C., Bouttes, N., and Lhardy, F.: Climate and ice sheet evolutions from the last glacial  
1567 maximum to the pre-industrial period with an ice-sheet–climate coupled model, *Clim. Past*, 17, 2179–2199,  
1568 <https://doi.org/10.5194/cp-17-2179-2021>, 2021.
- 1569 ~~Rabineau, M., Berné, S., Olivet, J. L., Aslanian, D., Guillocheau, F., and Joseph, P.: Paleo sea levels reconsidered from direct  
1570 observation of paleoshoreline position during Glacial Maxima (for the last 500,000 yr), *Earth Planet. Sci. Lett.*, 252, 119–137,  
1571 <https://doi.org/10.1016/j.epsl.2006.09.033>, 2006.~~
- 1572 [Reed, B., Green, J. A. M., Jenkins, A., and Gudmundsson, G. H.: Recent irreversible retreat phase of Pine Island Glacier, \*Nat.\*  
1573 \*Clim. Change\*, 14, 75–81, <https://doi.org/10.1038/s41558-023-01887-y>, 2024.](https://doi.org/10.1038/s41558-023-01887-y)
- 1574 Rignot, E. and Jacobs, S. S.: Rapid Bottom Melting Widespread near Antarctic Ice Sheet Grounding Lines, *Science*, 296,  
1575 2020–2023, <https://doi.org/10.1126/science.1070942>, 2002.
- 1576 Rignot, E., Mouginot, J., and Scheuchl, B.: Ice Flow of the Antarctic Ice Sheet, *Science*, 333, 1427–1430,  
1577 <https://doi.org/10.1126/science.1208336>, 2011.
- 1578 Rignot, E., Jacobs, S., Mouginot, J., and Scheuchl, B.: Ice-Shelf Melting Around Antarctica, *Science*, 341, 266–270,  
1579 <https://doi.org/10.1126/science.1235798>, 2013.
- 1580 Robel, A. A. and Tziperman, E.: The role of ice stream dynamics in deglaciation, *J. Geophys. Res. Earth Surf.*, 121, 1540–  
1581 1554, <https://doi.org/10.1002/2016JF003937>, 2016.
- 1582 Roberts, W. H. G., Valdes, P. J., and Payne, A. J.: Topography’s crucial role in Heinrich Events, *Proc. Natl. Acad. Sci.*, 111,  
1583 16688–16693, <https://doi.org/10.1073/pnas.1414882111>, 2014.
- 1584 [Roberts, W. H. G., Li, C., and Valdes, P. J.: The Mechanisms that Determine the Response of the Northern Hemisphere’s  
1585 Stationary Waves to North American Ice Sheets, <https://doi.org/10.1175/JCLI-D-18-0586.1>, 2019.](https://doi.org/10.1175/JCLI-D-18-0586.1)

- 1586 Roe, G. H. and Lindzen, R. S.: The Mutual Interaction between Continental-Scale Ice Sheets and Atmospheric Stationary  
1587 Waves, *J. Clim.*, 14, 1450–1465, [https://doi.org/10.1175/1520-0442\(2001\)014<1450:TMBCS>2.0.CO;2](https://doi.org/10.1175/1520-0442(2001)014<1450:TMBCS>2.0.CO;2), 2001.
- 1588 Rohling, E. J., Hibbert, F. D., Williams, F. H., Grant, K. M., Marino, G., Foster, G. L., Hennekam, R., de Lange, G. J., Roberts,  
1589 A. P., Yu, J., Webster, J. M., and Yokoyama, Y.: Differences between the last two glacial maxima and implications for ice-  
1590 sheet,  $\delta^{18}\text{O}$ , and sea-level reconstructions, *Quat. Sci. Rev.*, 176, 1–28, <https://doi.org/10.1016/j.quascirev.2017.09.009>, 2017.
- 1591 [Romé, Y.: Abrupt climate changes during the last ice age: a study of millennial-scale variability in climate simulations, phd,  
1592 University of Leeds, 2024.](#)
- 1593 Rougier, J., Maute, A., Guillas, S., and Richmond, A. D.: Expert Knowledge and Multivariate Emulation: The Thermosphere-  
1594 Ionosphere Electrodynamics General Circulation Model (TIE-GCM), *Technometrics*, 51, 414–424, 2009.
- 1595 Ryan, J. C., Smith, L. C., Cooley, S. W., Pearson, B., Wever, N., Keenan, E., and Lenaerts, J. T. M.: Decreasing surface albedo  
1596 signifies a growing importance of clouds for Greenland Ice Sheet meltwater production, *Nat. Commun.*, 13, 4205,  
1597 <https://doi.org/10.1038/s41467-022-31434-w>, 2022.
- 1598 Saltelli, A.: Making best use of model evaluations to compute sensitivity indices, *Comput. Phys. Commun.*, 145, 280–297,  
1599 [https://doi.org/10.1016/S0010-4655\(02\)00280-1](https://doi.org/10.1016/S0010-4655(02)00280-1), 2002.
- 1600 Scherrenberg, M., Berends, C., and Van De Wal, R.: Late Pleistocene glacial terminations accelerated by proglacial lakes,  
1601 <https://doi.org/10.5194/cp-2023-42>, 3 July 2023a.
- 1602 Scherrenberg, M. D. W., Berends, C. J., Stap, L. B., and van de Wal, R. S. W.: Modelling feedbacks between the Northern  
1603 Hemisphere ice sheets and climate during the last glacial cycle, *Clim. Past*, 19, 399–418, [https://doi.org/10.5194/cp-19-399-  
1604 2023](https://doi.org/10.5194/cp-19-399-2023), 2023b.
- 1605 ~~Schmidt, G. A., Annan, J. D., Bartlein, P. J., Cook, B. I., Guilyardi, E., Hargreaves, J. C., Harrison, S. P., Kageyama, M.,  
1606 LeGrande, A. N., Konecky, B., Lovejoy, S., Mann, M. E., Masson-Delmotte, V., Risi, C., Thompson, D., Timmermann, A.,  
1607 Tremblay, L. B., and Yiou, P.: Using palaeo-climate comparisons to constrain future projections in CMIP5, *Clim. Past*, 10,  
1608 221–250, <https://doi.org/10.5194/cp-10-221-2014>, 2014.~~
- 1609 Schmittner, A., Urban, N. M., Shakun, J. D., Mahowald, N. M., Clark, P. U., Bartlein, P. J., Mix, A. C., and Rosell-Melé, A.:  
1610 Climate Sensitivity Estimated from Temperature Reconstructions of the Last Glacial Maximum, *Science*, 334, 1385–1388,  
1611 <https://doi.org/10.1126/science.1203513>, 2011.
- 1612 Schneider von Deimling, T., Ganopolski, A., Held, H., and Rahmstorf, S.: How cold was the Last Glacial Maximum?,  
1613 *Geophys. Res. Lett.*, 33, <https://doi.org/10.1029/2006GL026484>, 2006.
- 1614 Schoof, C.: A variational approach to ice stream flow, *J. Fluid Mech.*, 556, 227–251,  
1615 <https://doi.org/10.1017/S0022112006009591>, 2006.
- 1616 Schoof, C. and Hindmarsh, R. C. A.: Thin-Film Flows with Wall Slip: An Asymptotic Analysis of Higher Order Glacier Flow  
1617 Models, *Q. J. Mech. Appl. Math.*, 63, 73–114, <https://doi.org/10.1093/qjmam/hbp025>, 2010.
- 1618 Sherriff-Tadano, S., [Abe-Ouchi, A., Yoshimori, M., Oka, A., and Chan, W.-L.: Influence of glacial ice sheets on the Atlantic  
1619 meridional overturning circulation through surface wind change, \*Clim. Dyn.\*, 50, 2881–2903, \[https://doi.org/10.1007/s00382-  
017-3780-0\]\(https://doi.org/10.1007/s00382-<br/>1620 017-3780-0\), 2018.](#)

- 1621 [Sherriff-Tadano, S., Abe-Ouchi, A., and Oka, A.: Impact of mid-glacial ice sheets on deep ocean circulation and global climate, \*Clim. Past\*, 17, 95–110, <https://doi.org/10.5194/cp-17-95-2021>, 2021.](#)
- 1622
- 1623 [Sherriff-Tadano, S., Ivanovic, R., Gregoire, L., Lang, C., Gandy, N., Gregory, J., Edwards, T. L., Pollard, O., and Smith, R. S.: Large-ensemble simulations of the North American and Greenland ice sheets at the Last Glacial Maximum with a coupled atmospheric general circulation–ice sheet model, \*Clim. Past\*, 20, 1489–1512, <https://doi.org/10.5194/cp-20-1489-2024>, 2024.](#)
- 1624
- 1625
- 1626 [Siahaan, A., Smith, R. S., Holland, P. R., Jenkins, A., Gregory, J. M., Lee, V., Mathiot, P., Payne, A. J., Ridley, J. K., and Jones, C. G.: The Antarctic contribution to 21st-century sea-level rise predicted by the UK Earth System Model with an interactive ice sheet, \*The Cryosphere\*, 16, 4053–4086, <https://doi.org/10.5194/tc-16-4053-2022>, 2022.](#)
- 1627
- 1628
- 1629 Simms, A. R., Lisiecki, L., Gebbie, G., Whitehouse, P. L., and Clark, J. F.: Balancing the last glacial maximum (LGM) sea-level budget, *Quat. Sci. Rev.*, 205, 143–153, <https://doi.org/10.1016/j.quascirev.2018.12.018>, 2019.
- 1630
- 1631 Smith, R. N. B.: A scheme for predicting layer clouds and their water content in a general circulation model, *Q. J. R. Meteorol. Soc.*, 116, 435–460, <https://doi.org/10.1002/qj.49711649210>, 1990.
- 1632
- 1633 [Smith, R. S. and Gregory, J.: The last glacial cycle: transient simulations with an AOGCM, \*Clim. Dyn.\*, 38, 1545–1559, <https://doi.org/10.1007/s00382-011-1283-y>, 2012.](#)
- 1634
- 1635 [Smith, R. S., George, S., and Gregory, J. M.: FAMOUS version xotzt \(FAMOUS-ice\): a general circulation model \(GCM\) capable of energy- and water-conserving coupling to an ice sheet model, \*Geosci. Model Dev.\*, 14, 5769–5787, <https://doi.org/10.5194/gmd-14-5769-2021>, 2021.](#)
- 1636
- 1637
- 1638 Sobol', I. M.: Global sensitivity indices for nonlinear mathematical models and their Monte Carlo estimates, *Math. Comput. Simul.*, 55, 271–280, [https://doi.org/10.1016/S0378-4754\(00\)00270-6](https://doi.org/10.1016/S0378-4754(00)00270-6), 2001.
- 1639
- 1640 [Sommers, A. N., Otto-Bliesner, B. L., Lipscomb, W. H., Lofverstrom, M., Shafer, S. L., Bartlein, P. J., Brady, E. C., Kluzek, E., Leguy, G., Thayer-Calder, K., and Tomas, R. A.: Retreat and Regrowth of the Greenland Ice Sheet During the Last Interglacial as Simulated by the CESM2-CISM2 Coupled Climate–Ice Sheet Model, \*Paleoceanogr. Paleoclimatology\*, 36, e2021PA004272, <https://doi.org/10.1029/2021PA004272>, 2021.](#)
- 1641
- 1642
- 1643
- 1644 Stokes, C. R. and Clark, C. D.: Palaeo-ice streams, *Quat. Sci. Rev.*, 20, 1437–1457, [https://doi.org/10.1016/S0277-3791\(01\)00003-8](https://doi.org/10.1016/S0277-3791(01)00003-8), 2001.
- 1645
- 1646 Stone, E. J. and Lunt, D. J.: The role of vegetation feedbacks on Greenland glaciation, *Clim. Dyn.*, 40, 2671–2686, <https://doi.org/10.1007/s00382-012-1390-4>, 2013.
- 1647
- 1648 Sutherland, J. L., Carrivick, J. L., Gandy, N., Shulmeister, J., Quincey, D. J., and Cornford, S. L.: Proglacial Lakes Control Glacier Geometry and Behavior During Recession, *Geophys. Res. Lett.*, 47, e2020GL088865, <https://doi.org/10.1029/2020GL088865>, 2020.
- 1649
- 1650
- 1651 Svendsen, J. I., Alexanderson, H., Astakhov, V. I., Demidov, I., Dowdeswell, J. A., Funder, S., Gataullin, V., Henriksen, M., Hjort, C., Houmark-Nielsen, M., Hubberten, H. W., Ingólfsson, Ó., Jakobsson, M., Kjær, K. H., Larsen, E., Lokrantz, H., Lunkka, J. P., Lyså, A., Mangerud, J., Matiouchkov, A., Murray, A., Möller, P., Niessen, F., Nikolskaya, O., Polyak, L., Saarnisto, M., Siegert, C., Siegert, M. J., Spielhagen, R. F., and Stein, R.: Late Quaternary ice sheet history of northern Eurasia, *Quat. Sci. Rev.*, 23, 1229–1271, <https://doi.org/10.1016/j.quascirev.2003.12.008>, 2004.
- 1652
- 1653
- 1654
- 1655

- 1656 Tarasov, L., Dyke, A. S., Neal, R. M., and Peltier, W. R.: A data-calibrated distribution of deglacial chronologies for the North  
1657 American ice complex from glaciological modeling, *Earth Planet. Sci. Lett.*, 315–316, 30–40,  
1658 <https://doi.org/10.1016/j.epsl.2011.09.010>, 2012.
- 1659 Tsai, V. C., Stewart, A. L., and Thompson, A. F.: Marine ice-sheet profiles and stability under Coulomb basal conditions, *J.*  
1660 *Glaciol.*, 61, 205–215, <https://doi.org/10.3189/2015JoG14J221>, 2015.
- 1661 Ullman, D. J., LeGrande, A. N., Carlson, A. E., Anslow, F. S., and Licciardi, J. M.: Assessing the impact of Laurentide Ice  
1662 Sheet topography on glacial climate, *Clim. Past*, 10, 487–507, <https://doi.org/10.5194/cp-10-487-2014>, 2014.
- 1663 Wainer, K. A. I., Rowe, M. P., Thomas, A. L., Mason, A. J., Williams, B., Tamisiea, M. E., Williams, F. H., Düsterhus, A.,  
1664 and Henderson, G. M.: Speleothem evidence for MIS 5c and 5a sea level above modern level at Bermuda, *Earth Planet. Sci.*  
1665 *Lett.*, 457, 325–334, <https://doi.org/10.1016/j.epsl.2016.10.005>, 2017.
- 1666 Wekerle, C., Colleoni, F., Näslund, J.-O., Brandefelt, J., and Masina, S.: Numerical reconstructions of the penultimate glacial  
1667 maximum Northern Hemisphere ice sheets: sensitivity to climate forcing and model parameters, *J. Glaciol.*, 62, 607–622,  
1668 <https://doi.org/10.1017/jog.2016.45>, 2016.
- 1669 Willeit, M., Calov, R., Talento, S., Greve, R., Bernales, J., Klemann, V., Bagge, M., and Ganopolski, A.: Glacial inception  
1670 through rapid ice area increase driven by albedo and vegetation feedbacks, *Clim. Past*, 20, 597–623, <https://doi.org/10.5194/cp-20-597-2024>, 2024.
- 1672 Williams, J. H. T., Smith, R. S., Valdes, P. J., Booth, B. B. B., and Osprey, A.: Optimising the FAMOUS climate model:  
1673 inclusion of global carbon cycling, *Geosci. Model Dev.*, 6, 141–160, <https://doi.org/10.5194/gmd-6-141-2013>, 2013.
- 1674 Williamson, D.: Exploratory ensemble designs for environmental models using k-extended Latin Hypercubes, *Environmetrics*,  
1675 26, 268–283, <https://doi.org/10.1002/env.2335>, 2015.
- 1676 ~~Williamson, D., Goldstein, M., Allison, L., Blaker, A., Challenor, P., Jackson, L., and Yamazaki, K.: History matching for  
1677 exploring and reducing climate model parameter space using observations and a large perturbed physics ensemble, *Clim. Dyn.*,  
1678 41, 1703–1729, <https://doi.org/10.1007/s00382-013-1896-4>, 2013.~~
- 1679 [Zhang, X., Lohmann, G., Knorr, G., and Purcell, C.: Abrupt glacial climate shifts controlled by ice sheet changes, \*Nature\*, 512,  
1680 290–294, <https://doi.org/10.1038/nature13592>, 2014.](https://doi.org/10.1038/nature13592)
- 1681 Zhang, X.-Y., Trame, M. N., Lesko, L. J., and Schmidt, S.: Sobol Sensitivity Analysis: A Tool to Guide the Development and  
1682 Evaluation of Systems Pharmacology Models, *CPT Pharmacomet. Syst. Pharmacol.*, 4, 69–79, <https://doi.org/10.1002/psp4.6>,  
1683 2015.
- 1684 Zhu, J., Otto-Bliesner, B. L., Brady, E. C., Gettelman, A., Bacmeister, J. T., Neale, R. B., Poulsen, C. J., Shaw, J. K., McGraw,  
1685 Z. S., and Kay, J. E.: LGM Paleoclimate Constraints Inform Cloud Parameterizations and Equilibrium Climate Sensitivity in  
1686 CESM2, *J. Adv. Model. Earth Syst.*, 14, e2021MS002776, <https://doi.org/10.1029/2021MS002776>, 2022.
- 1687 Ziemen, F. A., Rodehacke, C. B., and Mikolajewicz, U.: Coupled ice sheet–climate modeling under glacial and pre-industrial  
1688 boundary conditions, *Clim. Past*, 10, 1817–1836, <https://doi.org/10.5194/cp-10-1817-2014>, 2014.
- 1689 Zweck, C. and Huybrechts, P.: Modeling of the northern hemisphere ice sheets during the last glacial cycle and glaciological  
1690 sensitivity, *J. Geophys. Res. Atmospheres*, 110, <https://doi.org/10.1029/2004JD005489>, 2005.
- 1691